

UNIVERSITE TOULOUSE III, PAUL SABATIER

HABILITATION À DIRIGER LES RECHERCHES

Functionals, Integrals, Spheres & Cusps

Author:

Pierre-François Loos

*A thesis submitted in fulfillment of the requirements
for the degree of Habilitation à diriger les recherches*

in the

Université de Toulouse, CNRS, UPS, France
Laboratoire de Chimie et Physique quantiques

January 26, 2018

UNIVERSITE TOULOUSE III, PAUL SABATIER

Abstract

Laboratoire de Chimie et Physique quantiques

Habilitation à diriger les recherches

Functionals, Integrals, Spheres & Cusps

by Pierre-François Loos

In this memoir, after a brief introduction of the various quantum chemistry methods considered here, I summarise some of the projects we have been working on in the last ten years. First, I describe succinctly several studies we have been doing on model two-electron systems. In particular, we introduced a novel class of quasi-exactly solvable systems that we have been studying exhaustively in several papers. Following this work, we shed new lights on the universality of correlation effects in two-electron systems. The discovery we have made are discussed. Second, I present the work we performed on the mathematical properties of a new family of uniform electron gases as well as the development of a new class of density functionals based on this new paradigm. Third, new recurrence relations for three- and four-electron integrals as well as their fundamental integrals and upper bounds are discussed. In particular, our strategy to bound rigorously and efficiently these many-electron integrals is presented. This new way of calculating many-electron integrals represents an interesting alternative to what is currently done in explicitly-correlated methods. Finally, I present two lines of research we have been pursuing recently, namely the development of explicitly-correlated configuration interaction methods and a self-consistent correction to enforce the electron-nucleus cusp in molecular orbitals.

Contents

Introduction	1
1 Methods	7
1.1 Schrödinger equation	7
1.2 Hartree-Fock approximation	8
1.2.1 Roothaan-Hall equations	9
1.2.2 Self-consistent field calculation	10
1.3 Post Hartree-Fock methods	11
1.3.1 Configuration interaction methods	11
1.3.2 Density-functional theory	11
1.3.3 Kohn-Sham equations	12
1.3.4 Exchange-correlation functionals	13
1.4 Quantum Monte Carlo methods	14
1.4.1 Variational Monte Carlo	14
1.4.2 Diffusion Monte Carlo	15
1.4.3 Trial wave functions	15
1.4.4 Fixed-node approximation	15
2 Correlation in two-electron systems	17
2.1 Quasi-exactly solvable models	18
2.1.1 Singlet ground state	19
2.1.2 Triplet excited state	20
2.1.3 Other electronic states	22
2.1.4 Natural/unnatural parity	23
2.1.5 First-order cusp condition	23
2.1.6 Second-order cusp condition	24
2.2 Universality of correlation effects	25
2.2.1 High-density correlation energy	25
2.2.2 The conjecture	26
2.2.3 The proof	27
2.3 Summary	29
3 DFT using finite uniform electron gases	31
3.1 Uniform electron gases	32
3.1.1 Spherium atoms	32
3.1.2 Glomium atoms	33
3.1.3 The non-uniqueness problem	33
3.2 Exchange functionals based on finite uniform electron gases	34
3.2.1 Theory	35
3.2.2 GLDA exchange functionals	37
3.2.3 FMGGA exchange functionals	41
3.3 Summary	43

4	Many-electron integrals involving Gaussian geminals	45
4.1	History	45
4.2	Generalities	48
4.2.1	Gaussian functions	48
4.2.2	Many-electron integrals	48
4.2.3	Three- and four-electron operators	49
4.3	Fundamental integrals	50
4.4	Upper bounds	51
4.4.1	Integral bounds	52
4.4.2	Class bounds	52
4.4.3	Shell- <i>m</i> tuplet bounds	53
4.4.4	Screening algorithm	53
4.5	Recurrence relations	54
4.5.1	Vertical recurrence relations	54
4.5.2	Transfer recurrence relations	54
4.5.3	Horizontal recurrence relations	55
4.6	Algorithm	55
4.7	Summary	59
5	Future directions	61
5.1	Motivations	61
5.2	Explicitly-correlated FCI methods	62
5.2.1	Ansatz	63
5.2.2	Dressing	63
5.2.3	Matrix elements	64
5.2.4	An illustrative example	65
5.3	Self-consistent electron-nucleus cusp correction for molecular orbitals	66
5.3.1	Cusp-corrected orbitals	68
5.3.2	Self-consistent dressing of the Fock matrix	69
5.3.3	An illustrative example	71
5.4	Summary	71
	Conclusion	73
	Bibliography	79

Introduction

This memoir concerns the research activities I have been involved in after the end of my PhD.

In a nutshell, my PhD work deals with excited electronic states of macromolecules, such as proteins, enzymes and DNA fragments, as well as the development of QM/MM methods which combine quantum mechanics and molecular mechanics methods. Martin Karplus, Micheal Levitt and Arie Warshel have been awarded the 2013 Nobel Prize in Chemistry for the seminal development of these methods.

During the three years of my PhD, I worked on the development of a new efficient hybrid QM/MM method, as well as its implementation in a quantum chemistry package [1, 2]. Part of my research project aimed at investigating spectroscopic properties and solvation effects on large systems (core ionisations, UV/Vis and IR spectra of chromophoric units) with the help of density-functional theory (DFT) and its time-dependent version (TD-DFT) [3, 4]. I have also made a series of more technical contributions, including:

- combination of orthogonalisation procedures [3];
- non-orthogonal molecular orbitals (biorthogonal basis sets) [2];
- variationally-optimised strictly localized orbitals [2];
- coupled-perturbated Hartree-Fock equations with non-variational orbitals;
- TD-DFT/MM coupling [4].

Towards the end of my PhD, I turned to new chemical situations (DNA damage, Ru@DNA complexes, reducible disulfide bonds) for which one has to ensure a proper treatment of electronic attachment [5–10].

After completing my PhD, I worked for four years as a postdoctoral fellow at the Research School of Chemistry (RSC) at the Australian National University (ANU) under the supervision of Prof. Peter Gill. During these years, I worked extensively on two-electron systems [11–21]. I also co-supervised one third-year undergraduate student (Yan Zhao) [22] and one exchange student from Switzerland (Julian Strauss). Some of this work is summarised in Chapter 2.

From 2013 to 2017, I was a DECRA recipient (roughly equivalent to a “ANR JJC”), which allowed me to concentrate on my research and steadily build my research group. During that time, I was the group leader of the Mathematical and Theoretical Chemistry group at the RSC. In 2014, I was awarded a Discovery Project (equivalent to a “Projet ANR”), and I was promoted to senior lecturer. Thanks to this Discovery Project grant, I hired a postdoctoral fellow (Dr Davids Agboola) on a one-year contract, followed by Dr Marat Sibaev on a two-year contract. In 2016, I was a full-time lecturer at the ANU and a visiting Erskine fellow at the University of Canterbury. I also organise with Deborah Crittenden (University of Canterbury, New Zealand) the *2nd Quantum and Computational Chemistry Student Conference* in Christchurch NZ.

During my time at the ANU, I supervised three Master students (Anneke Knol, Sam Backwell and Fergus Rogers). I also co-supervised two PhD students (Caleb Ball and Giuseppe Barca), who have both recently successfully completed their PhD. In addition, I also supervised a dozen of undergraduate students: Dominic Weiller, Amy Kendrick, Ee-Faye Chong, Stuart Ferrie, Matt Plowman, Nathaniel Bloomfield, Anneke Knol, Daniel Hills, Nilupuli Senadhira, Wenqi Zhang, Harrison Barnett and Fergus Rogers.

During these years, I made several contributions on the uniform electron gas (UEG) models. In particular, we introduced a new paradigm to study the UEG based on spherical geometry [23]. We showed that this new model is mathematically simple and well-suited to address some unsolved problems in the field. I also worked on more conventional UEG models, and we published three papers reporting the derivation of the closed-form expression of energy expansion coefficients [24–26]. Some of the work we performed during that time is summarised in Chapter 3. More recently, I have devoted part of my time to the construction of accurate trial wave functions incorporating explicit electronic correlation. Some of this work is discussed in Chapter 4.

Since February 2017, I have been a CNRS researcher at the *Laboratoire de Chimie et Physique Quantiques* at the Université Paul Sabatier in Toulouse. The research projects we are currently pursuing are summarised in Chapter 5.

Publications

1. Garniron, Y.; Scemama, A.; Loos, P. F.; Caffarel, M. Hybrid stochastic-deterministic calculation of the second-order perturbative contribution of multireference perturbation theory, *J. Chem. Phys.*, **2017**, *147*, 034101.
2. Barca, G. M. J.; Loos, P. F. Three-electron and four-electron integrals involving Gaussian geminals: fundamental integrals, upper bounds and recurrence relations, *J. Chem. Phys.*, **2017**, *147*, 024103.
3. Barca, G. M. J.; Loos, P. F. Recurrence relations for four-electron integrals over Gaussian basis functions, *Adv. Quantum Chem.*, **2017**, (in press).
4. Loos, P. F.; Rivail, J.-L.; Assfeld, X. Iterative stochastic subspace self-consistent field method, *J. Mod. Mol.*, **2017**, *23*, 173.
5. Loos, P. F. Exchange functionals based on finite uniform electron gases, *J. Chem. Phys.*, **2017**, *146*, 114108.
6. Rogers, F. J. M.; Loos, P. F. Excited-state Wigner crystals, *J. Chem. Phys.*, **2017**, *146*, 044114.
7. Ball, C. J.; Loos, P. F.; Gill, P. M. W. Electronic structure calculations in one dimension, *Phys. Chem. Chem. Phys.*, **2017**, *19*, 3987.
8. Rogers, F. J. M.; Ball, C. J.; Loos, P. F. Symmetry-broken local-density approximation for one-dimensional systems, *Phys. Rev. B*, **2016**, *93*, 235114.
9. Loos, P. F.; Gill, P. M. W. The uniform electron gas, *WIREs Comput. Mol. Sci.*, **2016**, *6*, 410.

10. Barca, G. M. J.; Loos, P. F.; Gill, P. M. W. Many-electron integrals over Gaussian basis functions. I. Recurrence relations for three-electron integrals, *J. Chem. Theory Comput.*, **2016**, *12*, 1735.
11. Tognetti, V; Loos, P. F. Natural occupation numbers in two-electron quantum rings, *J. Chem. Phys.*, **2016**, *144*, 054108.
12. Loos, P. F.; Bloomfield, N. J.; Gill, P. M. W. Three-electron coalescence points in two and three dimensions, *J. Chem. Phys.*, **2015**, *143*, 181101.
13. Agboola, D.; Knol, A. L.; Gill, P. M. W.; Loos, P. F. Uniform electron gases: III. Low-density gases on three-dimensional spheres, *J. Chem. Phys.*, **2015**, *143*, 084114.
14. Loos, P. F.; Bressanini, D. Nodal surfaces and interdimensional degeneracies, *J. Chem. Phys.*, **2015**, *142*, 214112.
15. Loos, P. F.; Ball, C. J.; Gill, P. M. W. Chemistry in one dimension, *Phys. Chem. Chem. Phys.*, **2015**, *17*, 3196.
16. Gill, P. M. W.; Loos, P. F.; Agboola, D. Basis functions for electronic structure calculations on spheres, *J. Chem. Phys.*, **2014**, *141*, 244102.
17. Loos, P. F. Generalized local-density approximation and one-dimensional uniform electron gases, *Phys. Rev. A*, **2014**, *89*, 052523.
18. Loos, P. F.; Ball, C. J.; Gill, P. M. W. Uniform electron gases. II. The generalized local density approximation in one dimension, *J. Chem. Phys.*, **2014**, *140*, 18A524.
19. Loos, P. F.; Gill, P. M. W. Exact wave functions for concentric two-electron systems, *Phys. Lett. A*, **2014**, *378*, 329.
20. Bernard, Y. A.; Loos, P. F.; Gill, P. M. W. Distribution of $r_{12} \cdot p_{12}$ in quantum systems, *Mol. Phys.*, **2013**, *111*, 2414.
21. Loos, P. F.; Gill, P. M. W. Uniform electron gases. II. Electrons on a ring, *J. Chem. Phys.*, **2013**, *138*, 164124.
22. Loos, P. F. High-density correlation energy expansion of the one-dimensional uniform electron gas, *J. Chem. Phys.*, **2013**, *138*, 064108.
23. Loos, P. F. Understanding excitons using spherical geometry, *Phys. Lett. A*, **2012**, *376*, 1997.
24. Loos, P. F.; Gill, P. M. W. Harmonically trapped jellium model, *Mol. Phys.*, **2012**, *108*, 083002.
25. Loos, P. F.; Gill, P. M. W. Exact wave functions of two-electron quantum rings, *Phys. Rev. Lett.*, **2012**, *110*, 2337.
26. Loos, P. F.; Gill, P. M. W. Leading-order behavior of the correlation energy in the uniform electron gas, *Int. J. Quantum Chem.*, **2012**, *112*, 1712.
27. Gill, P. M. W.; Loos, P. F. Uniform electron gases, *Theor. Chem. Acc.*, **2012**, *131*, 1069.
28. Loos, P. F.; Gill, P. M. W. Thinking outside the box: the uniform electron gas on a hypersphere, *J. Chem. Phys.*, **2011**, *135*, 214111.

29. Zhao, Y.; Loos, P. F.; Gill, P. M. W. Correlation energy of anisotropic quantum dots, *Phys. Rev. A*, **2011**, *84*, 032513.
30. Loos, P. F.; Gill, P. M. W. Correlation energy of the spin-polarized uniform electron gas at high density, *Phys. Rev. B*, **2011**, *84*, 033103.
31. Loos, P. F.; Gill, P. M. W. Exact energy of the spin-polarized two-dimensional electron gas at high density, *Phys. Rev. B*, **2011**, *83*, 233102.
32. Loos, P. F.; Gill, P. M. W. A tale of two electrons: correlation at high density, *Chem. Phys. Lett.*, **2010**, *500*, 1.
33. Loos, P. F.; Gill, P. M. W. Invariance of the correlation energy at high density and large dimension for two-electron systems, *Phys. Rev. Lett.*, **2010**, *105*, 113001.
34. Loos, P. F.; Gill, P. M. W. Excited states of spherium, *Mol. Phys.*, **2010**, *108*, 2527.
35. Loos, P. F.; Gill, P. M. W. Correlation energy of two electrons in a ball, *J. Chem. Phys.*, **2010**, *132*, 234111.
36. Loos, P. F.; Gill, P. M. W. Ground state of two electrons on concentric spheres, *Phys. Rev. A*, **2010**, *81*, 052510.
37. Ambrosek, D. Loos, P. F.; Assfeld, X.; Daniel, C. Electronic absorption spectroscopy of Ru(II) polypyridyl DNA intercalators: a theoretical study, *J. Inorg. Biochem.*, **2010**, *104*, 893.
38. Loos, P. F. Hooke's law correlation in two-electron systems, *Phys. Rev. A*, **2010**, *81*, 032510.
39. Dumont, E.; Loos, P. F.; Laurent, A.; Assfeld, X. Electronic effects and ring strain influences on the electron uptake by selenium-containing bonds, *Int. J. Quantum Chem.*, **2010**, *110*, 513.
40. Loos, P. F.; Gill, P. M. W. Correlation energy of two electrons in the high-density limit, *J. Chem. Phys.*, **2009**, *131*, 241101.
41. Loos, P. F.; Gill, P. M. W. Two electrons on a hypersphere: a quasi-exactly solvable model, *Phys. Rev. Lett.*, **2009**, *103*, 123008.
42. Loos, P. F.; Gill, P. M. W. Ground state of two electrons on a sphere, *Phys. Rev. A*, **2009**, *79*, 062517.
43. Loos, P. F.; Dumont, E.; Laurent, A.; Assfeld, X. Important effects of neighboring nucleotides on electron induced DNA single-strand breaks, *Chem. Phys. Lett.*, **2009**, *475*, 120.
44. Dumont, E.; Laurent, A.; Loos, P. F.; Assfeld, X. Analyzing the selectivity and successiveness of a two-electron capture on a multiply disulfide-linked protein, *J. Chem. Theor. Comput.*, **2009**, *5*, 1700.
45. Dumont, E.; Loos, P. F.; Assfeld, X. Factors governing electron capture by small disulfide loops in two-cysteines peptides, *J. Phys. Chem. B*, **2008**, *112*, 13661.
46. Dumont, E.; Loos, P. F.; Laurent, A.; Assfeld, X. Huge disulfide-linkage's reducible potential variation induced by α -helix orientation, *J. Chem. Theor. Comput.*, **2008**, *4*, 1171.

47. Dumont, E.; Loos, P. F.; Assfeld, X. Effect of ring strain on disulfide electron attachment, *Chem. Phys. Lett.*, **2008**, *458*, 276.
48. Loos, P. F.; Preat, J.; Laurent, A.; Michaux, C.; Jacquemin, D.; Perpète, E. A.; Assfeld, X. Theoretical investigation of the geometries and UV/Vis spectra of Poly(L-glutamic acid) featuring photochromic azobenzene side chain, *J. Chem. Theor. Comput.*, **2008**, *4*, 637.
49. Loos, P. F.; Assfeld, X. On the frontier bond location in the QM/MM description of the peptides and proteins, *AIP Conf. Proc.*, **2007**, *963*, 308.
50. Loos, P. F.; Fornili, A.; Sironi, M.; Assfeld, X. Removing the extra frontier parameters in QM/MM methods: a tentative with the Local Self-Consistent Field approach, *Comput. Lett.* **2007**, *4*, 473.
51. Loos, P. F.; Assfeld, X. Core-ionized and core-excited states of macromolecules, *Int. J. Quantum Chem.*, **2007**, *107*, 2343.
52. Preat, J.; Loos, P. F.; Assfeld, X.; Jacquemin, D.; Perpète, E. A. A TD-DFT investigation of UV spectra of pyranoïdic dyes: a NCM vs. PCM comparison, *J. Mol. Struct. (THEOCHEM)*, **2007**, *808*, 85.
53. Loos, P. F.; Assfeld, X. Self-Consistent Strictly Localized Orbitals, *J. Chem. Theor. Comput.*, **2007**, *3*, 1047.
54. Loos, P. F.; Assfeld, X.; Rivail, J.-L. Intramolecular interactions and cis peptidic bonds, *Theor. Chem. Acc.*, **2007**, *118*, 165.
55. Preat, J.; Loos, P. F.; Assfeld, X.; Jacquemin, D.; Perpète, E. A. DFT and TD-DFT investigation of IR and UV spectra of solvated molecules: comparison of two SCRf continuum models, *Int. J. Quantum Chem.*, **2007**, *107*, 574.
56. Rivail, J.-L.; Bouchy, A.; Loos, P. F., Electronic factors favouring the cis conformation in proline peptidic bonds, *J. Argentine Chem. Soc.*, **2006**, *94*, 19.
57. Fornili, A.; Loos, P. F.; Sironi, M.; Assfeld, X. Frozen core orbitals as an alternative to specific frontier bond potential in hybrid Quantum Mechanics/Molecular Mechanics methods, *Chem. Phys. Lett.*, **2006**, *427*, 236.
58. Moreau, Y.; Loos, P. F.; Assfeld, X. Solvent effects on the asymmetric Diels-Alder reaction between cyclopentadiene and (-)-menthyl acrylate revisited with the three-layer hybrid local self-consistent field/molecular mechanics/self-consistent reaction field method, *Theor. Chem. Acc.*, **2004**, *112*, 228.

Chapter 1

Methods

1.1 Schrödinger equation

In this memoir, we consider atomic and molecular quantum systems (i.e. systems composed by nuclei and electrons) within the Born-Oppenheimer approximation [27, 28]. This means that we neglect the kinetic energy of the nuclei and treat the nuclear coordinates as parameters. We therefore concentrate our attention on the electronic degrees of freedom. Unless otherwise stated, atomic units are used throughout this memoir.

A chemical system is completely defined at a time t by its electronic wave function $\Psi(\mathbf{X}, t)$, solution of the time-dependent Schrödinger equation

$$i \frac{\partial \Psi(\mathbf{X}, t)}{\partial t} = \hat{H} \Psi(\mathbf{X}, t), \quad (1.1)$$

where \hat{H} is the so-called Hamiltonian and $\mathbf{X} = (x_1, \dots, x_n) = (\mathbf{s}, \mathbf{R})$ is a composite coordinate vector gathering the spin coordinates $\mathbf{s} = (s_1, \dots, s_n)$ and spatial coordinates $\mathbf{R} = (\mathbf{r}_1, \dots, \mathbf{r}_n)$ of the n electrons.

In the case of a stationary system, the time-independent Schrödinger equation reads

$$\hat{H} \Psi(\mathbf{X}, t) = E \Psi(\mathbf{X}, t), \quad (1.2)$$

where E is the energy of the system and the non-relativistic Hamiltonian is explicitly given by

$$\begin{aligned} \hat{H} &= \hat{T}_e + \hat{V}_{\text{en}} + \hat{V}_{\text{ee}} + \hat{V}_{\text{nn}} \\ &= - \sum_i^n \frac{\nabla_i^2}{2} - \sum_i^n \sum_A^{\text{nuc}} \frac{Z_A}{|\mathbf{r}_A - \mathbf{r}_i|} + \sum_{i < j}^n \frac{1}{|\mathbf{r}_i - \mathbf{r}_j|} + \sum_{A < B}^{\text{nuc}} \frac{Z_A Z_B}{|\mathbf{r}_B - \mathbf{r}_A|}, \end{aligned} \quad (1.3)$$

where ∇_i^2 is the Laplace operator associated with the i th electron, \mathbf{r}_A and Z_A are the nuclear coordinates and charge of nucleus A . The first term \hat{T}_e is the kinetic energy operator of the electrons, the next term \hat{V}_{en} corresponds to the Coulombic attraction between electrons and nuclei, while the last two terms corresponds to the interelectronic (\hat{V}_{ee}) and internuclear (\hat{V}_{nn}) Coulombic repulsions, respectively. Note that the last term \hat{V}_{nn} is a constant as, within the Born-Oppenheimer approximation, it does not depend on the electronic coordinates, and will be omitted for the sake of clarity.

1.2 Hartree-Fock approximation

Within the Hartree-Fock (HF) approximation [27], the electronic wave function Ψ_{HF} is written as a Slater determinant of n spin orbitals

$$\Psi_{\text{HF}}(\mathbf{x}_1, \dots, \mathbf{x}_n) = \frac{1}{\sqrt{n!}} \begin{vmatrix} \psi_1(\mathbf{x}_1) & \psi_2(\mathbf{x}_1) & \dots & \psi_n(\mathbf{x}_1) \\ \psi_1(\mathbf{x}_2) & \psi_2(\mathbf{x}_2) & \dots & \psi_n(\mathbf{x}_2) \\ \vdots & \vdots & \ddots & \vdots \\ \psi_1(\mathbf{x}_n) & \psi_2(\mathbf{x}_n) & \dots & \psi_n(\mathbf{x}_n) \end{vmatrix}. \quad (1.4)$$

Each spin orbital $\psi_i(\mathbf{x})$ is a product of a spin part $\omega(s)$ and a spatial part $\phi_i(\mathbf{r})$ — also known as a molecular orbital (MO) —

$$\psi_i(\mathbf{x}) = \omega(s)\phi_i(\mathbf{r}), \quad (1.5)$$

where

$$\omega(s) = \begin{cases} \alpha(s), & \text{for spin-up electrons,} \\ \beta(s), & \text{for spin-down electrons.} \end{cases} \quad (1.6)$$

The spin orbitals form an orthonormal set, i.e.

$$\langle \psi_i | \psi_j \rangle = \delta_{ij}, \quad (1.7)$$

where

$$\delta_{ij} = \begin{cases} 1, & \text{if } i = j, \\ 0, & \text{otherwise,} \end{cases} \quad (1.8)$$

is the Kronecker delta [29].

The HF energy is defined as

$$E_{\text{HF}} = \langle \Psi_{\text{HF}} | \hat{H} | \Psi_{\text{HF}} \rangle, \quad (1.9)$$

and yields the following expression:

$$\begin{aligned} E_{\text{HF}} &= \sum_i^n \langle \psi_i(\mathbf{r}_1) | \hat{H}^c | \psi_i(\mathbf{r}_1) \rangle \\ &+ \sum_{i < j}^n \left[\langle \psi_i(\mathbf{r}_1)\psi_j(\mathbf{r}_2) | r_{12}^{-1} | \psi_i(\mathbf{r}_1)\psi_j(\mathbf{r}_2) \rangle - \langle \psi_i(\mathbf{r}_1)\psi_j(\mathbf{r}_2) | r_{12}^{-1} | \psi_j(\mathbf{r}_1)\psi_i(\mathbf{r}_2) \rangle \right], \end{aligned} \quad (1.10)$$

where the so-called core Hamiltonian (i.e. the one-electron part of the electronic Hamiltonian) is defined as

$$\hat{H}^c = \hat{T}_e + \hat{V}_{\text{en}}. \quad (1.11)$$

We define the Fock operator as

$$\hat{F}\psi_i(\mathbf{r}_1) = \varepsilon_i\psi_i(\mathbf{r}_1), \quad (1.12)$$

$$\hat{F}(\mathbf{r}_1) = \hat{H}^c(\mathbf{r}_1) + \sum_i^n [\hat{J}_i(\mathbf{r}_1) - \hat{K}_i(\mathbf{r}_1)], \quad (1.13)$$

where $\hat{J}_i(\mathbf{r}_1)$ and $\hat{K}_i(\mathbf{r}_1)$ are the Coulomb and exchange operators respectively:

$$\hat{J}_i(\mathbf{r}_1)\psi_j(\mathbf{r}_1) = \psi_j(\mathbf{r}_1) \int \psi_i(\mathbf{r}_2)r_{12}^{-1}\psi_i(\mathbf{r}_2)d\mathbf{r}_2, \quad (1.14a)$$

$$\hat{K}_i(\mathbf{r}_1)\psi_j(\mathbf{r}_1) = \psi_i(\mathbf{r}_1) \int \psi_j(\mathbf{r}_2)r_{12}^{-1}\psi_i(\mathbf{r}_2)d\mathbf{r}_2. \quad (1.14b)$$

In the following, we adopt the restricted HF (RHF) formalism which means that we assume that the spatial part of the spin orbital is independent of the spin state of the electron occupying this orbital [27]. Moreover, unless otherwise stated, the systems treated here are closed-shell systems, i.e. each MO is doubly occupied by one spin-up and one spin-down electron.

1.2.1 Roothaan-Hall equations

Within the LCAO approximation, we expand each MO as a linear combination of N atomic orbitals (AOs), such as

$$\phi_i(\mathbf{r}) = \sum_{\mu} c_{\mu i} \chi_{\mu}(\mathbf{r}). \quad (1.15)$$

In practice, the AOs $\chi_{\mu}(\mathbf{r})$ are usually chosen as cartesian Gaussian functions due to their computational convenience. However, other choices (such a Slater functions) are possible depending on the type of systems and the target accuracy. We will come back to this particular point later in this memoir.

In the AO basis, we have

$$F_{\mu\nu} = \langle \chi_{\mu} | \hat{F} | \chi_{\nu} \rangle \equiv \langle \mu | \hat{F} | \nu \rangle = H_{\mu\nu}^c + \sum_{\lambda\sigma} P_{\lambda\sigma} \left[\langle \mu\lambda | \nu\sigma \rangle - \frac{1}{2} \langle \mu\lambda | \sigma\nu \rangle \right], \quad (1.16)$$

with

$$H_{\mu\nu}^c = \langle \mu | \hat{H}^c | \nu \rangle, \quad (1.17)$$

$$\langle \mu\lambda | \nu\sigma \rangle = \iint \chi_{\mu}(\mathbf{r}_1)\chi_{\lambda}(\mathbf{r}_2)r_{12}^{-1}\chi_{\nu}(\mathbf{r}_1)\chi_{\sigma}(\mathbf{r}_2)d\mathbf{r}_1d\mathbf{r}_2, \quad (1.18)$$

and where the density matrix is defined as

$$P_{\mu\nu} = 2 \sum_i^{\text{occ}} c_{\mu i} c_{\nu i}. \quad (1.19)$$

The HF electronic energy of the system is then given by

$$E_{\text{HF}} = \sum_{\mu\nu} P_{\mu\nu} H_{\mu\nu}^c + \frac{1}{2} \sum_{\mu\nu\lambda\sigma} P_{\mu\nu} P_{\lambda\sigma} G_{\mu\nu\lambda\sigma}. \quad (1.20)$$

In matrix form, the Fock matrix F can be decomposed as

$$F = H^c + G, \quad (1.21)$$

where

$$G_{\mu\nu} = \sum_{\lambda\sigma} P_{\lambda\sigma} G_{\mu\nu\lambda\sigma}, \quad G_{\mu\nu\lambda\sigma} = \langle \mu\lambda | \nu\sigma \rangle - \frac{1}{2} \langle \mu\lambda | \sigma\nu \rangle. \quad (1.22)$$

The stationnarity of the energy with respect to the coefficients $c_{\mu i}$ yields the Roothaan-Hall equations:

$$\sum_{\nu} F_{\mu\nu} c_{\nu i} = \sum_{\nu} S_{\mu\nu} c_{\nu i} \varepsilon_i, \quad (1.23)$$

or in matrix form

$$FC = SC\varepsilon, \quad (1.24)$$

where the elements of the overlap matrix S are given by

$$S_{\mu\nu} = \langle \mu | \nu \rangle. \quad (1.25)$$

The coefficient matrix C gathers the MO coefficients $c_{\mu i}$, while the diagonal matrix ε gathers the MO energies ε_i . We introduce the orthogonalization matrix X such as

$$X^{\dagger}SX = I \quad (1.26)$$

in order to work in an orthogonal AO basis (where I is the identity matrix). There are two main orthogonalisation methods, namely the Löwdin orthogonalisation for which $X = S^{-1/2}$ and the canonical orthogonalisation for which $X = \mathbf{U}\mathbf{s}^{-1/2}$ (where \mathbf{U} and \mathbf{s} are the eigenvectors of eigenvalues matrices of S , respectively). Nowadays, the usual procedure consists in performing a singular value decomposition (SVD) of the overlap matrix S . This procedure is efficient, numerically stable and allows to remove the linear dependencies which might be present in the AO basis.

Rotating the Fock matrix F into the orthogonal basis yields

$$F' C' = C' \varepsilon, \quad (1.27)$$

where

$$F' = X^{\dagger}FX. \quad (1.28)$$

The matrices C' and ε can be determined by a straightforward diagonalisation of Eq. (1.27), and the matrix C is obtained by back-transforming the eigenvectors in the original basis:

$$C = XC'. \quad (1.29)$$

1.2.2 Self-consistent field calculation

In order to obtain the MO coefficients C , one must diagonalise the Fock matrix F . However, this matrix does depend on the MO coefficients itself. Therefore, one must employ an iterative procedure called self-consistent field (SCF) method. The SCF algorithm is described below:

1. Obtain an estimate of the density matrix P .
2. Build the Fock matrix: $F = H^c + G$.
3. Transform the Fock matrix in the orthogonal matrix: $F' = X^{\dagger}FX$.
4. Diagonalize F' to obtain C' and ε .
5. Back-transform the MOs in the original basis: $C = XC'$.
6. Compute the new density matrix $P = CC^{\dagger}$, as well as the HF energy:

$$E_{\text{HF}} = \frac{1}{2} \text{Tr}\{P(H^c + F)\}. \quad (1.30)$$

7. Convergence test. If not satisfied, go back to 2.

Unfortunately, the HF method cannot be used to obtain the exact energy of the system even in the complete basis set (CBS) limit due to the approximate treatment of the electron-electron interaction. Within the HF method, this interaction is averaged over all the electrons. In other words, a given electron “feels” the averaged repulsion of the $n - 1$ remaining electrons (mean-field approach). We will see in the next section how one can go beyond the HF approximation.

1.3 Post Hartree-Fock methods

The correlation energy E_c is defined as the error in the HF approximation, i.e. the energy difference between the exact energy and the energy calculated within the HF approximation:

$$E_c = E - E_{\text{HF}}. \quad (1.31)$$

Thanks to the variational principle, E_c is always a negative quantity. The purpose of post HF methods is to recover some or all of the correlation energy [30, 31].

1.3.1 Configuration interaction methods

One of the most conceptually simple (albeit expensive) approach to recover a large fraction of the correlation energy is the configuration interaction (CI) method. The general idea is to expand the wave function as a linear combination of “excited” determinants. These excited determinants are built by promoting electrons from occupied to unoccupied (virtual) MOs usually based on the HF orbitals, i.e.

$$\Psi_{\text{CI}} = c_0 \Psi_{\text{HF}} + \sum_i^{\text{occ}} \sum_a^{\text{virt}} c_i^a \Psi_i^a + \sum_{ij}^{\text{occ}} \sum_{ab}^{\text{virt}} c_{ij}^{ab} \Psi_{ij}^{ab} + \sum_{ijk}^{\text{occ}} \sum_{abc}^{\text{virt}} c_{ijk}^{abc} \Psi_{ijk}^{abc} + \dots, \quad (1.32)$$

where Ψ_i^a , Ψ_{ij}^{ab} and Ψ_{ijk}^{abc} are singly-, doubly- and triply-excited determinants. Ψ_{ij}^{ab} corresponds to the excitations of two electrons from the occupied spinorbitals i and j to virtual spinorbitals a and b . It is easy to show that the CI energy

$$E_{\text{CI}} = \langle \Psi_{\text{CI}} | \hat{H} | \Psi_{\text{CI}} \rangle \quad (1.33)$$

is an upper bound to the exact energy of the system.

When all possible excitations are taken into account, the method is called full CI (FCI) and it recovers the entire correlation energy for a given basis set. Albeit elegant, FCI is very expensive due to the exponential increase of the number of excited determinants. For example, when only singles and doubles are taken into account, the method is called CISD. It recovers an important chunk of the correlation. However, it has the disadvantage to be size-inconsistent.

A method is said to be size-consistent if the correlation energy of two non-interaction systems is equal to twice the correlation energy of the isolated system. Size-extensivity means that the correlation energy grows linearly with the system size.

1.3.2 Density-functional theory

Density-functional theory (DFT) is based on two theorems known as the Hohenberg-Kohn (HK) theorems [32], which states that it exists a non-interacting reference

system with an electronic density $\rho(\mathbf{r})$ equal to the real, interaction system. The first theorem proves the existence of a one-to-one mapping between the electron density and the external potential, while the second HK theorem guarantees the existence of a variational principle for the ground-state electron density.

1.3.3 Kohn-Sham equations

Present-day DFT calculations are almost exclusively done within the so-called Kohn-Sham (KS) formalism, which corresponds to an exact dressed one-electron theory [33]. In analogy to the HF theory, the electrons are treated as independent particles moving in the average field of all others but now with exchange and correlation included by virtue of an “exchange-correlation” functional.

Following the work of Kohn and Sham [33], we introduce KS orbitals $\psi_i(\mathbf{r})$, and the energy can be decomposed as

$$E_{\text{KS}}[\rho(\mathbf{r})] = T_s[\rho(\mathbf{r})] + E_{\text{ne}}[\rho(\mathbf{r})] + J[\rho(\mathbf{r})] + E_{\text{xc}}[\rho(\mathbf{r})], \quad (1.34)$$

where

$$T_s[\rho(\mathbf{r})] = -\frac{1}{2} \sum_i^{\text{occ}} \langle \psi_i | \nabla_i^2 | \psi_i \rangle \quad (1.35)$$

is the non-interacting kinetic energy,

$$E_{\text{ne}}[\rho(\mathbf{r})] = - \sum_A^{\text{nuc}} \int \frac{Z_A \rho(\mathbf{r})}{|\mathbf{r}_A - \mathbf{r}|} d\mathbf{r} \quad (1.36)$$

is the electron-nucleus attraction energy,

$$J[\rho(\mathbf{r})] = \frac{1}{2} \iint \frac{\rho(\mathbf{r}_1)\rho(\mathbf{r}_2)}{|\mathbf{r}_1 - \mathbf{r}_2|} d\mathbf{r}_1 d\mathbf{r}_2 \quad (1.37)$$

is the classical electronic repulsion, and the one-electron density is

$$\rho(\mathbf{r}) = \sum_i^{\text{occ}} |\psi_i(\mathbf{r})|^2. \quad (1.38)$$

The exchange-correlation energy

$$E_{\text{xc}}[\rho(\mathbf{r})] = \{T[\rho(\mathbf{r})] - T_s[\rho(\mathbf{r})]\} + \{E_{\text{ee}}[\rho(\mathbf{r})] - J[\rho(\mathbf{r})]\} \quad (1.39)$$

is the sum of two terms: one coming from the difference between the exact kinetic energy $T[\rho(\mathbf{r})]$ and the non-interacting kinetic energy $T_s[\rho(\mathbf{r})]$, and the other one coming from the difference between the exact interelectronic repulsion $E_{\text{ee}}[\rho(\mathbf{r})]$ and the classical Coulomb repulsion $J[\rho(\mathbf{r})]$. Here, we will only consider the second term as the “kinetic” correlation energy is usually much smaller than its “Coulomb” counterpart. Also, as it is usually done, we will split the exchange-correlation energy as a sum of an exchange and correlation components, i.e.

$$E_{\text{xc}}[\rho(\mathbf{r})] = E_x[\rho(\mathbf{r})] + E_c[\rho(\mathbf{r})]. \quad (1.40)$$

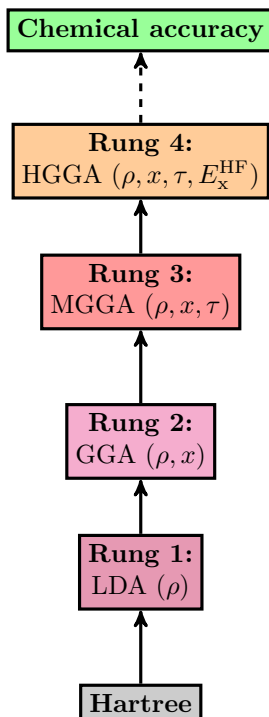


FIGURE 1.1: Jacob's ladder of DFT. ρ , x , τ and E_x^{HF} are the electron density, the reduced gradient, the kinetic energy density, and the HF exchange energy, respectively.

Similarly to the Roothaan-Hall equations, the condition of stationarity of the KS energy with respect to the electron density

$$\frac{\delta E[\rho(\mathbf{r})]}{\delta \rho(\mathbf{r})} = \mu \quad (1.41)$$

(where μ is the chemical potential) yields the KS equations

$$\left[-\frac{\nabla_r^2}{2} - \sum_A^{\text{nuc}} \frac{Z_A}{|\mathbf{r} - \mathbf{r}_A|} + \int \frac{\rho(\mathbf{r}')}{|\mathbf{r} - \mathbf{r}'|} d\mathbf{r}' + \frac{\delta E_{\text{xc}}[\rho(\mathbf{r})]}{\delta \rho(\mathbf{r})} \right] \psi_i(\mathbf{r}) = \varepsilon_i \psi_i(\mathbf{r}), \quad (1.42)$$

which can be re-written as

$$\hat{F}_{\text{KS}} \psi_i(\mathbf{r}) = \varepsilon_i \psi_i(\mathbf{r}). \quad (1.43)$$

These equations are solved iteratively, just like the HF equations, by expanding the KS MOs in a AO basis, yielding

$$F_{\text{KS}} C = S C \varepsilon. \quad (1.44)$$

1.3.4 Exchange-correlation functionals

Due to its moderate computational cost and its reasonable accuracy, KS DFT [32, 33] has become the workhorse of electronic structure calculations for atoms, molecules and solids [34]. To obtain accurate results within DFT, one only requires the exchange and correlation functionals, which can be classified in various families depending on their physical input quantities [35, 36]. These various types of functionals are classified by the Jacob's ladder of DFT [37, 38] (see Fig. 1.1).

- The local-density approximation (LDA) sits on the first rung of the Jacob's ladder and only uses as input the electron density ρ . The oldest and probably most famous LDA functional is the Dirac exchange functional (D30) [39] based on the uniform electron gas (UEG) [40]. Based on the work of Ceperley and Alder who used quantum Monte Carlo calculations (see below) to determine the correlation energy of the UEG with respect to the density [41], Vosko, Wilk and Nusair (VWN) proposed a LDA correlation functional by fitting their data [42].
- The generalized-gradient approximation (GGA) corresponds to the second rung and adds the gradient of the electron density $\nabla\rho$ as an extra ingredient. The well-known B88, G96, PW91 and PBE exchange functionals are examples of GGA exchange functionals [43–46]. Probably the most famous GGA correlation functional is LYP [47], which gave birth to the GGA exchange-correlation functional BLYP [48] by combination with B88.
- The third rung is composed by the so-called meta-GGA (MGGA) functionals [49] which uses, in addition to ρ and $\nabla\rho$, the kinetic energy density

$$\tau = \sum_i^{\text{occ}} |\nabla\psi_i|^2. \quad (1.45)$$

The M06-L functional from Zhao and Truhlar [50], the mBEEF functional from Wellendorff et al. [51] and the SCAN [52] and MS [53, 54] family of functionals from Sun et al. are examples of widely-used MGGA functionals.

- The fourth rung (hyper-GGAs or HGGAs) includes the widely-used hybrid functionals, introduced by Becke in 1993 [55], which add a certain percentage of HF exchange. Example of such functionals are B3LYP [55], B3PW91 [55–57], BH&HLYP [58] or PBE0 [59]. Hybrids functionals are known for their accuracy in electronic structure theory. However, they are more computationally expensive than LDA or GGA functionals due to the calculation of the costly HF exchange.
- The fifth rung includes double hybrids and RPA-like functionals but we will not be discussing such types of functionals in the present memoir.

1.4 Quantum Monte Carlo methods

1.4.1 Variational Monte Carlo

In the VMC method, the expectation value of the Hamiltonian with respect to a trial wave function is obtained using a stochastic integration technique. Within this approach a variational trial wave function $\Psi_T(\mathbf{R})$ is introduced, and one then calculates its variational energy

$$E_{\text{VMC}} = \frac{\int \Psi_T(\mathbf{R}) \hat{H} \Psi_T(\mathbf{R}) d\mathbf{R}}{\int \Psi_T(\mathbf{R})^2 d\mathbf{R}}, \quad (1.46)$$

using the Metropolis Monte Carlo method of integration [60]. The resulting VMC energy is an upper bound to the exact ground-state energy, within the statistical Monte Carlo error. Unfortunately, any resulting observables are biased by the form of the trial wave function, and the method is therefore only as good as the chosen Ψ_T .

1.4.2 Diffusion Monte Carlo

DMC is a stochastic projector technique for solving the many-body Schrödinger equation [61–63]. Its starting point is the time-dependent Schrödinger equation in imaginary time

$$-\frac{\partial \Psi(\mathbf{R}, \tau)}{\partial \tau} = (\hat{H} - S)\Psi(\mathbf{R}, \tau). \quad (1.47)$$

For $\tau \rightarrow \infty$, the steady-state solution of Eq. (1.47) for S close to the ground-state energy is the ground-state $\Psi(\mathbf{R})$ [64]. DMC generates configurations distributed according to the product of the trial and exact ground-state wave functions. If the trial wave function has the correct nodes, the DMC method yields the exact energy, within a statistical error that can be made arbitrarily small by increasing the number of Monte Carlo steps. Thus, as in VMC, a high quality trial wave function is essential in order to achieve high accuracy [65, 66].

1.4.3 Trial wave functions

Within QMC, trial wave functions are usually defined as [66–68]

$$\Psi_T(\mathbf{R}) = e^{J(\mathbf{R})} \sum_I c_I D_I^\uparrow(\mathbf{r}^\uparrow) D_I^\downarrow(\mathbf{r}^\downarrow), \quad (1.48)$$

where D_I^σ are determinants of the spin- σ electrons. The fermionic nature of the wave function is imposed by a single- or multi-determinant expansion of Slater determinants made of HF or KS MOs. $J(\mathbf{R})$ is called the Jastrow factor and $e^{J(\mathbf{R})}$ is a nodeless function. Hence, the nodes of Ψ_T are completely determined by the determinantal part of the trial wave function.

1.4.4 Fixed-node approximation

Considering an antisymmetric (real) electronic wave function $\Psi(\mathbf{R})$, the nodal hypersurface (or simply “nodes”) is a $(nD - 1)$ -dimensional manifold defined by the set of configuration points \mathbf{N} for which $\Psi(\mathbf{N}) = 0$. The nodes divide the configuration space into nodal cells or domains which are either positive or negative depending on the sign of the electronic wave function in each of these domains. In recent years, strong evidence has been gathered showing that, for the lowest state of any given symmetry, there is a single nodal hypersurface (up to all permutations) that divides configuration space into only two nodal domains (one positive and one negative) [69–79]. Except in some particular cases, electronic or more generally fermionic nodes are poorly understood due to their high dimensionality and complex topology [69, 73]. The number of systems for which the exact nodes are known analytically is very limited [72, 73, 80, 81].

The quality of fermion nodes is of prime importance in QMC calculations due to the fermion sign problem, which continues to preclude the application of in principle exact QMC methods to large systems. The dependence of the DMC energy on the quality of Ψ_T is often significant in practice, and is due to the fixed-node approximation which segregates the walkers in regions defined by Ψ_T [69]. The fixed-node error is only proportional to the square of the nodal displacement error, but it is uncontrolled and its accuracy difficult to assess [82–84].

The DMC method then finds the best energy for that chosen nodal surface, providing an upper bound for the ground-state energy. The exact ground-state energy is reached only if the nodal surface is exact. Therefore, one of greatest challenge of QMC methods

is to design a well-defined protocol to control the fixed-node error or, equivalently, to be able to build chemical meaningful nodal surfaces for any chemical system.

Chapter 2

Correlation in two-electron systems

By solving the Schrödinger equation, one can predict some of the chemistry and most of the physics of a given system. However, although this statement is true and philosophically important, it was realised many years ago that, for more than *one* electron, it is usually far too difficult from the mathematical point of view to solve this mighty equation. As Dirac pointed out,

“The aim of science is to make difficult things understandable in a simpler way.”

Consequently, it is essential to develop simple approximations that are accurate enough to have chemical and physical usefulness. To do this, quantum chemists and physicists have developed a variety of simple models that, despite their simplicity, contain the key physics of more complicated and realistic systems. A few examples are:

- the Born-Oppenheimer model: the motions of nuclei and electrons are independent;
- the orbital model: electrons occupy orbitals and move independently of one another;
- the local density model: the molecular electron density is built as an assembly of uniform electron gas densities.

Nowadays, all of these models are routinely applied in theoretical and/or computational studies. Spherical models are another example. One of the most popular starting points for modelling complex real life phenomenon by a highly simplified scientific model is the spherical geometry, and the most famous illustration of this is probably the so-called *spherical cow* (Fig. 2.1). While appearing completely nonsensical to most people outside the scientific area, these spherical models can be extremely powerful for understanding, explaining and even predicting physical and chemical phenomena in a wide range of disciplines of physics and chemistry. Besides, they offer unparalleled mathematical simplicity, while retaining much of the key physics.

An explicit example is the spherical model introduced by Haldane [85] to explain the fractional quantum Hall effect (FQHE), for which Laughlin, Störmer and Tsui received the Nobel prize in physics. This geometry has been instrumental in establishing the validity of the FQHE theory, and provides the cleanest proof for many properties. In this chapter, we will show that the spherical geometry can be also useful to better understand the structure of the exact electronic wave function.

Almost ten years ago, following this idea, we undertook a comprehensive study of two electrons on the surface of a sphere of radius R [11, 14, 18]. We used quantum chemistry electronic structure models ranging from HF to state-of-the-art explicitly correlated treatments, the last of which leads to near-exact wave functions and



FIGURE 2.1: A spherical cow.

energies. This helped us to understand not only the complicated relative motion of electrons, but also the errors inherent to each method. It eventually led to the important discovery that the system composed of two electrons restricted to the surface of a D -sphere (where D is the dimensionality of the surface of the sphere) is exactly solvable for a countable infinite set of values of R [17, 19, 20, 86]. In other words, it means that the *exact* solution of the Schrödinger equation can be obtained for certain “magic” values of the radius of the sphere [17]. This discovery propelled the two-electrons-on-a-sphere model (subsequently named spherium), into the exclusive family of exactly solvable two-electron models. Moreover, after an exhaustive study of the ground state of two electrons confined by various external potentials [12, 15], we noticed that the correlation energy is weakly dependent on the external potential, and we conjectured that the behaviour of the two-electron correlation energy, in the limit of large dimension, is *universal*! The rigorous proof of this conjecture has been published in Ref. [16]. In particular, we showed that the limiting correlation energy at high-density in helium and spherium are amazingly similar [13]. However, while the closed-form expression of the limiting correlation energy has never been found for helium, the value for spherium is quite simple to obtain. This shows the superiority of the spherical geometry approach and that it can be used in quantum chemistry to provide robust and trustworthy models for understanding, studying and explaining “real world” chemical systems.

In this chapter, we will summarise some of our key discoveries.

2.1 Quasi-exactly solvable models

Quantum mechanical models for which it is possible to solve explicitly for a finite portion of the energy spectrum are said to be quasi-exactly solvable [87]. They have ongoing value and are useful both for illuminating more complicated systems and for testing and developing theoretical approaches, such as DFT [32–34] and explicitly-correlated methods [88–91]. One of the most famous quasi-solvable model is the Hooke’s law atom which consists of a pair of electrons, repelling Coulombically but trapped in a harmonic external potential with force constant k . This system was first considered nearly 50 years ago by Kestner and Sinanoglu [92], solved analytically in 1989 for one particular k value [93], and later for a countably infinite set of k values [94].

A related system consists of two electrons trapped on the surface of a sphere of radius R . This has been used by Berry and collaborators [95–98] to understand both weakly and strongly correlated systems and to suggest an “alternating” version of Hund’s rule [99]. Seidl utilised this system to develop new correlation functionals [100, 101] within the adiabatic connection in DFT [102]. As mentioned earlier, we will use the term “spherium” to describe this two-electron system.

In Ref. [11], we examined various schemes and described a method for obtaining near-exact estimates of the 1S ground state energy of spherium for any given R . Because the corresponding HF energies are also known exactly, this is now one of the most complete theoretical models for understanding electron correlation effects.

In this section, we consider the D -dimensional generalisation of this system in which the two electrons are trapped on a D -sphere of radius R . We adopt the convention that a D -sphere is the surface of a $(D + 1)$ -dimensional ball. Here, we show that the Schrödinger equation for the 1S and the 3P states can be solved exactly for a countably infinite set of R values and that the resulting wave functions are polynomials in the interelectronic distance $r_{12} = |\mathbf{r}_1 - \mathbf{r}_2|$. Other spin and angular momentum states can be addressed in the same way using the ansatz derived by Breit [103] and we will discuss these excited states later in this section [19]. We have also published dedicated studies of the 1D system (that we dubbed ringium) [20, 104, 105]. The case of two concentric spheres has also been considered in two separate publications [14, 86], as well as the extension to excitonic wave functions [21]. Finally, the nodal structures of these systems has been investigated in collaboration with Dario Bressanini [81].

2.1.1 Singlet ground state

The electronic Hamiltonian is

$$\hat{H} = -\frac{\nabla_1^2}{2} - \frac{\nabla_2^2}{2} + \frac{1}{r_{12}}, \quad (2.1)$$

and because each electron moves on a D -sphere, it is natural to adopt hyperspherical coordinates [106].

For 1S states, it can be then shown [11] that the wave function $S(r_{12})$ satisfies the Schrödinger equation

$$\left[\frac{r_{12}^2}{4R^2} - 1 \right] \frac{d^2 S(r_{12})}{dr_{12}^2} + \left[\frac{(2D-1)r_{12}}{4R^2} - \frac{D-1}{r_{12}} \right] \frac{dS(r_{12})}{dr_{12}} + \frac{S(r_{12})}{r_{12}} = E S(r_{12}). \quad (2.2)$$

By introducing the dimensionless variable $x = r_{12}/2R$, this becomes a Heun equation [107] with singular points at $x = -1, 0, +1$. Based on our previous work [11] and the known solutions of the Heun equation [108], we seek wave functions of the form

$$S(r_{12}) = \sum_{k=0}^{\infty} s_k r_{12}^k, \quad (2.3)$$

and substitution into (2.2) yields the recurrence relation

$$s_{k+2} = \frac{s_{k+1} + \left[k(k+2D-2)\frac{1}{4R^2} - E \right] s_k}{(k+2)(k+D)}, \quad (2.4)$$

with the starting values

$$\{s_0, s_1\} = \begin{cases} \{0, 1\}, & D = 1, \\ \{1, 1/(D-1)\}, & D \geq 2. \end{cases} \quad (2.5)$$

TABLE 2.1: Radius R , energy E and wave function $S(r_{12})$ or $T(r_{12})$ of the first 1S and 3P polynomial solutions for two electrons on a D -sphere

State	D	$2R$	E	$S(r_{12})$ or $T(r_{12})$
1S	1	$\sqrt{6}$	$2/3$	$r_{12}(1 + r_{12}/2)$
	2	$\sqrt{3}$	1	$1 + r_{12}$
	3	$\sqrt{10}$	$1/2$	$1 + r_{12}/2$
	4	$\sqrt{21}$	$1/3$	$1 + r_{12}/3$
3P	1	$\sqrt{6}$	$1/2$	$1 + r_{12}/2$
	2	$\sqrt{15}$	$1/3$	$1 + r_{12}/3$
	3	$\sqrt{28}$	$1/4$	$1 + r_{12}/4$
	4	$\sqrt{45}$	$1/5$	$1 + r_{12}/5$

Thus, the Kato cusp conditions [109] are

$$S(0) = 0, \quad \frac{S''(0)}{S'(0)} = 1, \quad (2.6)$$

for electrons on a ring ($D = 1$), i.e. ringium, and

$$\frac{S'(0)}{S(0)} = \frac{1}{D-1}, \quad (2.7)$$

in higher dimensions. We note that the “normal” Kato value of $1/2$ arises for $D = 3$ — a system we called glomium as the name of a 3-sphere is a glome — suggesting that this may be the most appropriate model for atomic or molecular systems. We will return to this point below.

The wave function (2.3) reduces to the polynomial

$$S_{n,m}(r_{12}) = \sum_{k=0}^n s_k r_{12}^k, \quad (2.8)$$

(where m the number of roots between 0 and $2R$) if, and only if, $s_{n+1} = s_{n+2} = 0$. Thus, the energy $E_{n,m}$ is a root of the polynomial equation $s_{n+1} = 0$ (where $\deg s_{n+1} = \lfloor (n+1)/2 \rfloor$) and the corresponding radius $R_{n,m}$ is found from (2.4) which yields

$$R_{n,m}^2 E_{n,m} = \frac{n}{2} \left(\frac{n}{2} + D - 1 \right). \quad (2.9)$$

$S_{n,m}(r_{12})$ is the exact wave function of the m -th excited state of 1S symmetry for the radius $R_{n,m}$.

2.1.2 Triplet excited state

If we write the 3P state wave function as [103]

$$^3\Psi = (\cos \theta_1 - \cos \theta_2) T(r_{12}), \quad (2.10)$$

where θ_1 and θ_2 are the D -th hyperspherical angles of the two electrons [106], the symmetric part satisfies the Schrödinger equation

$$\left[\frac{r_{12}^2}{4R^2} - 1 \right] \frac{d^2 T(r_{12})}{dr_{12}^2} + \left[\frac{(2D+1)r_{12}}{4R^2} - \frac{D+1}{r_{12}} \right] \frac{dT(r_{12})}{dr_{12}} + \frac{T(r_{12})}{r_{12}} = E T(r_{12}), \quad (2.11)$$

and the antisymmetric part provides an additional kinetic energy contribution $D/(2R^2)$. Substituting the power series expansion

$$T(r_{12}) = \sum_{k=0}^{\infty} t_k r_{12}^k \quad (2.12)$$

into (2.11) yields the recurrence relation

$$t_{k+2} = \frac{t_{k+1} + [k(k+2D)\frac{1}{4R^2} - E]t_k}{(k+2)(k+D+2)}, \quad (2.13)$$

with the starting values

$$\{t_0, t_1\} = \{1, 1/(D+1)\}, \quad (2.14)$$

yielding the cusp condition

$$\frac{T'(0)}{T(0)} = \frac{1}{D+1}. \quad (2.15)$$

The wave function (2.12) reduces to the polynomial

$$T_{n,m}(r_{12}) = \sum_{k=0}^n t_k r_{12}^k, \quad (2.16)$$

when the energy $E_{n,m}$ is a root of $t_{n+1} = 0$ and the corresponding radius $R_{n,m}$ is found from (2.13) which yields

$$R_{n,m}^2 E_{n,m} = \frac{n}{2} \left(\frac{n}{2} + D \right). \quad (2.17)$$

$T_{n,m}(r_{12})$ is the exact wave function of the m -th excited state of 3P symmetry for the radius $R_{n,m}$.

It is illuminating to begin by examining the simplest 1S and 3P polynomial solutions. Except in the $D = 1$ case, the first 1S solution has

$$R_{1,0} = \sqrt{\frac{(2D-1)(2D-2)}{8}}, \quad E_{1,0} = \frac{1}{D-1}, \quad (2.18)$$

and the first 3P solution has

$$R_{1,0} = \sqrt{\frac{(2D+1)(2D+2)}{8}}, \quad E_{1,0} = \frac{1}{D+1}. \quad (2.19)$$

These are tabulated for $D = 1, 2, 3, 4$, together with the associated wave functions, in Table 2.1.

In the ringium ($D = 1$) case (*i.e.* two electrons on a ring), the first singlet and triplet solutions have $E_{2,0} = 2/3$ and $E_{1,0} = 1/2$, respectively, for the same value of the radius ($\sqrt{6}/2 \approx 1.2247$). The corresponding wave functions are related by $S_{2,0} = r_{12} T_{1,0}$. Unlike $T_{1,0}$, the singlet wavefunction $S_{2,0}$ vanishes at $r_{12} = 0$, and exhibits a second-order cusp condition, as shown in (2.6).

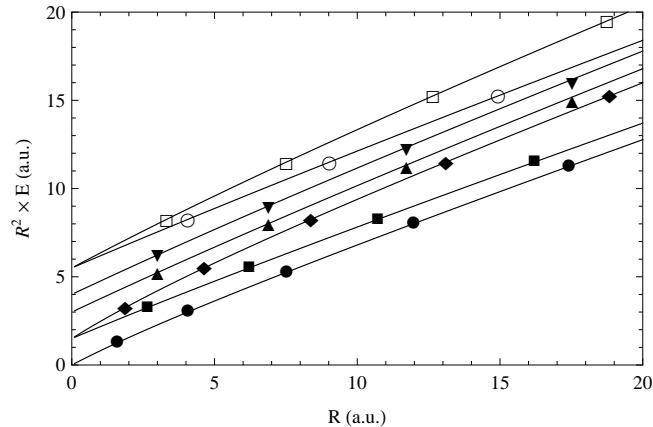


FIGURE 2.2: Energy of the S , P and D states of glomium (${}^1S^e < {}^3P^o \leq {}^1P^o < {}^3P^e < {}^3D^e < {}^1D^o \leq {}^3D^o$). The quasi-exact solutions are shown by the markers.

For spherium ($D = 2$ case), we know from our previous work [11] that the HF energy of the lowest 1S state is $E_{\text{HF}} = 1/R$. It follows that the exact correlation energy for $R = \sqrt{3}/2$ is $E_c = 1 - 2/\sqrt{3} \approx -0.1547$ which is much larger than the limiting correlation energies of the helium-like ions (-0.0467) [110] or Hooke's law atoms (-0.0497) [111]. This confirms our view that electron correlation on the surface of a sphere is qualitatively different from that in three-dimensional physical space.

For glomium ($D = 3$ case), in contrast, possesses the same singlet and triplet cusp conditions — Eqs. (2.7) and (2.15) — as those for electrons moving in three-dimensional physical space. Indeed, the wave functions in Table 2.1

$$S_{1,0}(r_{12}) = 1 + r_{12}/2, \quad (R = \sqrt{5/2}), \quad (2.20)$$

$$T_{1,0}(r_{12}) = 1 + r_{12}/4, \quad (R = \sqrt{7}), \quad (2.21)$$

have precisely the form of the ansatz used in Kutzelnigg's increasingly popular R12 methods [88, 89]. Moreover, it can be shown [12] that, as $R \rightarrow 0$, the correlation energy E_c approaches -0.0476 , which nestles nicely between the corresponding values for the helium-like ions (-0.0467) [110] and the Hooke's law atom (-0.0497) [111]. Again, this suggests that the $D = 3$ model ("electrons on a glome") bears more similarity to common physical systems than the $D = 2$ model ("electrons on a sphere"). We will investigate this observation further in the next section.

2.1.3 Other electronic states

As shown in Ref. [19], one can determine exact wave functions for other electronic states, but not all of them. These states are inter-connected by subtle interdimensional degeneracies (see Table 2.2) using the transformation $(D, L) \rightarrow (D + 2, L - 1)$, where L is the total angular momentum of the state. We refer the interested readers to Refs. [19, 81, 112–114] for more details.

The energies of the S , P and D states ($m = 0$) for glomium are plotted in Fig. 2.2 (the quasi-exact solutions are indicated by markers), while density plots of spherium ($n = 1$ and $m = 0$) are represented on Fig. 2.3.

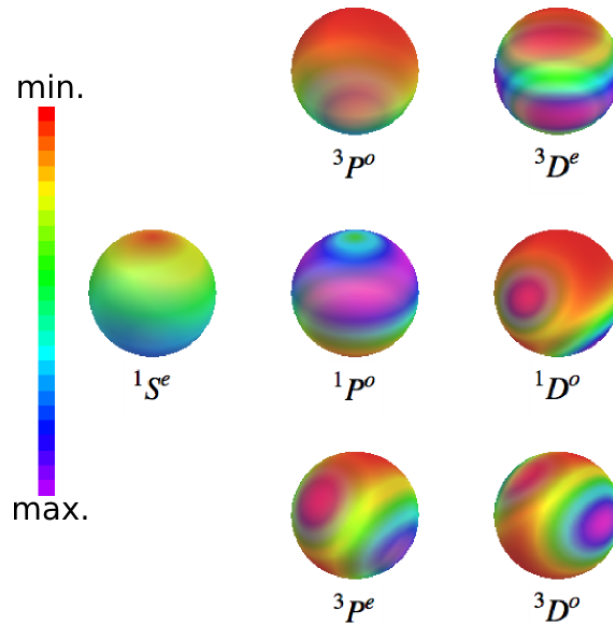


FIGURE 2.3: Density plots of the S , P and D states of spherium. The squares of the wave functions when one electron is fixed at the north pole are represented. The radii are $\sqrt{3}/2$, $\sqrt{15}/2$, $\sqrt{5}/2$, $\sqrt{21}/2$, $\sqrt{21}/2$, $3\sqrt{5}/2$ and $3\sqrt{3}/2$ for the $1S^e$, $3P^o$, $1P^o$, $3P^e$, $3D^e$, $1D^o$ and $3D^o$ states, respectively.

2.1.4 Natural/unnatural parity

In attempting to explain Hund's rules [115] and the "alternating" rule [116, 117] (see also Refs. [99, 118]), Morgan and Kutzelnigg [119–121] have proposed that the two-electron atomic states be classified as:

A two-electron state, composed of one-electron spatial orbitals with individual parities $(-1)^{\ell_1}$ and $(-1)^{\ell_2}$ and hence with overall parities $(-1)^{\ell_1+\ell_2}$, is said to have natural parity if its parity is $(-1)^L$. [...] If the parity of the two-electron state is $-(-1)^L$, the state is said to be of unnatural parity.

After introducing spin, three classes emerge. In a three-dimensional space, the states with a cusp value of $1/2$ are known as the *natural parity singlet states* [109, 122], those with a cusp value of $1/4$ are the *natural and unnatural parity triplet states* [123], and those with a cusp value of $1/6$, are the *unnatural parity singlet states* [119].

Most of the higher angular momentum states of glomium, possess the "normal" cusp values of $1/2$ and $1/4$. However, the unnatural $1D^o$ and $1F^e$ states have the cusp value of $1/6$.

2.1.5 First-order cusp condition

The wave function, radius and energy of the lowest states are given by

$$\Psi_{1,0}(r_{12}) = 1 + \gamma r_{12}, \quad R_{1,0}^2 = \frac{\delta}{4\gamma}, \quad E_{1,0} = \gamma, \quad (2.22)$$

TABLE 2.2: Ground state and excited states of two electrons on a D -sphere

State	Configuration	δ	γ^{-1}	Λ	κ	Degeneracy
$^1S^e$	s^2	$2D - 1$	$D - 1$	0	0	$^3P^e$
$^3P^o$	sp	$2D + 1$	$D + 1$	$D/2$	1	$^1D^o$
$^1P^o$	sp	$2D + 1$	$D - 1$	$D/2$	0	$^3D^o$
$^3P^e$	p^2	$2D + 3$	$D + 1$	D	1	
$^3D^e$	sd	$2D + 3$	$D + 1$	$D + 1$	1	$^1F^e$
$^1D^o$	pd	$2D + 5$	$D + 3$	$3D/2 + 1$	2	
$^3D^o$	pd	$2D + 5$	$D + 1$	$3D/2 + 1$	1	
$^1F^e$	pf	$2D + 7$	$D + 3$	$2D + 3$	2	

which are closely related to the Kato cusp condition [109]

$$\frac{\Psi'(0)}{\Psi(0)} = \gamma. \quad (2.23)$$

We now generalise the Morgan-Kutzelnigg classification [120] to a D -dimensional space. Writing the interparticle wave function as

$$\Psi(r_{12}) = 1 + \frac{r_{12}}{2\kappa + D - 1} + O(r_{12}^2), \quad (2.24)$$

we have

$$\begin{aligned} \kappa &= 0, \text{ for natural parity singlet states,} \\ \kappa &= 1, \text{ for triplet states,} \\ \kappa &= 2, \text{ for unnatural parity singlet states.} \end{aligned} \quad (2.25)$$

The labels for states of two electrons on a D -sphere are given in Table 2.2.

2.1.6 Second-order cusp condition

The second solution is associated with

$$\Psi_{2,0}(r_{12}) = \Psi_{1,0}(r_{12}) + \frac{\gamma^2(\delta + 2)}{2\gamma(\delta + 2) + 4\delta + 6} r_{12}^2, \quad (2.26)$$

$$R_{2,0}^2 = \frac{(\gamma + 2)(\delta + 2) - 1}{2\gamma}, \quad (2.27)$$

$$E_{2,0} = \frac{\gamma(\delta + 1)}{(\gamma + 2)(\delta + 2) - 1}. \quad (2.28)$$

For two electrons on a D -sphere, the second-order cusp condition is

$$\frac{\Psi''(0)}{\Psi(0)} = \frac{1}{2D} \left(\frac{1}{D - 1} - E \right). \quad (2.29)$$

Following (2.29), the classification (2.25) can be extended to the second-order coalescence condition, where the wave function (correct up to second-order in u) is

$$\Psi(r_{12}) = 1 + \frac{r_{12}}{2\kappa + D - 1} + \frac{r_{12}^2}{2(2\kappa + D)} \left(\frac{1}{2\kappa + D - 1} - E \right) + O(r_{12}^3). \quad (2.30)$$

Thus, we have, for $D = 3$,

$$\frac{\Psi''(0)}{\Psi(0)} = \begin{cases} \frac{1}{6}(\frac{1}{2} - E), & \text{for } \kappa = 0, \\ \frac{1}{10}(\frac{1}{4} - E), & \text{for } \kappa = 1, \\ \frac{1}{14}(\frac{1}{6} - E), & \text{for } \kappa = 2. \end{cases} \quad (2.31)$$

For the natural parity singlet states ($\kappa = 0$), the second-order cusp condition of glomium is precisely the second-order coalescence condition derived by Tew [124], reiterating that glomium is an appropriate model for normal physical systems.

2.2 Universality of correlation effects

Understanding and calculating the electronic correlation energy is one of the most important and difficult problems in theoretical chemistry. In this pursuit, the study of high-density correlation energy using perturbation theory has been particularly profitable, shedding light on the physically relevant density regime and providing *exact* results for key systems, such as the uniform electron gas [125] and two-electron systems [126]. The former is the cornerstone of the most popular density functional paradigm (the local-density approximation) in solid-state physics [34]; the latter provide important test cases in the development of new explicitly-correlated methods [88, 127] for electronic structure calculations [28].

2.2.1 High-density correlation energy

The high-density correlation energy of the helium-like ions is obtained by expanding both the exact [128] and HF [129] energies as series in $1/Z$, yielding

$$E(Z, D, V) = E^{(0)}(D, V)Z^2 + E^{(1)}(D, V)Z + E^{(2)}(D, V) + \frac{E^{(3)}(D, V)}{Z} + \dots, \quad (2.32a)$$

$$E_{\text{HF}}(Z, D, V) = E^{(0)}(D, V)Z^2 + E^{(1)}(D, V)Z + E_{\text{HF}}^{(2)}(D, V) + \frac{E_{\text{HF}}^{(3)}(D, V)}{Z} + \dots, \quad (2.32b)$$

where Z is the nuclear charge, D is the dimension of the space and V is the external Coulomb potential. Equations (2.32a) and (2.32b) share the same zeroth- and first-order energies because the exact and the HF treatment have the same zeroth-order Hamiltonian. Thus, in the high-density (large- Z) limit, the correlation energy is

$$\begin{aligned} E_c^{(2)}(D, V) &= \lim_{Z \rightarrow \infty} E_c(Z, D, V) \\ &= \lim_{Z \rightarrow \infty} [E(Z, D, V) - E_{\text{HF}}(Z, D, V)] \\ &= E^{(2)}(D, V) - E_{\text{HF}}^{(2)}(D, V). \end{aligned} \quad (2.33)$$

Despite intensive study [110, 130], the coefficient $E^{(2)}(D, V)$ has not yet been reported in closed form. However, the accurate numerical estimate

$$E^{(2)} = -0.157\ 666\ 429\ 469\ 14 \quad (2.34)$$

has been determined for the important $D = 3$ case [110]. Combining (2.34) with the exact result [129]

$$E_{\text{HF}}^{(2)} = \frac{9}{32} \ln \frac{3}{4} - \frac{13}{432} \quad (2.35)$$

yields a value of

$$E_c^{(2)} = -0.046\,663\,253\,999\,48 \quad (2.36)$$

for the helium-like ions in a three-dimensional space.

In the large- D limit, the quantum world reduces to a simpler semi-classical one [131] and problems that defy solution in $D = 3$ sometimes become exactly solvable. In favorable cases, such solutions provide useful insight into the $D = 3$ case and this strategy has been successfully applied in many fields of physics [132, 133]. Indeed, just as one learns something about interacting systems by studying non-interacting ones and introducing the interaction perturbatively, one learns something about $D = 3$ by studying the large- D case and introducing dimension-reduction perturbatively.

Singularity analysis [134] reveals that the energies of two-electron atoms possess first- and second-order poles at $D = 1$, and that the Kato cusp [109, 120] is directly responsible for the second-order pole. In our previous work [12, 15], we have expanded the correlation energy as a series in $1/(D - 1)$ but, although this is formally correct if summed to infinite order, such expansions falsely imply higher-order poles at $D = 1$. For this reason, we now follow Herschbach and Goodson [135, 136], and expand both the exact and HF energies as series in $1/D$. Although various possibilities exist for this dimensional expansion [134, 137–139], it is convenient to write

$$E^{(2)}(D, V) = \frac{E^{(2,0)}(V)}{D^2} + \frac{E^{(2,1)}(V)}{D^3} + \dots, \quad (2.37a)$$

$$E_{\text{HF}}^{(2)}(D, V) = \frac{E_{\text{HF}}^{(2,0)}(V)}{D^2} + \frac{E_{\text{HF}}^{(2,1)}(V)}{D^3} + \dots, \quad (2.37b)$$

$$E_c^{(2)}(D, V) = \frac{E_c^{(2,0)}(V)}{D^2} + \frac{E_c^{(2,1)}(V)}{D^3} + \dots, \quad (2.37c)$$

where

$$E_c^{(2,0)}(V) = E^{(2,0)}(V) - E_{\text{HF}}^{(2,0)}(V), \quad (2.38a)$$

$$E_c^{(2,1)}(V) = E^{(2,1)}(V) - E_{\text{HF}}^{(2,1)}(V). \quad (2.38b)$$

Such double expansions of the correlation energy were originally introduced for the helium-like ions, and have led to accurate estimations of correlation [140, 141] and atomic energies [142, 143] *via* interpolation and renormalisation techniques. Equations (2.37a), (2.37b) and (2.37c) apply equally to the 1S ground state of any two-electron system confined by a spherical potential $V(r)$.

2.2.2 The conjecture

For the helium-like ions, it is known [135, 136, 144] that

$$E_c^{(2,0)}(V) = -\frac{1}{8}, \quad E_c^{(2,1)}(V) = -\frac{163}{384}, \quad (2.39)$$

and we have recently found [12] that $E_c^{(2,0)}(V)$ takes the same value in hookium (two electrons in a parabolic well [92–94, 145]), spherium (two electrons on a sphere [11, 17, 95, 102]) and ballium (two electrons in a ball [15, 146, 147]). In contrast, we found

TABLE 2.3: $E^{(2,0)}$, $E_{\text{HF}}^{(2,0)}$, $E_c^{(2,0)}$ and $E_c^{(2,1)}$ coefficients for various systems and $v(r) = 1$.

System	m	$-E^{(2,0)}$	$-E_{\text{HF}}^{(2,0)}$	$-E_c^{(2,0)}$	$-E_c^{(2,1)}$
Helium	-1	5/8	1/2	1/8	0.424479
Airium	1	7/24	1/6	1/8	0.412767
Hookium	2	1/4	1/8	1/8	0.433594
Quartium	4	5/24	1/12	1/8	0.465028
Sextium	6	3/16	1/16	1/8	0.486771
Ballium	∞	1/8	0	1/8	0.664063

that $E_c^{(2,1)}(V)$ is V -dependent. The fact that the term $E_c^{(2,0)}$ is invariant, while $E_c^{(2,1)}$ varies with the confinement potential allowed us to explain why the high-density correlation energy of the previous two-electron systems are similar, but not identical, for $D = 3$ [12, 15]. On this basis, we conjectured [12] that

$$E_c^{(2)}(D, V) \sim -\frac{1}{8D^2} - \frac{C(V)}{D^3} \quad (2.40)$$

holds for *any* spherical confining potential, where the coefficient $C(V)$ varies slowly with $V(r)$.

2.2.3 The proof

Here, we will summarise our proof of the conjecture (2.40). More details can be found in Ref. [16]. We prove that $E_c^{(2,0)}$ is universal, and that, for large D , the high-density correlation energy of the 1S ground state of two electrons is given by (2.40) for any confining potential of the form

$$V(r) = \text{sgn}(m)r^m v(r), \quad (2.41)$$

where $v(r)$ possesses a Maclaurin series expansion

$$v(r) = v_0 + v_1 r + v_2 \frac{r^2}{2} + \dots \quad (2.42)$$

After transforming both the dependent and independent variables [16], the Schrödinger equation can be brought to the simple form

$$\left(\frac{1}{\Lambda} \hat{\mathcal{T}} + \hat{\mathcal{U}} + \hat{\mathcal{V}} + \frac{1}{Z} \hat{\mathcal{W}} \right) \Phi_D = \mathcal{E}_D \Phi_D, \quad (2.43)$$

in which, for S states, the kinetic, centrifugal, external potential and Coulomb operators are, respectively,

$$-2\hat{T} = \left(\frac{\partial^2}{\partial r_1^2} + \frac{\partial^2}{\partial r_2^2} \right) + \left(\frac{1}{r_1^2} + \frac{1}{r_2^2} \right) \left(\frac{\partial^2}{\partial \theta^2} + \frac{1}{4} \right), \quad (2.44)$$

$$\hat{U} = \frac{1}{2 \sin^2 \theta} \left(\frac{1}{r_1^2} + \frac{1}{r_2^2} \right), \quad (2.45)$$

$$\hat{V} = V(r_1) + V(r_2), \quad (2.46)$$

$$\hat{W} = \frac{1}{\sqrt{r_1^2 + r_2^2 - 2r_1 r_2 \cos \theta}}, \quad (2.47)$$

and the dimensional perturbation parameter is

$$\Lambda = \frac{(D-2)(D-4)}{4}. \quad (2.48)$$

In this form, double perturbation theory can be used to expand the energy in terms of both $1/Z$ and $1/\Lambda$.

For $D = \infty$, the kinetic term vanishes and the electrons settle into a fixed (“Lewis”) structure [135] that minimises the effective potential

$$\hat{X} = \hat{U} + \hat{V} + \frac{1}{Z}\hat{W}. \quad (2.49)$$

The minimization conditions are

$$\frac{\partial \hat{X}(r_1, r_2, \theta)}{\partial r_1} = \frac{\partial \hat{X}(r_1, r_2, \theta)}{\partial r_2} = 0, \quad (2.50)$$

$$\frac{\partial \hat{X}(r_1, r_2, \theta)}{\partial \theta} = 0, \quad (2.51)$$

and the stability condition implies $m > -2$. Assuming that the two electrons are equivalent, the resulting exact energy is

$$\mathcal{E}_\infty = \hat{X}(r_\infty, r_\infty, \theta_\infty). \quad (2.52)$$

It is easy to show that

$$r_\infty = \alpha + \frac{\alpha^2}{m+2} \left(\frac{1}{2\sqrt{2}} - \Lambda \frac{m+1}{m} \frac{v_1}{v_0} \right) \frac{1}{Z} + \dots, \quad (2.53)$$

$$\cos \theta_\infty = -\frac{\alpha}{4\sqrt{2}} \frac{1}{Z} + \dots, \quad (2.54)$$

where $\alpha^{-(m+2)} = \text{sgn}(m)mv_0$.

For the HF treatment, we have $\theta_\infty^{\text{HF}} = \pi/2$. Indeed, the HF wave function itself is independent of θ , and the only θ dependence comes from the D -dimensional Jacobian, which becomes a Dirac delta function centred at $\pi/2$ as $D \rightarrow \infty$. Solving (2.50), one finds that r_∞^{HF} and r_∞ are equal to second-order in $1/Z$. Thus, in the large- D limit, the HF energy is

$$\mathcal{E}_\infty^{\text{HF}} = \hat{X}\left(r_\infty^{\text{HF}}, r_\infty^{\text{HF}}, \frac{\pi}{2}\right), \quad (2.55)$$

and correlation effects originate entirely from the fact that θ_∞ is slightly greater than $\pi/2$ for finite Z .

Expanding (2.52) and (2.55) in terms of Z and D yields

$$E^{(2,0)}(V) = -\frac{1}{8} - \frac{1}{2(m+2)}, \quad (2.56)$$

$$E_{\text{HF}}^{(2,0)}(V) = -\frac{1}{2(m+2)}, \quad (2.57)$$

thus showing that both $E^{(2,0)}$ and $E_{\text{HF}}^{(2,0)}$ depend on the leading power m of the external potential but not on $v(r)$.

Subtracting these energies yields

$$E_c^{(2,0)}(V) = -\frac{1}{8}, \quad (2.58)$$

and this completes the proof that, in the high-density limit, the leading coefficient $E_c^{(2,0)}$ of the large- D expansion of the correlation energy is universal, *i.e.* it does not depend on the external potential $V(r)$.

The result (2.58) is related to the cusp condition [109, 120, 148]

$$\left. \frac{\partial \Psi_D}{\partial r_{12}} \right|_{r_{12}=0} = \frac{1}{D-1} \Psi_D(r_{12}=0), \quad (2.59)$$

which arises from the cancellation of the Coulomb operator singularity by the D -dependent angular part of the kinetic operator [28].

The $E^{(2,1)}$ and $E_{\text{HF}}^{(2,1)}$ coefficients can be found by considering the Langmuir vibrations of the electrons around their equilibrium positions [135, 136]. The general expressions depend on v_0 and v_1 , but are not reported here. However, for $v(r) = 1$, which includes many of the most common external potentials, we find

$$E_c^{(2,1)}(V) = -\frac{85}{128} - \frac{9/32}{(m+2)^{3/2}} + \frac{1/2}{(m+2)^{1/2}} + \frac{1/16}{(m+2)^{1/2} + 2}, \quad (2.60)$$

showing that $E_c^{(2,1)}$, unlike $E_c^{(2,0)}$, is potential-dependent. Numerical values of $E_c^{(2,1)}$ are reported in Table 2.3 for various systems.

2.3 Summary

In the first section of this chapter, we have reported exact solutions of a Coulomb correlation problem, consisting of two electrons on a D -dimensional sphere. The Coulomb problem can be solved exactly for an infinite set of values of the radius R for both the ground and excited states, on both the singlet and triplet manifolds. The corresponding exact solutions are polynomials in the interelectronic distance r_{12} . The cusp conditions, which are related to the behaviour of the wave function at the electron-electron coalescence point, have been analysed and classified according to the natural or unnatural parity of the state considered.

In the second section, we proved that the leading term in the large- D expansion of the high-density correlation energy of an electron pair is invariant to the nature of the confining potential. For any such system, the correlation energy is given by $E_c \sim -\gamma^2/8$, where $\gamma = 1/(D-1)$ is the Kato cusp factor in a D -dimensional space.

Chapter 3

DFT using finite uniform electron gases

The final decades of the twentieth century witnessed a major revolution in solid-state and molecular physics, as the introduction of sophisticated exchange-correlation models [34] propelled DFT from qualitative to quantitative usefulness. The apotheosis of this development was probably the award of the 1998 Nobel Prize for Chemistry to Walter Kohn and John Pople but its origins can be traced to the prescient efforts by Thomas [149], Fermi [150] and Dirac [39], more than 70 years earlier, to understand the behaviour of ensembles of electrons without explicitly constructing their full wave functions. These days, DFT so dominates the popular perception of molecular orbital calculations that many non-specialists now regard the two as synonymous.

In principle, the cornerstone of modern DFT is the HK theorem [32] but, in practice, it rests largely on the presumed similarity between the electronic behaviour in a real system and that in the hypothetical “infinite” uniform electron gas (IUEG) or jellium [24, 25, 39, 40, 125, 149–160]. In 1965, Kohn and Sham [33] showed that the knowledge of an analytical parametrisation of the IUEG correlation energy allows one to perform approximate calculations for atoms, molecules and solids. The idea — the local-density approximation (LDA) — is attractively simple: if we know the properties of jellium, we can understand the electron cloud in a molecule by dividing it into tiny chunks of density and treating each as a piece of jellium.

The good news is that the properties of jellium are known from DMC calculations [41, 82, 161–169]. Such calculations are possible because jellium is characterised by just a *single* parameter ρ , the electron density.

This spurred the development of a wide variety of spin-density correlation functionals (VWN [42], PZ [170], PW92 [56], etc), each of which requires information on the high- and low-density regimes of the spin-polarised IUEG, and are parametrised using numerical results from QMC calculations [41, 171], together with analytic perturbative results.

The bad news is that jellium has an infinite number of electrons in an infinite volume and this unboundedness renders it, in some respects, a poor model for the electrons in molecules. Indeed, the simple LDA described above predicts bond energies that are much too large and this led many chemists in the 70’s to dismiss DFT as a quantitatively worthless theory.

Most of the progress since these days has resulted from concocting ingenious corrections for jellium’s deficiencies (GGAs, MGGAs, HGGAs, etc).

However, notwithstanding the impressive progress since the 70’s, modern DFT approximations still exhibit fundamental deficiencies in large systems [172], conjugated molecules [173], charge-transfer excited states [174], dispersion-stabilised systems [175], systems with fractional spin or charge [176], isodesmic reactions [177], and elsewhere. Because DFT is in principle an exact theory, many of these problems

TABLE 3.1: The lowest free-particle orbitals on a 2-sphere

Name	l	m	$\sqrt{4\pi} Y_{lm}(\theta, \phi)$
s	0	0	1
p_0	1	0	$3^{1/2} \cos \theta$
p_{+1}	1	+1	$(3/2)^{1/2} \sin \theta \exp(+i\phi)$
p_{-1}	1	-1	$(3/2)^{1/2} \sin \theta \exp(-i\phi)$
d_0	2	0	$(5/4)^{1/2} (3 \cos^2 \theta - 1)$
d_{+1}	2	+1	$(15/2)^{1/2} \sin \theta \cos \theta \exp(+i\phi)$
d_{-1}	2	-1	$(15/2)^{1/2} \sin \theta \cos \theta \exp(-i\phi)$
d_{+2}	2	+2	$(15/8)^{1/2} \sin^2 \theta \exp(+2i\phi)$
d_{-2}	2	-2	$(15/8)^{1/2} \sin^2 \theta \exp(-2i\phi)$

TABLE 3.2: Number of electrons in L -spherium and L -glomium atoms

L	0	1	2	3	4	5	6	7
L -spherium	2	8	18	32	50	72	98	128
L -glomium	2	10	28	60	110	182	280	408

can be traced ultimately to the use of jellium as a reference system and the *ad hoc* corrections that its use subsequently necessitates.

3.1 Uniform electron gases

In the previous chapter, we considered the behaviour of electrons that are confined to the surface of a sphere. This work yielded a number of unexpected discoveries [11–14, 16–19, 23] but the one of relevance here is that such systems provide a beautiful new family of UEGs. These finite UEGs (FUEGs) have been thoroughly studied in Ref. [23]. Here, we only report their main characteristics [178].

3.1.1 Spherium atoms

The surface of a three-dimensional ball is called a 2-sphere (for it is two-dimensional) and its free-particle orbitals (Table 3.1) are the spherical harmonics $Y_{lm}(\theta, \phi)$. It is known that

$$\sum_{m=-l}^l |Y_{lm}(\theta, \phi)|^2 = \frac{2l+1}{4\pi}, \quad (3.1)$$

and doubly occupying all the orbitals with $0 \leq l \leq L$ thus yields a UEG. We call this system L -spherium and will compare it to *two*-dimensional jellium [160].

The number of electrons (Table 3.2) in L -spherium is

$$n = 2(L+1)^2, \quad (3.2)$$

the volume of a 2-sphere is $V = 4\pi R^2$ and, therefore,

$$\rho = \frac{(L+1)^2}{2\pi R^2}. \quad (3.3)$$

TABLE 3.3: The lowest free-particle orbitals on a glome (*i.e.* a 3-sphere)

Name	l	m	n	$\pi Y_{lmn}(\chi, \theta, \phi)$
1s	0	0	0	$2^{-1/2}$
2s	1	0	0	$2^{1/2} \cos \chi$
2p ₀	1	1	0	$2^{1/2} \sin \chi \cos \theta$
2p ₊₁	1	1	+1	$\sin \chi \sin \theta \exp(+i\phi)$
2p ₋₁	1	1	-1	$\sin \chi \sin \theta \exp(-i\phi)$
3s	2	0	0	$2^{-1/2}(4 \cos^2 \chi - 1)$
3p ₀	2	1	0	$12^{1/2} \sin \chi \cos \chi \cos \theta$
3p ₊₁	2	1	+1	$6^{1/2} \sin \chi \cos \chi \sin \theta \exp(+i\phi)$
3p ₋₁	2	1	-1	$6^{1/2} \sin \chi \cos \chi \sin \theta \exp(-i\phi)$
3d ₀	2	2	0	$\sin^2 \chi (3 \cos^2 \theta - 1)$
3d ₊₁	2	2	+1	$6^{1/2} \sin^2 \chi \sin \theta \cos \theta \exp(+i\phi)$
3d ₋₁	2	2	-1	$6^{1/2} \sin^2 \chi \sin \theta \cos \theta \exp(-i\phi)$
3d ₊₂	2	2	+2	$(3/2)^{1/2} \sin^2 \chi \sin^2 \theta \exp(+2i\phi)$
3d ₋₂	2	2	-2	$(3/2)^{1/2} \sin^2 \chi \sin^2 \theta \exp(-2i\phi)$

3.1.2 Glomium atoms

The surface of a four-dimensional ball is a 3-sphere (or “glome”) and its free-particle orbitals (Table 3.3) are the hyperspherical harmonics $Y_{lmn}(\chi, \theta, \phi)$. It is known [179] that

$$\sum_{m=0}^l \sum_{n=-m}^m |Y_{lmn}(\chi, \theta, \phi)|^2 = \frac{(l+1)^2}{2\pi^2}, \quad (3.4)$$

and doubly occupying all the orbitals with $0 \leq l \leq L$ thus yields a UEG. We call this system L -glomium and will compare it to *three*-dimensional jellium [160].

The number of electrons (Table 3.2) in L -glomium is

$$n = (L+1)(L+2)(2L+3)/3, \quad (3.5)$$

the volume of a 3-sphere is $V = 2\pi^2 R^3$ and, therefore,

$$\rho = \frac{(L+1)(L+2)(2L+3)}{6\pi^2 R^3}. \quad (3.6)$$

3.1.3 The non-uniqueness problem

The deeply disturbing aspect of jellium-based DFT models — and the launching-pad for the remainder of this chapter — is the countercultural claim, that

“The uniform electron gas with density ρ is not unique.”

Though it may seem heretical to someone who has worked with jellium for many years, or to someone who suspects that the claim violates the HK theorem, we claim that two D -dimensional UEGs with the same density parameter ρ may have different energies. To illustrate this, we now show that density functionals [39, 56, 166] which are exact for jellium are wrong for 0-spherium and 0-glomium.

The energy contributions for 0-spherium and 0-glomium are easy to find. There is no external potential, so $E_{ne} = 0$. The density $\rho(\mathbf{r})$ is constant, so the KS orbital $\psi(\mathbf{r}) = \sqrt{\rho(\mathbf{r})}$ is constant, and $T_s = 0$. The Hartree energy is the self-repulsion of a

TABLE 3.4: Exact and KS reduced energies of the ground states of 0-spherium and 0-glomium for various eigenradii R

	$2R$	Exact					Jellium-based KS DFT				Error $E_{\text{KS}} - E$
		T	E_{ee}	E	T_{s}	E_{ne}	J	$-E_{\text{x}}$	$-E_{\text{c}}$	E_{KS}	
0-spherium	$\sqrt{3}$	0.051982	0.448018	1/2	0	0	1.154701	0.490070	0.1028	0.562	0.062
	$\sqrt{28}$	0.018594	0.124263	1/7	0	0	0.377964	0.160413	0.0593	0.158	0.015
0-glomium	$\sqrt{10}$	0.014213	0.235787	1/4	0	0	0.536845	0.217762	0.0437	0.275	0.025
	$\sqrt{66}$	0.007772	0.083137	1/11	0	0	0.208967	0.084764	0.0270	0.097	0.006

uniform spherical shell of charge of radius R and one finds [12]

$$J = \frac{\Gamma(D-1)}{\Gamma(D-1/2)} \frac{\Gamma(D/2+1/2)}{\Gamma(D/2)} \frac{1}{R}, \quad (3.7)$$

where $\Gamma(x)$ is the Gamma function [29]. The exchange energy is predicted to be [23]

$$E_{\text{x}} = -\frac{2D}{(D^2-1)\pi R} \left(\frac{D!}{2}\right)^{1/D}, \quad (3.8)$$

and the correlation energy is predicted by conventional jellium-based functionals [39, 56, 166].

Applying these formulae to the exactly solvable states of 0-spherium and 0-glomium considered in the previous chapter yields the results in the right half of Table 3.4. In all cases, the KS-DFT energies are too high by 10 – 20%, indicating that the correlation functional that is exact for the UEG in jellium grossly underestimates the correlation energy of the UEGs in 0-spherium and 0-glomium.

We know that it is possible for two UEGs to have the same density ρ but different reduced energies E . But how can this be, given that the probability of finding an electron in a given volume is identical in the two systems? The key insight is that the probability of finding *two* electrons in that volume is different.

This is illustrated in Fig. 3.1, which compare the probability distributions of the interelectronic distance u [14, 180, 181] in various two-dimensional UEGs. These reveal that, although similar for $u \approx 0$ (because of the Kato cusp condition [109]), the specific Coulomb holes (i.e. the holes per unit volume [182]) in two gases with the same one-electron density ρ can be strikingly different. In each case, the jellium hole is both deeper and wider than the corresponding spherium hole, indicating that the jellium electrons exclude one another more strongly, and one is much less likely to find two electrons in a given small volume of jellium than in the same volume of spherium.

We conclude from these comparisons that (at least) two parameters are required to characterise a UEG. Although the parameter choice is not unique, we believe that the first should be a one-electron quantity, such as the density ρ and the second should be a two-electron quantity. A possible choice of a two-electron local variable will be presented in the next section.

3.2 Exchange functionals based on finite uniform electron gases

In this section, we show how to use these finite UEGs (FUEGs) to create a new type of exchange functionals applicable to atoms, molecules and solids [183]. We have

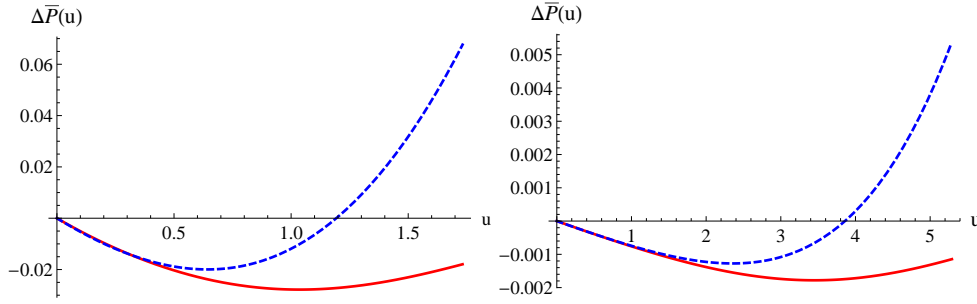


FIGURE 3.1: Specific Coulomb holes for 0-spherium (dotted) with $R = \sqrt{3}/2$ (left) and $R = \sqrt{7}$ (right), and 2D jellium (solid). Both are uniform gases with $\rho = 2/(3\pi)$ (left) and $\rho = 1/(14\pi)$ (right)

successfully applied this strategy to one-dimensional systems [184–187], for which we have created a correlation functional based on this idea [188, 189].

3.2.1 Theory

Within DFT, one can write the total exchange energy as the sum of its spin-up ($\sigma = \uparrow$) and spin-down ($\sigma = \downarrow$) contributions:

$$E_x = E_{x,\uparrow} + E_{x,\downarrow}, \quad (3.9)$$

where

$$E_{x,\sigma} = \int e_{x,\sigma}(\rho_\sigma, \nabla\rho_\sigma, \tau_\sigma, \dots) \rho_\sigma(\mathbf{r}) d\mathbf{r}, \quad (3.10)$$

and ρ_σ is the electron density of the spin- σ electrons. Although, for sake of simplicity, we sometimes remove the subscript σ , we only use spin-polarised quantities from hereon.

The first-rung LDA exchange functional (or D30 [39]) is based on the IUEG [40] and reads

$$e_{x,\sigma}^{\text{LDA}}(\rho_\sigma) = C_x^{\text{LDA}} \rho_\sigma^{1/3}, \quad (3.11)$$

where

$$C_x^{\text{LDA}} = -\frac{3}{2} \left(\frac{3}{4\pi} \right)^{1/3}. \quad (3.12)$$

A GGA functional (second rung) is defined as

$$e_{x,\sigma}^{\text{GGA}}(\rho_\sigma, x_\sigma) = e_{x,\sigma}^{\text{LDA}}(\rho_\sigma) F_x^{\text{GGA}}(x_\sigma), \quad (3.13)$$

where F_x^{GGA} is the GGA enhancement factor depending only on the reduced gradient

$$x = \frac{|\nabla\rho|}{\rho^{4/3}}, \quad (3.14)$$

and

$$\lim_{x \rightarrow 0} F_x^{\text{GGA}}(x) = 1, \quad (3.15)$$

i.e. a well thought-out GGA functional reduces to the LDA for homogeneous systems.

Similarly, motivated by the work of Becke [190] and our previous investigations [188, 189], we define an alternative second-rung functional (see Fig. 3.2) that we call

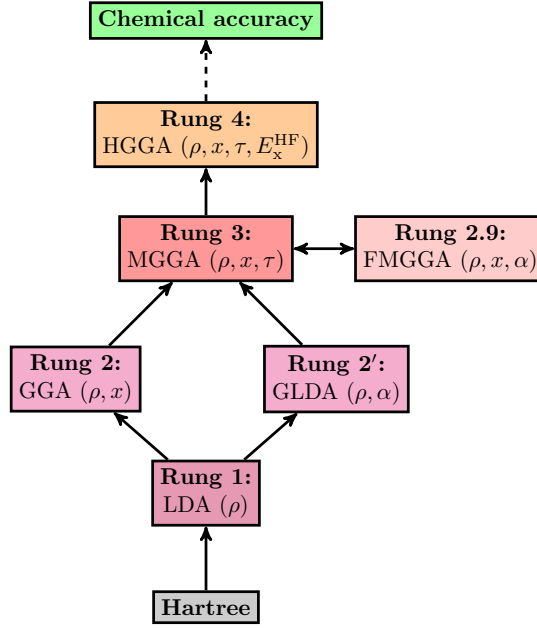


FIGURE 3.2: Jacob's ladder of DFT revisited.

generalised LDA (GLDA)

$$e_{x,\sigma}^{\text{GLDA}}(\rho_\sigma, \alpha_\sigma) = e_{x,\sigma}^{\text{LDA}}(\rho_\sigma) F_x^{\text{GLDA}}(\alpha_\sigma). \quad (3.16)$$

By definition, a GLDA functional only depends on the electron density and the curvature of the Fermi hole (see Fig. 3.2):

$$\alpha = \frac{\tau - \tau_W}{\tau_{\text{UEG}}} = \frac{\tau}{\tau_{\text{UEG}}} - \frac{x^2}{4C_F}, \quad (3.17)$$

which measures the tightness of the exchange hole around an electron [191, 192]. In Eq. (3.17),

$$\tau_W = \frac{|\nabla\rho|^2}{4\rho} \quad (3.18)$$

is the von Weizsäcker kinetic energy density [193], and

$$\tau_{\text{UEG}} = C_F \rho^{5/3} \quad (3.19)$$

is the kinetic energy density of the IUEG [40], where

$$C_F = \frac{3}{5}(6\pi^2)^{2/3}. \quad (3.20)$$

The dimensionless parameter α has two characteristic features: i) $\alpha = 0$ for any one-electron system, and ii) $\alpha = 1$ for the IUEG. Some authors call α the inhomogeneity parameter but we will avoid using this term as we are going to show that α can have distinct values in homogeneous systems. For well-designed GLDA functionals, we must ensure that

$$\lim_{\alpha \rightarrow 1} F_x^{\text{GLDA}}(\alpha) = 1, \quad (3.21)$$

i.e. the GLDA reduces to the LDA for the IUEG.¹

Although any functional depending on the reduced gradient x and the kinetic energy density τ is said to be of MGGA type, here we will define a third-rung MGGA functional as depending on ρ , x and α :

$$e_{x,\sigma}^{\text{MGGA}}(\rho_\sigma, x_\sigma, \alpha_\sigma) = e_{x,\sigma}^{\text{LDA}}(\rho_\sigma) F_x^{\text{MGGA}}(x_\sigma, \alpha_\sigma), \quad (3.22)$$

where one should ensure that

$$\lim_{x \rightarrow 0} \lim_{\alpha \rightarrow 1} F_x^{\text{MGGA}}(x, \alpha) = 1, \quad (3.23)$$

i.e. the MGGA reduces to the LDA for an infinite homogeneous system.

The Fermi hole curvature α has been shown to be a better variable than the kinetic energy density τ as one can discriminate between covalent ($\alpha = 0$), metallic ($\alpha \approx 1$) and weak bonds ($\alpha \gg 0$) [52–54, 196–201]. The variable α is also related to the electron localisation function (ELF) designed to identify chemical bonds in molecules [191, 202]. Moreover, by using the variables x and α , we satisfy the correct uniform coordinate density-scaling behaviour [203].

In conventional MGGA, the dependence in x and α can be strongly entangled, while, in GGAs for example, ρ and x are strictly disentangled as illustrated in Eq. (3.13). Therefore, it feels natural to follow the same strategy for MGGA. Thus, we consider a special class of MGGA functionals (rung 2.9 in Fig. 3.2) that we call factorable MGGA (FMGGA)

$$e_{x,\sigma}^{\text{FMGGA}}(\rho_\sigma, x_\sigma, \alpha_\sigma) = e_{x,\sigma}^{\text{LDA}}(\rho_\sigma) F_x^{\text{FMGGA}}(x_\sigma, \alpha_\sigma), \quad (3.24)$$

where the enhancement factor is written as

$$F_x^{\text{FMGGA}}(x, \alpha) = F_x^{\text{GGA}}(x) F_x^{\text{GLDA}}(\alpha). \quad (3.25)$$

By construction, F_x^{FMGGA} fulfills Eq. (3.23) and the additional physical limits

$$\lim_{x \rightarrow 0} F_x^{\text{FMGGA}}(x, \alpha) = F_x^{\text{GLDA}}(\alpha), \quad (3.26a)$$

$$\lim_{\alpha \rightarrow 1} F_x^{\text{FMGGA}}(x, \alpha) = F_x^{\text{GGA}}(x). \quad (3.26b)$$

The MVS functional designed by Sun, Perdew and Ruzsinszky is an example of FMGGA functional [200].

Unless otherwise stated, all calculations have been performed self-consistently with a development version of the Q-Chem4.4 package [204] using the aug-cc-pVTZ basis set [205–210]. To remove quadrature errors, we have used a very large quadrature grids consisting of 100 radial points (Euler-MacLaurin quadrature) and 590 angular points (Lebedev quadrature). As a benchmark, we have calculated the (exact) unrestricted HF (UHF) exchange energies.

3.2.2 GLDA exchange functionals

As stated in the previous section, the orbitals for an electron on a 3-sphere of unit radius are the normalised hyperspherical harmonics $Y_{\ell\mu}$, where ℓ is the principal quantum number and μ is a composite index of the remaining two quantum numbers

¹While some functionals only use the variable τ [194, 195], we are not aware of any functional only requiring α .

[179, 211]. We confine our attention to ferromagnetic (i.e. spin-polarised) systems in which each orbital with $\ell = 0, 1, \dots, L_\sigma$ is occupied by one spin-up or spin-down electron. As mentioned in the previous section, this yields an electron density that is uniform over the surface of the sphere. Note that the present paradigm is equivalent to the jellium model [40] for $L_\sigma \rightarrow \infty$. We refer the reader to Ref. [23] for more details about this paradigm.

The number of spin- σ electrons is

$$n_\sigma = \frac{1}{3}(L_\sigma + 1)(L_\sigma + 3/2)(L_\sigma + 2), \quad (3.27)$$

and their one-electron uniform density around the 3-sphere is

$$\rho_\sigma = \frac{n_\sigma}{V} = \frac{(L_\sigma + 2)(L_\sigma + 3/2)(L_\sigma + 1)}{6\pi^2 R^3}, \quad (3.28)$$

where $V = 2\pi^2 R^3$ is the surface of a 3-sphere of radius R . Moreover, using Eq. (3.17), one can easily derive that [188, 189]

$$\alpha_\sigma = \frac{L_\sigma(L_\sigma + 3)}{[(L_\sigma + 1)(L_\sigma + 3/2)(L_\sigma + 2)]^{2/3}}, \quad (3.29)$$

which yields

$$\lim_{n_\sigma \rightarrow 1} \alpha_\sigma = 0, \quad \lim_{n_\sigma \rightarrow \infty} \alpha_\sigma = 1. \quad (3.30)$$

We recover the results that $\alpha = 0$ in a one-electron system (here a one-electron FUEG), and that $\alpha = 1$ in the IUEG.

In particular, we have shown that the exchange energy of these systems can be written as [23, 212]

$$E_{x,\sigma}(L_\sigma) = C_x(L_\sigma) \int \rho_\sigma^{4/3} dr. \quad (3.31)$$

where

$$C_x(L) = C_x^{\text{LDA}} \frac{\frac{1}{2}(L + \frac{5}{4})(L + \frac{7}{4}) \left[\frac{1}{2}H_{2L+\frac{5}{2}} + \ln 2 \right] + (L + \frac{3}{2})^2 (L^2 + 3L + \frac{13}{8})}{[(L+1)(L+\frac{3}{2})(L+2)]^{4/3}} \quad (3.32)$$

and H_k is an harmonic number [29].

Therefore, thanks to the one-to-one mapping between L_σ and α_σ evidenced by Eq. (3.29), we have created the gX functional

$$F_x^{\text{gX}}(\alpha) = \frac{C_x^{\text{GLDA}}(0)}{C_x^{\text{GLDA}}(1)} + \alpha \frac{c_0 + c_1 \alpha}{1 + (c_0 + c_1 - 1)\alpha} \left[1 - \frac{C_x^{\text{GLDA}}(0)}{C_x^{\text{GLDA}}(1)} \right], \quad (3.33)$$

where $c_0 = +0.827411$, $c_1 = -0.643560$, and

$$C_x^{\text{GLDA}}(1) = C_x^{\text{LDA}} = -\frac{3}{2} \left(\frac{3}{4\pi} \right)^{1/3}, \quad (3.34)$$

$$C_x^{\text{GLDA}}(0) = -\frac{4}{3} \left(\frac{2}{\pi} \right)^{1/3}. \quad (3.35)$$

The parameters c_0 and c_1 of the gX enhancement factor (3.33) have been obtained by

fitting the exchange energies of these FUEGs for $1 \leq L \leq 10$ given by Eq. (3.31). F_x^{gX} automatically fulfils the constraint given by Eq. (3.21). Moreover, because $1 \leq F_x^{\text{gX}} \leq 1.233$, it breaks only slightly the tight Lieb-Oxford bound [213–215] $F_x < 1.174$ derived by Perdew and coworkers for two-electron systems [216, 217]. This is probably due to the non-zero curvature of these FUEGs.

Albeit very simple, the functional form (3.33) is an excellent fit to Eq. (3.32). In particular, F_x^{gX} is linear in α for small α , which is in agreement with Eq. (3.32) [23]. Also, Eq. (3.32) should have an infinite derivative at $\alpha = 1$ and approached as $\sqrt{1 - \alpha} \ln(1 - \alpha)$. Equation (3.33) does not behave that way. However, it has a marginal impact on the numerical results.

As one can see in Fig. 3.3, albeit being created with FUEGs, the gX functional has a fairly similar form to the common MGGAs, such as MS0 [53], MS1 [54], MS2 [54], MVS [200], and SCAN [52] for $0 \leq \alpha \leq 1$. This is good news for DFT as it shows that we recover functionals with similar physics independently of the paradigm used to design them. However, around $\alpha \approx 1$, the behaviour of F_x^{gX} is very different from other MGGAs (except for MVS) due to the constraint of the second-order gradient expansion (which is not satisfied in our case) [218]. For $0 \leq \alpha \leq 1$, it is also instructive to note that the gX functional is an upper bound of all the MGGAs. Taking into account the inhomogeneity of the system via the introduction of x should have the effect of decreasing the MGA enhancement factor (at least for $0 \leq \alpha \leq 1$).

Unlike other functionals, we follow a rather different approach and guide our functional between $\alpha = 0$ and 1 using FUEGs. For example, the MS0 functional uses the exact exchange energies of non-interacting hydrogenic anions to construct the functional from $\alpha = 0$ to 1 [53, 219], while revTPSS has no constraint to guide itself for this range of α [198]. Nonetheless, because these uniform systems only give valuable information in the range $0 \leq \alpha \leq 1$, we must find a different way to guide our functional for $\alpha > 1$.²

To do so, we have extended the gX functional beyond $\alpha = 1$ using a simple one-parameter extrapolation:

$$F_x^{\text{GX}}(\alpha) = \begin{cases} F_x^{\text{gX}}(\alpha), & 0 \leq \alpha \leq 1, \\ 1 + (1 - \alpha_\infty) \frac{1 - \alpha}{1 + \alpha}, & \alpha > 1, \end{cases} \quad (3.36)$$

where α_∞ is an adjustable parameter governing the value of F_x^{GX} when $\alpha \rightarrow \infty$. For large α , F_x^{GX} converges to α_∞ as α^{-1} , similarly to the MVS functional [200]. Far from claiming that this choice is optimal, we have found that the simple functional form (3.36) for $\alpha > 1$ yields satisfactory results (see below).

Following the seminal work of Sham [220] and Kleinman [221–223] (see also Ref. [224]), it is also possible, using linear response theory, to derive a second-order gradient-corrected functional. However, it does not provide any information for $\alpha > 1$.

The performance of the GX functional is illustrated in Table 3.5. Although GX is an improvement compared to LDA, even for one- and two-electron systems, we observe that the GX functional cannot compete with GGAs and MGGAs in terms of accuracy.

²Except for one- and two-electron systems, any atomic and molecular systems has region of space with $\alpha_r > 1$, as discussed in details by Sun et al.[199]

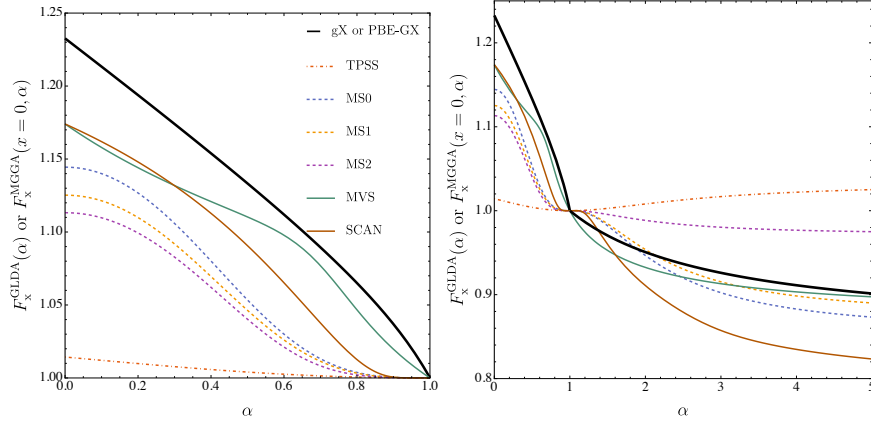


FIGURE 3.3: Enhancement factors $F_x^{\text{GLDA}}(\alpha)$ or $F_x^{\text{MGGA}}(x=0, \alpha)$ as a function of α for various GLDA and MGGA exchange functionals. The TPSS functional is represented as a dot-dashed line, the MS family of functionals (MS0, MS1 and MS2) are represented as dashed lines, while the MVS and SCAN functionals are depicted with solid lines. The new functionals gX and PBE-GX are represented with thick black lines. Note that $F_x^{\text{gX}}(\alpha) = F_x^{\text{PBE-GX}}(0, \alpha)$ for $0 \leq \alpha \leq 1$. For $F_x^{\text{PBE-GX}}$, $\alpha_\infty = +0.852$.

TABLE 3.5: Reduced (i.e. per electron) mean error (ME) and mean absolute error (MAE) (in kcal/mol) of the error (compared to UHF) in the exchange energy of the hydrogen-like ions, helium-like ions and first 18 neutral atoms for various LDA, GGA, GLDA, FMGGA and MGGA functionals. For the hydrogen-like ions, the exact density has been used for all calculations.

		hydrogen-like ions		helium-like ions		neutral atoms	
		ME	MAE	ME	MAE	ME	MAE
LDA	D30	153.5	69.7	150.6	69.5	70.3	9.1
GGA	B88	9.5	4.3	9.3	4.7	2.8	0.5
	G96	4.4	2.0	4.4	2.2	2.1	0.5
	PW91	19.4	8.8	19.1	9.3	4.5	0.8
	PBE	22.6	10.3	22.3	10.7	7.4	0.6
GLDA	GX	61.8	123.5	61.0	122.0	—	—
FMGGA	MVS	0.0	0.0	0.3	0.2	2.7	0.9
	PBE-GX	0.0	0.0	0.7	0.4	1.0	1.1
MGGA	M06-L	44.4	88.8	12.0	24.0	4.2	2.9
	TPSS	0.0	0.0	0.7	0.4	0.7	1.1
	revTPSS	0.0	0.0	0.5	0.3	3.5	2.5
	MS0	0.0	0.0	0.4	0.2	1.3	2.4
	SCAN	0.0	0.0	0.3	0.2	1.2	1.6

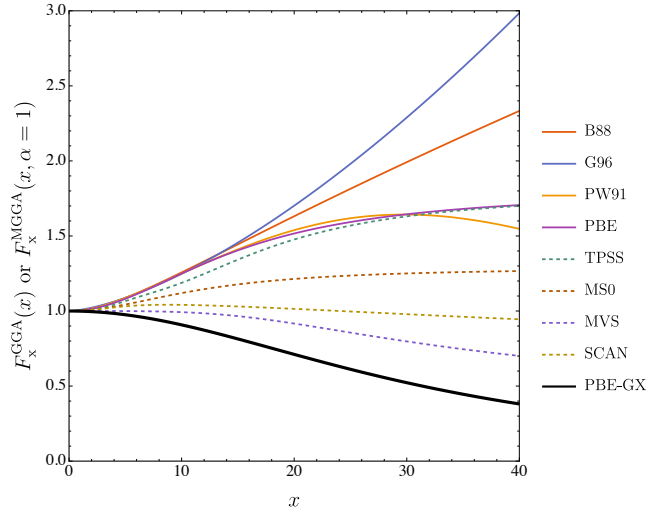


FIGURE 3.4: Enhancement factors $F_x^{\text{GGA}}(x)$ or $F_x^{\text{MGGA}}(x, \alpha = 1)$ as a function of x for various GGA, FMGGA and MGGA exchange functionals. The GGA functionals are represented in solid lines, while MGGAs are depicted in dashed lines. The new functional PBE-GX is represented with a thick black line.

3.2.3 FMGGA exchange functionals

One of the problem of GLDA functionals is that they cannot discriminate between homogeneous and inhomogeneous one-electron systems, for which we have $\alpha = 0$ independently of the value of the reduced gradient x . For example, the GX functional is exact for one-electron FUEGs, while it is inaccurate for the hydrogen-like ions. Unfortunately, it is mathematically impossible to design a GLDA functional exact for these two types of one-electron systems.

To cure this problem, we couple the GX functional designed above with a GGA enhancement factor to create a FMGGA functional. We have chosen a PBE-like GGA factor, i.e.

$$F_x^{\text{PBE-GX}}(x, \alpha) = F_x^{\text{PBE}}(x) F_x^{\text{GX}}(\alpha), \quad (3.37)$$

where

$$F_x^{\text{PBE}}(x) = \frac{1}{1 + \mu x^2}. \quad (3.38)$$

Similarly to various MGGAs (such as TPSS [197], MVS [200], or SCAN [52]), we use the hydrogen atom as a “norm”, and determine that $\mu = +0.001015549$ reproduces the exact exchange energy of the ground state of the hydrogen atom. Also, we have found that $\alpha_\infty = +0.852$ yields excellent exchange energies for the first 18 neutral atoms. Unlike GX, PBE-GX is accurate for both the (inhomogeneous) hydrogen-like ions and the (homogeneous) one-electron FUEGs, and fulfils the negativity constraint and uniform density scaling [52, 225]. The right graph of Fig. 3.3 shows the behaviour of the MGGA enhancement factor for $x = 0$ as a function of α . Looking at the curves for $\alpha > 1$, we observe that TPSS has a peculiar enhancement factor which slowly raises as α increases. All the other functionals (including PBE-GX) decay more or less rapidly with α . We note that PBE-GX and MVS behave similarly for $\alpha > 1$, though their functional form is different.

Figure 3.4 evidences a fundamental difference between GGAs and MGGAs: while the enhancement factor of conventional GGAs does increase monotonically with x and favour inhomogeneous electron densities, F_x^{MGGA} decays monotonically with

TABLE 3.6: Reduced (i.e. per electron) mean error (ME) and mean absolute error (MAE) (in kcal/mol) of the error (compared to the experimental value) in the atomisation energy ($E_{\text{atoms}} - E_{\text{molecule}}$) of diatomic molecules at experimental geometry for various LDA, GGA and MGGAs exchange-correlation functionals. Experimental geometries are taken from Ref. [227].

	functional		diatomics	
	exchange	correlation	ME	MAE
LDA	D30	VWN5	1.8	3.7
GGA	B88	LYP	0.6	1.2
	PBE	PBE	0.7	1.2
MGGAs	M06-L	M06-L	0.4	0.7
	TPSS	TPSS	0.6	1.1
	revTPSS	revTPSS	0.6	1.2
	MVS	regTPSS	0.5	0.9
	SCAN	SCAN	0.4	0.7
	PBE-GX	PBE	0.6	1.2
	PBE-GX	regTPSS	0.6	1.1
	PBE-GX	LYP	0.6	1.1
	PBE-GX	TPSS	0.7	1.3
	PBE-GX	revTPSS	0.8	1.5
PBE-GX	SCAN	0.6	1.0	

respect to x . This is a well-known fact: the x - and α -dependence are strongly coupled, as suggested by the relationship (3.17). Therefore, the x -dependence can be sacrificed if the α -dependence is enhanced [52, 53, 200]. Similarly to $F_x^{\text{PBE-GX}}$, F_x^{MVS} and F_x^{SCAN} decay monotonically with x (although not as fast as PBE-GX), while earlier MGGAs such as TPSS and MS0 have a slowly-increasing enhancement factor. We have observed that one needs to use a bounded enhancement factor at large x (as in Eq. (3.38)) in order to be able to converge self-consistent field (SCF) calculations. Indeed, using an unbounded enhancement factor (as in B88 [43] or G96 [44]) yields divergent SCF KS calculations. Finally, we note that, unlike TPSS, PBE-GX does not suffer from the order of limits problem [226].

How good are FMGGAs? This is the question we would like to answer here. In other words, we would like to know whether or not our new simple FMGGA functional called PBE-GX is competitive within MGGAs. Unlike GGAs and some of the MGGAs (like M06-L), by construction, PBE-GX reproduces exactly the exchange energy of the hydrogen atom and the hydrogenic ions (He^+ , Li^{2+} , ...) due to its dimensional consistency (see Table 3.5). PBE-GX also reduces the error for the helium-like ions (H^- , He , Li^+ , ...) by one order of magnitude compared to GGAs, and matches the accuracy of MGGAs. For the first 18 neutral atoms (Table 3.5 and Fig. 3.5), PBE-GX is as accurate as conventional MGGAs with a mean error (ME) and mean absolute error (MAE) of 1.0 and 1.1 kcal/mol. From the more conventional MGGAs, the TPSS and SCAN functionals are the best performers for neutral atoms with MEs of 0.7 and 1.2 kcal/mol, and MAEs of 1.1 and 1.6 kcal/mol. PBE-GX lies just in-between these two MGGAs.

We now turn our attention to diatomic molecules for which errors in the atomisation energy ($E_{\text{atoms}} - E_{\text{molecule}}$) are reported in Table 3.6 for various combinations of exchange and correlation functionals. In particular, we have coupled our new PBE-GX exchange functional with the PBE [46], regTPSS [226] (also called vPBEc)

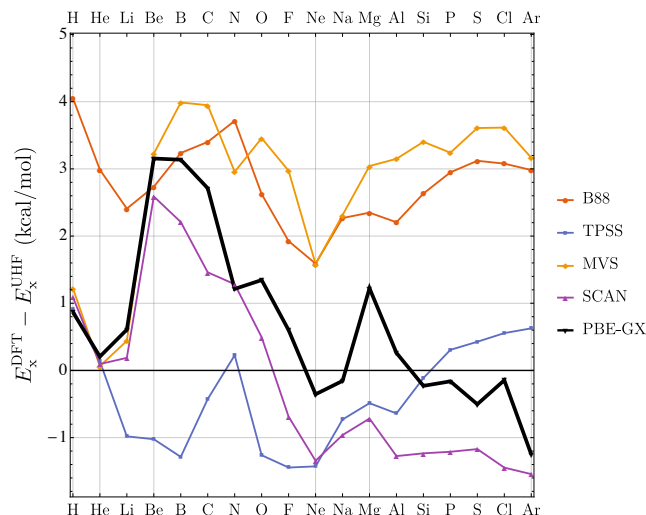


FIGURE 3.5: Reduced (i.e. per electron) error (in kcal/mol) in atomic exchange energies of the first 18 neutral atoms of the periodic table for the B88 (red), TPSS (blue), MVS (orange), SCAN (purple) and PBE-GX (thick black) functionals.

and LYP [47] GGA correlation functionals, as well as the TPSS, [197] revTPSS [198] and SCAN [52] MGGGA correlation functionals.

Although very lightly parametrised on atoms, PBE-GX is also accurate for molecules. Interestingly, the results are mostly independent of the choice of the correlation functional with MEs ranging from 0.6 and 0.8 kcal/mol, and MAEs from 1.0 and 1.5 kcal/mol. PBE-GX is only slightly outperformed by the SCAN functional and the highly-parametrized M06-L functional, which have both a ME of 0.4 kcal/mol and a MAE of 0.7 kcal/mol.

3.3 Summary

In the first section, we have shown that uniform electron gases (UEGs) on a D -sphere are an attractive generalisation of D -jellium. However, although it is pleasing to know that the spherical and conventional gases become equivalent in the thermodynamic limit, we believe that it is more important to recognise that they are *not* equivalent for finite number of electrons. This has immediate chemical ramifications, suggesting that the traditional jellium paradigm is suboptimal for modelling molecular densities, even in regions of space where the density is nearly uniform.

In the second section, using *finite* UEGs (FUEGs), we have created a *generalized* LDA (GLDA) exchange functional which only depends on the curvature of the Fermi hole α . We have also combined our newly-designed GLDA functional with a PBE-type GGA functional to create a new type of MGGAs that we have called *factorizable* MGGAs (FMGGAs).

Chapter 4

Many-electron integrals involving Gaussian geminals

The time-independent electronic Schrödinger equation (1.2) is the starting point for a fundamental understanding of the behaviour of electrons and, thence, of chemical structure, bonding and reactivity. Indeed, the past 80 years have provided overwhelming evidence that, as Dirac observed in the early days of the quantum mechanical revolution [228],

“the underlying physical laws necessary for the mathematical theory of a large part of physics and the whole of chemistry are thus completely known, and the difficulty is only that the exact application of these laws leads to equations much too complicated to be soluble.”

Contemporary quantum chemistry has developed in two directions: wave function-based models [28] and density-based models [34]. Both spring from the Schrödinger equation but each reformulates this second-order partial differential equation in terms of integrals. For this reason, it is no exaggeration to say that the mathematical operation of integration lies at the heart of the field. If integration of functions were a trivial task, quantum chemistry would be likewise trivialised. But, it is not.

4.1 History

It is well known that highly-accurate wave functions require the fulfilment (or near-fulfilment) of the electron-electron cusp conditions [17, 19, 20, 109, 120, 122–124, 229–232]. For correlated wave functions expanded in terms of products of one-electron Gaussian basis functions, the energy converges as $\mathcal{O}(L^{-3})$, where L is the maximum angular momentum of the basis set [88]. This slow convergence can be tracked down to the inadequacy of these products to properly model the Coulomb correlation hole [233, 234].

In the late 20's, Hylleraas solved this issue for the helium atom by introducing explicitly the interelectronic distance $r_{12} = |\mathbf{r}_1 - \mathbf{r}_2|$ as an additional two-electron basis function [235, 236]. As Kutzelnigg later showed, this leads to a prominent improvement of the energy convergence from $\mathcal{O}(L^{-3})$ to $\mathcal{O}(L^{-7})$ [88].

Around the same time, Slater, while studying the Rydberg series of helium [237], suggested a new correlation factor known nowadays as a Slater geminal:

$$S_{12} = \exp(-\lambda_{12} r_{12}). \quad (4.1)$$

Unfortunately, the increase in mathematical complexity brought by r_{12} or S_{12} has been found to be rapidly computationally overwhelming.¹

In 1960, Boys [239] and Singer [240] independently proposed to use the Gaussian geminal (GG) correlation factor

$$G_{12} = \exp(-\lambda_{12} r_{12}^2), \quad (4.2)$$

as [239]

“there are explicit formulas for all of the necessary many-dimensional integrals”.

Interestingly, in the same article, a visionary Boys argued that, even if GGs do not fulfil the electron-electron cusp conditions, they could be used to fit S_{12} .

During the following years, variational calculations involving GGs flourished, giving birth to various methods, such as the exponentially-correlated Gaussian method [241–244]. However, this method was restricted to fairly small systems as it requires the optimisation of a large number of non-linear parameters. In the 70’s, the first MP2 calculations including GGs appeared thanks to the work by Pan and King [245, 246], Adamowicz and Sadlej [247–249], and later Szalewicz *et al.* [250, 251]. Even if these methods represented a substantial step forward in terms of computational burden, they still require the optimization of a large number of non-linear parameters.

In 1985, Kutzelnigg derived a first form of the MP2-R12 equations using r_{12} as a correlation factor [88]. Kutzelnigg’s idea, which was more formally described together with Klopper in 1987 [252], dredged up an old problem: in addition to two-electron integrals (traditional ones and new ones), three-electron and four-electron integrals were required. At that time, the only way to evaluate them would have been via an expensive one- or two-dimensional Gauss-Legendre quadrature [253, 254]. Additionally, citing Kutzelnigg and Klopper [89],

“even if fast procedures for the evaluation of these integrals were available, one would have to face the problem of the large number of these integrals; while that of two-electron integrals is $\sim N^4$, there are $\sim N^6$ three-electron and $\sim N^8$ four-electron integrals. The storing and manipulating of these integrals could be handled only for extremely small basis sets.”

Undoubtedly, in the late 80’s, the two-electron integrals technology was still in development [255–262]. Nowadays, though still challenging, these integrals could be computed much more effectively via judicious recursive schemes, designing the quadrature only to the fundamental integrals [263]. Another important remark is that the actual number of *significant* (i.e. greater than a given threshold) three- and four-electron integrals in a large system, is, at worst, $\mathcal{O}(N^3)$ or $\mathcal{O}(N^4)$. These kinds of scaling are achievable, for example, by exploiting robust density fitting [264] or upper bound-based screening methods, as discussed below [265].

Nevertheless, the success of the R12 method was triggered by the decision to avoid the computation of these three- and four-electron integrals through the use of the *resolution of the identity* (RI) approximation [89, 233, 266]. In this way, three- and four-electron integrals are approximated as linear combinations of products of

¹Note that, although Slater was the first to propose such correlation factor, he suggested to set $\lambda_{12} = -1/2$ in order to ensure that the wave function fulfils Kato’s electron-electron cusp condition. However, Hartree and Ingman [238] found this correlation factor physically unreasonable due to its behaviour at large r_{12} , and suggested that a correlation factor of the form $1 - c \exp(-\lambda_{12} r_{12})$ (with $\lambda_{12} > 0$) would be more appropriate. We refer the interested reader to the review of Hattig *et al.* [233] for a detailed historical overview.

two-electron integrals. Several key developments and improvements of the original MP2-R12 approach have been proposed in the last decade [233, 234, 266, 267]. Of course, the accuracy of the RI approximation relies entirely on the assumption that the auxiliary basis set is sufficiently large, i.e. $N_{\text{RI}} \gg N$, where N and N_{RI} are the number of basis functions in the primary and auxiliary basis sets, respectively.

The use of RI as method of choice does not seem definitive to us. In fact, eschewing the RI approximation would offer at least two advantages: i) smaller one-electron basis as the larger auxiliary basis set would not be required anymore; ii) the three- and four-electron integrals would be computed exactly. Moreover, one could avoid the commutator rearrangements involved in the computation of integrals over the kinetic energy operator [268].

In 1996, Persson and Taylor killed two birds with one stone. Using a pre-optimized GG expansion fitting r_{12}

$$r_{12} \approx \sum_k a_k [1 - \exp(-\lambda_k r_{12}^2)], \quad (4.3)$$

they avoided the non-linear optimisation, and eschewed the RI approximation thanks to the analytical integrability of three- and four-electron integrals over GGs [269]. They were able to show that a six- or ten-term fit introduces a 0.5 mE_h or $20 \mu\text{E}_h$ error, respectively [269]. Unfortunately, further improvements were unsuccessful due to the failure of r_{12} in modelling the correct behaviour of the wave function for intermediate and large r_{12} [270, 271]. In fact, Ten-no showed that S_{12} is near-optimal at describing the correlation hole, and that a 10-term GG fit of S_{12} yields very similar results. This suggests that, albeit not catching the cusp per se, the Coulomb correlation hole can be accurately represented by GGs [272–275].

Methods for evaluating many-electron integrals involving GGs have already been developed. As mentioned previously, Persson and Taylor [276] derived recurrence relations based on Hermite Gaussians, analogously to the work of McMurchie and Davidson for two-electron integrals [255]. These recurrence relations were implemented by Dahle [277–279]. Saito and Suzuki [280] also proposed an approach based on the work by Obara and Saika [260, 281]. More recently, a general formulation using Rys polynomials [257–259] was published by Komornicki and King [282]. Even if limited to the three-centre case, it is worth mentioning that May has also developed recurrence relations for two types of three-electron integrals [283]. These recurrence relations were implemented by Womack using automatically-generated code [284]. Recently, we have developed recurrence relations for three- and four-electron integrals for generic correlation factors [263, 285]. All these recursive schemes have variable computational cost depending on the degree of contraction of the integral class to be computed. Unsurprisingly, these algorithms are, to a large extent, complementary, and none of the algorithms has proven optimal under all circumstances.

A major limitation of all these approaches is that they do not include any integral screening. Indeed, a remarkable consequence of the short-range nature of the Slater and Gaussian correlation factors is that, even if formally scaling as $\mathcal{O}(N^6)$ and $\mathcal{O}(N^8)$, there are only $\mathcal{O}(N^2)$ significant (i.e. greater than a given threshold) three- and four-electron integrals in a large system [263, 265]. Therefore, it is paramount to devise rigorous upper bounds to avoid computing the large number of negligible integrals.

This chapter is organised as follows. First, we discuss Gaussian basis functions, many-electron integrals and the structure of the three- and four-electron operators considered here. In the next three sections, we introduce the main ingredients for the efficient computation of three- and four-electron integrals involving GGs: i)

fundamental integrals (FIs), ii) upper bounds (UBs), and iii) recurrence relations (RRs). Finally, we give an overall view of our algorithm which is an extension of the late-contraction path of PRISM, also known as the Head-Gordon-Pople (HGP) algorithm (see Refs. [261, 262] and references therein). Note that the HGP algorithm corresponds to the Obara-Saika scheme where one has introduced additional RRs and provides a precise description of how these RRs can be used in tandem to good effects.

4.2 Generalities

4.2.1 Gaussian functions

A primitive Gaussian function (PGF) is specified by an orbital exponent α , a center $\mathbf{A} = (A_x, A_y, A_z)$, and angular momentum $\mathbf{a} = (a_x, a_y, a_z)$:

$$\varphi_{\mathbf{a}}^{\mathbf{A}}(\mathbf{r}) = (x - A_x)^{a_x} (y - A_y)^{a_y} (z - A_z)^{a_z} e^{-\alpha |\mathbf{r} - \mathbf{A}|^2}. \quad (4.4)$$

A contracted Gaussian function (CGF) is defined as a sum of PGFs

$$\psi_{\mathbf{a}}^{\mathbf{A}}(\mathbf{r}) = \sum_{k=1}^{K_a} D_{ak} (x - A_x)^{a_x} (y - A_y)^{a_y} (z - A_z)^{a_z} e^{-\alpha_k |\mathbf{r} - \mathbf{A}|^2}, \quad (4.5)$$

where K_a is the degree of contraction and the D_{ak} are contraction coefficients. A CGF-pair

$$|\mathbf{ab}\rangle \equiv \psi_{\mathbf{a}}^{\mathbf{A}}(\mathbf{r}) \psi_{\mathbf{b}}^{\mathbf{B}}(\mathbf{r}) = \sum_{i=1}^{K_a} \sum_{j=1}^{K_b} |\mathbf{ab}\rangle_{ij} \quad (4.6)$$

is a two-fold sum of PGF-pairs $|\mathbf{ab}\rangle = \varphi_{\mathbf{a}}^{\mathbf{A}}(\mathbf{r}) \varphi_{\mathbf{b}}^{\mathbf{B}}(\mathbf{r})$.

A primitive shell $|a\rangle$ is a set of PGFs sharing the same total angular momentum a , exponent α and center \mathbf{A} . Similarly, a contracted shell $|a\rangle$ is a set of CGFs sharing the same PGFs and total angular momentum. A contracted shell-pair is the set of CGF-pairs obtained by the tensor product $|\mathbf{ab}\rangle = |a\rangle \otimes |b\rangle$. Similarly, a primitive shell-pair $|\mathbf{ab}\rangle = |a\rangle \otimes |b\rangle$ is the set of PGF-pairs. Finally, primitive and contracted shell-quartets, -sextets and -octets are obtained in an analogous way. For example, $|a_1 b_1 a_2 b_2\rangle = |a_1 b_1\rangle \otimes |a_2 b_2\rangle$ and $|a_1 a_2 b_1 b_2\rangle = |a_1 b_1\rangle \otimes |a_2 b_2\rangle$. Note that $|1\rangle$ is a set of three p -type PGFs, a $|11\rangle \equiv |pp\rangle$ shell-pair is a set of nine PGF-pairs, and a $|2222\rangle \equiv |dddd\rangle$ shell-quartet is a set of 1,296 PGF-quartets.

4.2.2 Many-electron integrals

Throughout this chapter, we use physicists notations, and we write the integral over a n -electron operator $f_{1\dots n}$ of CGFs as

$$\begin{aligned} \langle \mathbf{a}_1 \cdots \mathbf{a}_n | \mathbf{b}_1 \cdots \mathbf{b}_n \rangle &\equiv \langle \mathbf{a}_1 \cdots \mathbf{a}_n | f_{1\dots n} | \mathbf{b}_1 \cdots \mathbf{b}_n \rangle \\ &= \int \cdots \int \psi_{\mathbf{a}_1}^{\mathbf{A}_1}(\mathbf{r}_1) \cdots \psi_{\mathbf{a}_n}^{\mathbf{A}_n}(\mathbf{r}_n) f_{1\dots n} \psi_{\mathbf{b}_1}^{\mathbf{B}_1}(\mathbf{r}_1) \cdots \psi_{\mathbf{b}_n}^{\mathbf{B}_n}(\mathbf{r}_n) d\mathbf{r}_1 \cdots d\mathbf{r}_n. \end{aligned} \quad (4.7)$$

Additionally, square-bracketed integrals denote integrals over PGFs:

$$[a_1 \cdots a_n | b_1 \cdots b_n] = \int \cdots \int \varphi_{a_1}^{\mathbf{A}_1}(\mathbf{r}_1) \cdots \varphi_{a_n}^{\mathbf{A}_n}(\mathbf{r}_n) f_{1 \cdots n} \varphi_{b_1}^{\mathbf{B}_1}(\mathbf{r}_1) \cdots \varphi_{b_n}^{\mathbf{B}_n}(\mathbf{r}_n) d\mathbf{r}_1 \cdots d\mathbf{r}_n. \quad (4.8)$$

The FIs (i.e. the integral in which all $2n$ basis functions are s -type PGFs) is defined as $[\mathbf{0}] \equiv [\mathbf{0} \cdots \mathbf{0} | \mathbf{0} \cdots \mathbf{0}]$ with $\mathbf{0} = (0, 0, 0)$. The Gaussian product rule reduces it from $2n$ to n centers:

$$[\mathbf{0}] = \left(\prod_{i=1}^n S_i \right) \int \cdots \int \varphi_{\mathbf{0}}^{\mathbf{Z}_1}(\mathbf{r}_1) \cdots \varphi_{\mathbf{0}}^{\mathbf{Z}_n}(\mathbf{r}_n) f_{1 \cdots n} d\mathbf{r}_1 \cdots d\mathbf{r}_n, \quad (4.9)$$

where

$$\zeta_i = \alpha_i + \beta_i, \quad (4.10a)$$

$$\mathbf{Z}_i = \frac{\alpha_i \mathbf{A}_i + \beta_i \mathbf{B}_i}{\zeta_i}, \quad (4.10b)$$

$$S_i = \exp\left(-\frac{\alpha_i \beta_i}{\zeta_i} |\mathbf{A}_i \mathbf{B}_i|^2\right), \quad (4.10c)$$

and $\mathbf{A}_i \mathbf{B}_i = \mathbf{A}_i - \mathbf{B}_i$. We also define the quantity $\mathbf{Y}_{ij} = \mathbf{Z}_i - \mathbf{Z}_j$ which will be used later on.

For conciseness, we will adopt a notation in which missing indices represent s -type Gaussians. For example, $[a_2 a_3]$ is a shorthand for $[\mathbf{0} a_2 a_3 \mathbf{0} | \mathbf{0} \mathbf{0} \mathbf{0} \mathbf{0}]$. We will also use unbold indices, e.g. $[a_1 a_2 a_3 a_4 | b_1 b_2 b_3 b_4]$ to indicate a complete class of integrals from a shell-octet.

4.2.3 Three- and four-electron operators

In this chapter, we are particularly interested in the “master” four-electron operator $C_{12} G_{13} G_{14} G_{23} G_{34}$ (where $C_{12} = r_{12}^{-1}$ is the Coulomb operator) because the three types of three-electron integrals and the three types of four-electron integrals that can be required in F12 calculations can be easily generated from it (see Fig. 4.1). These three types of three-electron integrals are composed by a single type of integrals over the cyclic operator $C_{12} G_{13} G_{23}$, and two types of integrals over the three-electron chain (or 3-chain) operators $C_{12} G_{23}$ and $G_{13} G_{23}$. F12 calculations may also require three types of four-electron integrals: two types of integrals over the 4-chain operators $C_{12} G_{14} G_{23}$ and $C_{12} G_{13} G_{34}$, as well as one type over the trident operator $C_{12} G_{13} G_{14}$. Explicitly-correlated methods also requires two-electron integrals. However, their computation has been thoroughly studied in the literature [89, 233, 234, 272, 273, 275, 276, 282, 286–295]. Similarly, the nuclear attraction integrals can be easily obtained by taking the large-exponent limit of a s -type shell-pair.

Starting with the “master” operator $C_{12} G_{13} G_{14} G_{23} G_{34}$, one can easily obtain all the FIs as well as the RRs required to compute three- and four-electron integrals within F12 calculations. This is illustrated in Fig. 4.1 where we have used a diagrammatic representation of the operators. The number N_{sig} of significant integrals in a large system with N CGFs is also reported.

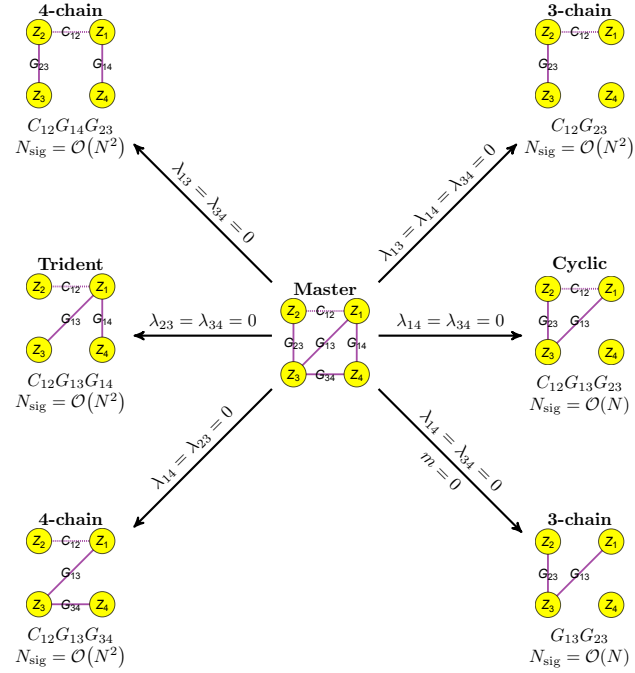


FIGURE 4.1: Diagrammatic representation of the three- and four-electron integrals required in F12 theory. The number N_{sig} of significant integrals in a large system with N CGFs is also reported.

4.3 Fundamental integrals

Following Persson and Taylor [269], the $[0]^m$ are derived starting from the momentumless integral (4.9) using the following Gaussian integral representation for the Coulomb operator

$$C_{12} = \frac{2}{\sqrt{\pi}} \int_0^\infty \exp(-u^2 r_{12}^2) du. \quad (4.11)$$

After a lengthy derivation which is not presented here for the sake of simplicity, one can show that the closed-form expression of the FIs is

$$[0]^m = \frac{2}{\sqrt{\pi}} [0]_G \sqrt{\frac{\delta_0}{\delta_1 - \delta_0}} \left(\frac{\delta_1}{\delta_1 - \delta_0} \right)^m F_m \left[\frac{\delta_1 (Y_1 - Y_0)}{\delta_1 - \delta_0} \right], \quad (4.12)$$

where m is an auxiliary index, $F_m(t)$ is the generalised Boys function, and

$$[0]_G = \left(\prod_{i=1}^4 S_i \right) \left(\frac{\pi^4}{\delta_0} \right)^{3/2} \exp(-Y_0) \quad (4.13)$$

is the FI of the “pure” GG operator $G_{13}G_{14}G_{23}G_{34}$ from which one can easily get the FI of the 3-chain operator $G_{13}G_{23}$ by setting $\lambda_{14} = \lambda_{34} = 0$. While the FIs involving a Coulomb operator contain an auxiliary index m , the FIs over “pure” GG operators (like $G_{13}G_{23}$) do not, thanks to the factorisation properties of GGs [296]. This is a major computational saving as the computation of these auxiliary integrals can take a significant fraction of the CPU time, even for two-electron integrals.

The various quantities required to compute (4.12) are

$$\delta_u = \zeta + \lambda_u = \zeta + \mathbf{G} + u^2 \mathbf{C}, \quad (4.14)$$

where

$$\zeta = \begin{pmatrix} \zeta_1 & 0 & 0 & 0 \\ 0 & \zeta_2 & 0 & 0 \\ 0 & 0 & \zeta_3 & 0 \\ 0 & 0 & 0 & \zeta_4 \end{pmatrix}, \quad \mathbf{C} = \begin{pmatrix} 1 & -1 & 0 & 0 \\ -1 & 1 & 0 & 0 \\ 0 & 0 & 0 & 0 \\ 0 & 0 & 0 & 0 \end{pmatrix}, \quad (4.15a)$$

$$\mathbf{G} = \begin{pmatrix} \lambda_{13} + \lambda_{14} & 0 & -\lambda_{13} & -\lambda_{14} \\ 0 & \lambda_{23} & -\lambda_{23} & 0 \\ -\lambda_{13} & -\lambda_{23} & \lambda_{13} + \lambda_{23} + \lambda_{34} & -\lambda_{34} \\ -\lambda_{14} & 0 & -\lambda_{34} & \lambda_{14} + \lambda_{34} \end{pmatrix}, \quad (4.15b)$$

and

$$\Delta_u = \zeta \cdot \delta_u^{-1} \cdot \zeta, \quad \mathbf{Y}^k = \begin{pmatrix} 0 & \mathbf{Y}_{12}^k & \mathbf{Y}_{13}^k & \mathbf{Y}_{14}^k \\ 0 & 0 & \mathbf{Y}_{23}^k & \mathbf{Y}_{24}^k \\ 0 & 0 & 0 & \mathbf{Y}_{34}^k \\ 0 & 0 & 0 & 0 \end{pmatrix}, \quad (4.16a)$$

$$\delta_u = \det(\delta_u), \quad Y_u = \text{Tr}(\Delta_u \cdot \mathbf{Y}^2). \quad (4.16b)$$

The generalised Boys function $F_m(t)$ in Eq. (4.12) can be computed efficiently using well-established algorithms [297–299].

4.4 Upper bounds

In this section, instead of reporting the mathematical expressions of UBs (which can be found in Ref. [300]), we present general concepts about UBs for three- and four-electron integrals. We refer the interested reader to Refs. [296, 301] for additional information about UBs.

As mentioned earlier in this chapter, computing $\mathcal{O}(N^6)$ or $\mathcal{O}(N^8)$ integrals in a large system would be extremely challenging, but it turns out that the number of *significant* three- and four-electron integrals is, at worst, $\mathcal{O}(N^3)$ and $\mathcal{O}(N^4)$, respectively. Moreover, if the correlation factor is a short-range operator (as in modern F12 methods [269, 270, 272, 274–276, 291]), it can be shown that the number drops to only $\mathcal{O}(N^2)$. However, to exploit this fully, one must devise rigorous UBs and then use these to avoid computing vast numbers of negligible integrals. If this can be achieved, it may enable large-scale F12 calculations without the need to introduce RI approximations.

From a general point of view, an effective UB should be:

- simple, i.e. much cheaper than the true integral;
- strong, i.e. as close as possible to the true integral;
- scaling-consistent, i.e. $N_{\text{sig}} = \mathcal{O}(N_{\text{UB}})$, where N_{UB} is the number estimated by the UB.

Many two-electron integral UBs are known [301–305] but few satisfy all three requirements. Moreover, to the best of our knowledge, the only three-electron integral UB that has been proposed is a simple application of the Cauchy-Schwartz inequality [277].

To construct UBs, we will depend heavily on the absolute value inequality

$$\left| \int \phi(\mathbf{r}) d\mathbf{r} \right| \leq \int |\phi(\mathbf{r})| d\mathbf{r}, \quad (4.17)$$

and the Hölder inequality [29]

$$\left| \int \phi_1(\mathbf{r})\phi_2(\mathbf{r})d\mathbf{r} \right| \leq \left[\int |\phi_1(\mathbf{r})|^p d\mathbf{r} \right]^{1/p} \left[\int |\phi_2(\mathbf{r})|^q d\mathbf{r} \right]^{1/q}, \quad (4.18)$$

where $p^{-1} + q^{-1} = 1$ and $p, q > 1$. Hölder yields the Cauchy-Schwartz inequality [29] if one chooses $p = q = 2$. Note, however, that we eschewed bounds descending from the Cauchy-Schwartz inequality because they are usually weaker than ours [301] and, for three-electron integrals, they are usually not simple.

4.4.1 Integral bounds

An integral bound is a number that bounds *a particular integral*. For example, the Cauchy-Schwartz inequality yields the well-known [303] two-electron integral bound

$$|[a_1 a_2 | b_1 b_2]| \leq [a_1 a_1 | b_1 b_1]^{1/2} [a_2 a_2 | b_2 b_2]^{1/2}. \quad (4.19)$$

If one has pre-computed and stored $\mathcal{O}(N^2)$ Cauchy-Schwartz factors $[a_1 a_1 | b_1 b_1]$, these yield cheap upper bounds on $\mathcal{O}(N^4)$ two-electron integrals.

However, despite their attractive features, integral bounds are poorly suited to modern hardware and software. Bounding every integral before deciding whether or not to compute its exact value places logical branches within inner loops and leads to slow code. Moreover, using bounds to eliminate a few integrals from a class is incompatible with recursive methods for integral generation. This leads naturally to a class strategy.

4.4.2 Class bounds

A class bound is a number that bounds *all the integrals in a class*. These are particularly effective for large classes because, if the class bound is below τ , a large number of integrals can be skipped on the basis of one test. Spherical bounding Gaussians (SBGs) \hat{a} , as introduced in Ref. [296, 300], lead naturally to class bounds, for example,

$$|[a_1 a_2 | b_1 b_2]| \leq [\hat{a}_1 \hat{a}_2 | \hat{b}_1 \hat{b}_2]. \quad (4.20)$$

Non-separable class bounds, such as (4.20), involve quantities that have the same asymptotic scaling as the integrals. Such bounds are therefore always scaling-consistent.

Separable class bounds, such as the Cauchy-Schwartz bound derived from (4.20)

$$|[a_1 a_2 | b_1 b_2]| \leq [\hat{a}_1 \hat{a}_1 | \hat{b}_1 \hat{b}_1]^{1/2} [\hat{a}_2 \hat{a}_2 | \hat{b}_2 \hat{b}_2]^{1/2} \quad (4.21)$$

involve factors that may scale differently from the integrals themselves. Such bounds may not be scaling-consistent.

A specific example may be helpful. The number of significant two-electron integrals over long-range and short-range operators is $\mathcal{O}(N^2)$ and $\mathcal{O}(N)$, respectively. However, the separable bound (4.21) predicts $\mathcal{O}(N^2)$ in both cases and is therefore scaling-inconsistent for short-range operators. In situations when one cannot find a scaling-consistent separable bound, one should use a non-separable bound.

Note that bounding an entire class of integrals with a single UB is a particularly desirable feature, especially when dealing with three- or four-electron integrals where the size of a class can be extremely large. For example, the simple $[ppp|ppp]$ and $[pppp|pppp]$ classes are made of 729 and 4,096 integrals!

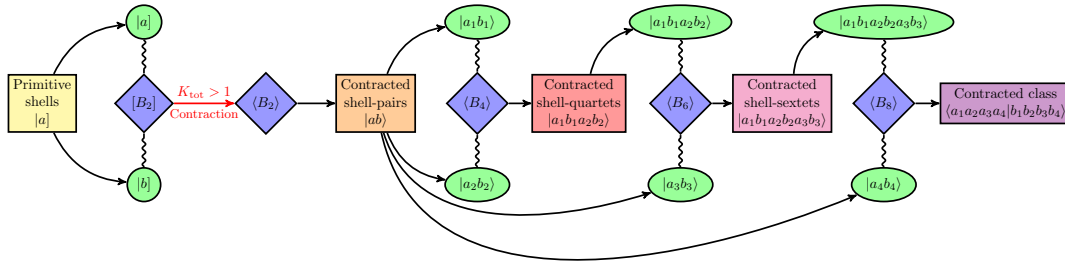


FIGURE 4.2: Schematic representation of the screening algorithm used to compute contracted four-electron integrals.

4.4.3 Shell-*mtuplet* bounds

A shell-*mtuplet* bound B_m relies only on shell-*mtuplet* information, where m is the shell multiplicity: shell-pair ($m = 2$), shell-quartet ($m = 4$), shell-sextet ($m = 6$), etc. If $B_m > \tau$, it indicates that the shell-*mtuplet* is significant, i.e. it could yield significant integrals. A shell-*mtuplet* bound is a class bound that depends only on the operator, the basis set and the shell multiplicity m , independent of the maximum shell multiplicity n of the integrals. It is also scaling-consistent at its specific shell-multiplet level.

4.4.4 Screening algorithm

Our screening algorithms are based on primitive, $[B_m]$, and contracted, $\langle B_m \rangle$, shell-*mtuplet* bounds. Figure 4.2 is a schematic representation of the overall screening scheme for contracted four-electron integrals. First, we use a primitive shell-pair bound $[B_2]$ to create a list of significant primitive shell-pairs. For a given contracted shell-pair, if at least one of its primitive shell-pairs has survived, a contracted shell-pair bound $\langle B_2 \rangle$ is used to decide whether or not this contracted shell-pair is worth keeping. The second step consists in using a shell-quartet bound $\langle B_4 \rangle$ to create a list of significant contracted shell-quartets by pairing the contracted shell-pairs with themselves. Then, we combine the significant shell-quartets and shell-pairs, and a shell-sextet bound $\langle B_6 \rangle$ identifies the significant contracted shell-sextets. Finally, the shell-sextets are paired with the shell-pairs. If the resulting shell-octet quantity is found to be significant, the contracted integral class $\langle a_1a_2a_3a_4|b_1b_2b_3b_4 \rangle$ must be computed via RRs, as discussed in the next section. Following this strategy, the size of any shell-*mtuplet* list is, at worst, quadratic in a large system.

During the shell-pair screening, either a contracted or a primitive path is followed depending on the degree of contraction of the integral class $K_{\text{tot}} = \prod_{i=1}^n K_{a_i} K_{b_i}$. If $K_{\text{tot}} > 1$, the contracted path is enforced, otherwise the primitive path is followed. This enables to adopt the more effective primitive bounds for primitive integral classes which are usually associated with medium and high angular momentum PGFs and, therefore, are more expensive to evaluate via RRs [300]. The scheme for primitive four-electron integrals differs only by the use of primitive bounds instead of contracted ones. The three-electron integrals screening scheme can be easily deduced from Fig. 4.2.

4.5 Recurrence relations

4.5.1 Vertical recurrence relations

Following Obara and Saika [260, 281], vertical RRs (VRRs) are obtained by differentiation of Eq. (4.12) with respect to the centers coordinates [263, 306]. For the integrals considered in this chapter, one can show that

$$\begin{aligned} [\cdots \mathbf{a}_i^+ \cdots]^m &= (\mathbf{Z}_i \mathbf{A}_i - \hat{D}_i Y_0) [\cdots \mathbf{a}_i \cdots]^m - (\hat{D}_i Y_1 - \hat{D}_i Y_0) [\cdots \mathbf{a}_i \cdots]^{m+1} \\ &+ \sum_{j=1}^n \mathbf{a}_j \left\{ \left(\frac{\delta_{ij}}{2\zeta_i} - \hat{D}_{ij} Y_0 \right) [\cdots \mathbf{a}_j^- \cdots]^m - (\hat{D}_{ij} Y_1 - \hat{D}_{ij} Y_0) [\cdots \mathbf{a}_j^- \cdots]^{m+1} \right\}, \end{aligned} \quad (4.22)$$

where δ_{ij} is the Kronecker delta [29],

$$\hat{D}_i = \frac{\nabla_{A_i}}{2\alpha_i}, \quad \hat{D}_{ij} = \hat{D}_i \hat{D}_j, \quad (4.23)$$

and

$$\hat{D}_i Y_u = \text{Tr}(\Delta_u \cdot \hat{D}_i \mathbf{Y}^2), \quad (\hat{D}_i \mathbf{Y}^2)_{kl} = \kappa_{ikl}(\mathbf{Y})_{kl}, \quad (4.24a)$$

$$\hat{D}_{ij} Y_u = \text{Tr}(\Delta_u \cdot \hat{D}_{ij} \mathbf{Y}^2), \quad (\hat{D}_{ij} \mathbf{Y}^2)_{kl} = \frac{\kappa_{ikl} \kappa_{jkl}}{2}, \quad (4.24b)$$

with

$$\varepsilon_{ij} = \begin{cases} 1, & \text{if } i \leq j, \\ 0, & \text{otherwise,} \end{cases} \quad \kappa_{ijk} = \frac{\varepsilon_{ij} \delta_{ki} - \delta_{ij} \varepsilon_{ki}}{\zeta_i}. \quad (4.25)$$

One can easily derive VRRs for other three- and four-electron operators following the simple rules given in Fig. 4.1. The number of terms for each of these VRRs is reported in Table 4.1 for various two-, three- and four-electron operators.

Note that for a pure GG operator, we have $m = 0$ and $Y_1 = Y_0$. Therefore, Eq. (4.22) reduces to a simpler expression:

$$[\cdots \mathbf{a}_i^+ \cdots] = (\mathbf{Z}_i \mathbf{A}_i - \hat{D}_i Y_0) [\cdots \mathbf{a}_i \cdots] + \sum_{j=1}^n \mathbf{a}_j \left(\frac{\delta_{ij}}{2\zeta_i} - \hat{D}_{ij} Y_0 \right) [\cdots \mathbf{a}_j^- \cdots]. \quad (4.26)$$

4.5.2 Transfer recurrence relations

Transfer RRs (TRRs) redistribute angular momentum between centres referring to different electrons [263]. Using the translational invariance, one can derive

$$[\cdots \mathbf{a}_i^+ \cdots] = \sum_{j=1}^n \frac{\mathbf{a}_j}{2\zeta_i} [\cdots \mathbf{a}_j^- \cdots] - \sum_{j \neq i}^n \frac{\zeta_j}{\zeta_i} [\cdots \mathbf{a}_j^+ \cdots] - \frac{\sum_{j=1}^n \beta_j \mathbf{A}_j \mathbf{B}_j}{\zeta_i} [\cdots \mathbf{a}_j \cdots]. \quad (4.27)$$

Note that Eq. (4.27) can only be used to build up angular momentum on the last center. Moreover, to increase the momentum by one unit on this last center, one must increase the momentum by the same amount on all the other centres (as evidenced by the second term in the right-hand side of (4.27)). Therefore, the TRR is computationally expensive for three- and four-electron integrals due to the large number of centres

TABLE 4.1: Number of intermediates required to compute various integral classes for two-, three- and four-electron operators. The path generating the minimum number of intermediates is highlighted in bold. The number of terms in the RRs and the associated incremental center are also reported.

Integral	type	operator	path	number of terms	centers	integral class				
						$[p\dots p]$	$[d\dots d]$	$[f\dots f]$	$[g\dots g]$	
two-electron	chain	G_{12}	VV	(2,3)	(A₂,A₁)	3	6	10	15	
			VT	(2,4)	(A ₂ ,A ₁)	4	9	16	25	
	C_{12}	VV	(4,6)	(A₂,A₁)	4	13	25	48		
		VT	(4,4)	(A ₂ ,A ₁)	7	19	37	61		
three-electron	chain	$G_{13}G_{23}$	VVV	(2,3,4)	(A₃,A₂,A₁)	5	13	26	45	
			VVT	(2,3,6)	(A ₃ ,A ₁ ,A ₂)	8	25	56	105	
		$C_{12}G_{23}$	VVV	(4,5,7)	(A ₃ ,A ₁ ,A ₂)	11	39	96	195	
			VVV	(4,6,6)	(A₃,A₂,A₁)	10	39	96	196	
	cyclic	$C_{12}G_{13}G_{23}$	VVT	(4,5,6)	(A ₃ ,A ₁ ,A ₂)	16	66	173	359	
			VVT	(4,6,6)	(A ₃ ,A ₂ ,A ₁)	15	65	171	357	
			VVV	(4,6,8)	(A₃,A₂,A₁)	12	46	119	250	
			VVT	(4,6,6)	(A ₃ ,A ₂ ,A ₁)	16	66	173	359	
four-electron	chain	$C_{12}G_{14}G_{23}$	VVVV	(4,5,7,8)	(A ₄ ,A ₃ ,A ₂ ,A ₁)	21	108	344	847	
			VVVV	(4,6,6,8)	(A₄,A₁,A₃,A₂)	19	88	260	607	
			VVVT	(4,5,7,8)	(A ₄ ,A ₃ ,A ₂ ,A ₁)	33	208	736	1,926	
			VVVT	(4,6,6,8)	(A ₄ ,A ₁ ,A ₃ ,A ₂)	33	204	716	1,866	
			$C_{12}G_{13}G_{34}$	VVVV	(4,6,6,9)	(A ₄ ,A ₃ ,A ₂ ,A ₁)	22	113	360	888
				VVVV	(4,6,8,7)	(A₄,A₃,A₁,A₂)	20	98	302	726
	trident	$C_{12}G_{13}G_{14}$	VVVT	(4,6,6,8)	(A ₄ ,A ₃ ,A ₂ ,A ₁)	33	204	716	1,866	
			VVVT	(4,6,8,8)	(A ₄ ,A ₃ ,A ₁ ,A ₂)	34	214	756	1,976	
			VVVV	(4,6,6,9)	(A ₄ ,A ₃ ,A ₂ ,A ₁)	22	113	360	888	
			VVVV	(4,6,8,7)	(A₄,A₃,A₁,A₂)	20	98	302	726	
			VVVT	(4,6,6,8)	(A ₄ ,A ₃ ,A ₂ ,A ₁)	33	204	716	1,866	
			VVVT	(4,6,8,8)	(A ₄ ,A ₃ ,A ₁ ,A ₂)	34	214	756	1,976	

(see below). As mentioned by Ahlrichs [306], the TRR can be beneficial for very high angular momentum two-electron integral classes.

4.5.3 Horizontal recurrence relations

The so-called horizontal RRs (HRRs) enable to shift momentum between centres over the same electronic coordinate [263]:

$$\langle \dots a_i \dots | \dots b_i^+ \dots \rangle = \langle \dots a_i^+ \dots | \dots b_i \dots \rangle + \mathbf{A}_i \mathbf{B}_i \langle \dots a_i \dots | \dots b_i \dots \rangle. \quad (4.28)$$

Note that HRRs can be applied to contracted integrals because they are independent of the contraction coefficients and exponents.

4.6 Algorithm

In this section, we present our recursive algorithm for the computation of a class of three- or four-electron integrals of arbitrary angular momentum. The present recursive algorithm is based on a late-contraction scheme inspired by the HGP algorithm [261] following a BOVVVCCCCHHHH path. The general skeleton of the algorithm is shown in Fig. 4.3 for the trident operator $C_{12}G_{13}G_{14}$. We will use this example to illustrate each step.

Based on the shell data, the first step of the algorithm (step B) is to decide whether or not a given class of integrals is significant or negligible. If the integral class is

found to be significant by the screening algorithm depicted in Fig. 4.2, an initial set of FIs is computed (step O).

Starting with these FIs, angular momentum is then built up over the different bra centres \mathbf{A}_1 , \mathbf{A}_2 , \mathbf{A}_3 and \mathbf{A}_4 using the VRRs derived in the previous section. To minimise the computational cost, one has to think carefully how to perform this step. Indeed, the cost depends on the order in which this increase in angular momentum is performed. This is illustrated in Fig. 4.4, where we have represented the various possible pathways for the 3-chain operator $C_{12}G_{23}$ (left) and the trident operator $C_{12}G_{13}G_{14}$ (right). The red path corresponds to the path generating the least intermediates (i.e. requiring the smallest number of classes in order to compute a given class). Different paths are compared in Table 4.1 for various two-, three- and four-electron operators, where we have reported the number of intermediates generated by each path for various integral classes.

Taking the 3-chain operator $C_{12}G_{23}$ as an example, one can see that, to compute a $[ppp]$ class, it is more advantageous to build momentum over center \mathbf{A}_3 , then over centres \mathbf{A}_2 , and finally over center \mathbf{A}_1 using VRRs with 4, 6 and 6 terms, respectively. The alternative path corresponding to building momentum over \mathbf{A}_3 , \mathbf{A}_1 , and then \mathbf{A}_2 with 4-, 5- and 7-term VRRs is slightly more expensive for a $[ppp]$ class but becomes affordable for high angular momentum classes. For both paths, using the TRR instead of the last VRR implies a large increase in the number of intermediates.

For the trident operator, we successively build angular momentum over \mathbf{A}_4 , \mathbf{A}_3 , \mathbf{A}_1 and \mathbf{A}_2 using VRRs with 4, 6, 8 and 7 terms. The pathway using VRRs with 4, 6, 6, and 9 terms is more expensive due to the large number of terms of the VRR building up momentum over the last center. Again, using the TRR instead of the last VRR significantly increases the number of intermediates.

The path involving the minimal number of intermediates is given in Table 4.1 for various two-, three- and four-electron operators. It is interesting to point out that it is never beneficial to use the TRR derived in Eq. (4.27).

One can easily show that, for operators involving the Coulomb operator, the number of intermediates required to compute a n -electron integral class $[a \dots a]$ increases as $\mathcal{O}(a^{n+1})$ for the VRR-only paths (see Table 4.1). This number is reduced to $\mathcal{O}(a^n)$ if one uses the TRR to build up angular momentum on the last center. However, the prefactor is much larger and the crossover happens for extremely high angular momentum for three- and four-electron integrals. For “pure” GG operators, such as G_{12} or $G_{13}G_{23}$, the number of intermediates required to compute a class $[a \dots a]$ increases as $\mathcal{O}(a^n)$ for any type of paths.

Finally, we note that the optimal path for the trident $C_{12}G_{13}G_{14}$ and the 4-chain $C_{12}G_{13}G_{34}$ is similar, thanks to their similar structure. Indeed, these two operators can be seen as two “linked” GGs ($G_{13}G_{14}$ or $G_{13}G_{34}$) interacting with the Coulomb operator C_{12} (see Fig. 4.1), while the other 4-chain operator $C_{12}G_{14}G_{23}$ can be seen as two “unlinked” GGs (G_{14} and G_{23}) interacting with the Coulomb operator.

When angular momentum has been built over all the bra centres, following the HGP algorithm [261], we contract $[a_1 a_2 a_3 a_4 | 0000]$ to form $\langle a_1 a_2 a_3 a_4 | 0000 \rangle$ (step CCCC). We can perform the contraction at this point because all of the subsequent RRs are independent of the contraction coefficients and exponents. More details about this contraction step can be found in Ref. [262].

The last step of the algorithm (step HHHH) shifts momentum from the bra center \mathbf{A}_1 , \mathbf{A}_2 , \mathbf{A}_3 and \mathbf{A}_4 to the ket centres \mathbf{B}_1 , \mathbf{B}_2 , \mathbf{B}_3 and \mathbf{B}_4 using the two-term HRRs given by Eq. (4.28).

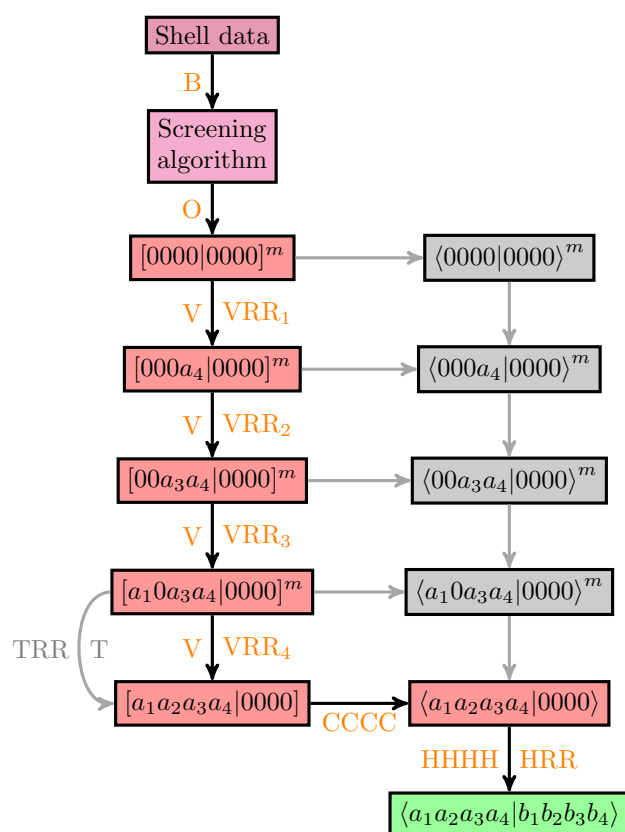


FIGURE 4.3: PRISM representation [307] of the recursive algorithm used to compute a four-electron integral class $\langle a_1 a_2 a_3 a_4 | b_1 b_2 b_3 b_4 \rangle$ over the trident operator $C_{12} G_{13} G_{14}$. In our algorithm, we consider the (orange) BOVVVCCCCCHHHH path.

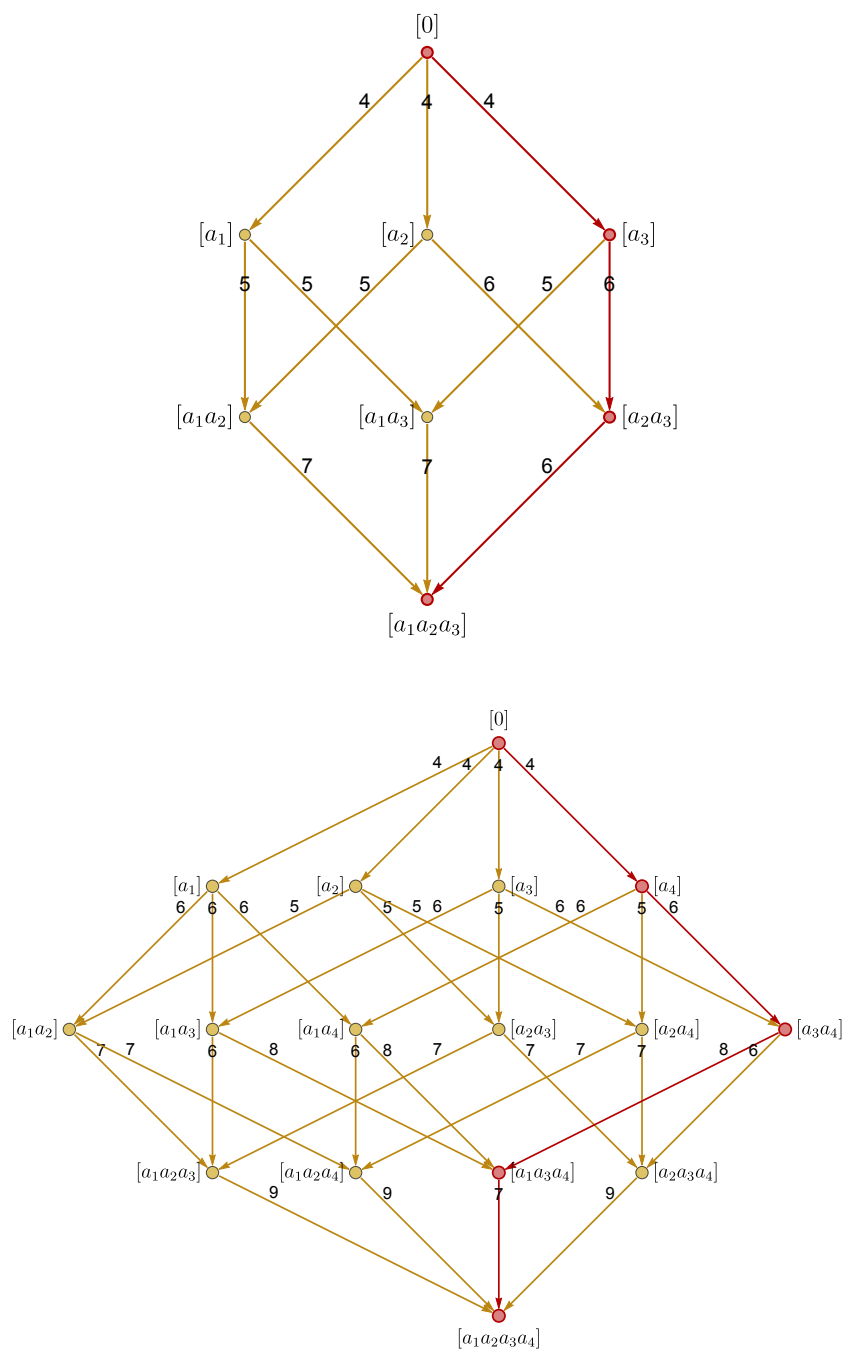


FIGURE 4.4: Graph representation of the VRRs for the 3-chain operator $C_{12}G_{23}$ (left) and trident operator $C_{12}G_{13}G_{14}$ (right). The edge label gives the number of terms in the corresponding VRR. The red path corresponds to the algorithm generating the smallest number of intermediates.

4.7 Summary

We have presented the three main ingredients to compute three- and four-electron integrals involving GGs. Firstly, a straightforward method to compute the FIs is given. Secondly, our UBs strategy is briefly discussed. Finally, the significant integrals are computed via a recursive scheme based on vertical and horizontal RRs, which can be viewed as an extension of the PRISM late-contraction path to three- and four-electron integrals. We believe our approach represents a major step towards an accurate and efficient computational scheme for three- and four-electron integrals. It also paves the way to contraction-effective methods for these types of integrals. In particular, an early-contraction scheme (including the contraction of both basis functions and Gaussian geminals) would have significant computational benefits.

Chapter 5

Future directions

5.1 Motivations

In the last decade, the advent of massively parallel computational platforms and their ever-growing capabilities in terms of number of computing nodes (exceeding now one million!) has unveiled new horizons for studying large quantum systems with genuine physical and/or chemical relevance (see Fig. 5.1). It is now widely recognised that there is an imperative need to revisit most of the standard algorithms (or design totally new ones!) to make sure that they take full advantage of these new supercomputer architectures and scale up to an arbitrary number of cores.

Unfortunately, because most of the computational chemistry methods developed so far are mainly based on iterative schemes for solving very large linear systems with stringent I/O and memory constraints, they intrinsically do not scale up, i.e. they are not able to deliver the result in an elapsed time (restitution time) inversely proportional to the number of cores (in the very large number of cores regime).

A class of methods known to scale up nicely are stochastic approaches. Taking advantage of this attractive feature, a number of authors has recently proposed to systematically revisit the traditional quantum chemistry methods to make them stochastic in nature. Note that the fundamental equations are identical, only the way of solving them is different. Let us mention the stochastic MP2 method of Hirata [308, 309], the FCI-QMC approach of Alavi and coworkers [310, 311], the stochastic coupled-cluster theory [312], and the stochastic CASSCF method [313]. Quite remarkably, in each case, it is found that the stochastic version is able to surpass the limits of the corresponding deterministic one. To give a concrete example, the authors of Ref. [313] have been able to perform a CASSCF calculation for the coronene molecule in a complete active space of 24 π electrons in 24 orbitals, a calculation impossible to perform using standard deterministic CASSCF implementations. Despite these impressive improvements, major limitations remain...

In this final chapter, we present two (unfinished) ideas. First, we present an explicitly-correlated version of the CI method. The key idea here is to combine QMC methods and traditional CI-type approaches. More precisely, we propose to exploit the extremely fast convergence properties of explicitly-correlated methods, and the multi-decade experience of quantum chemistry in building compact albeit accurate wave functions. The ultimate goal is to design a new highly accurate, black-box QMC method applicable to a wide range of chemical systems and able to run efficiently on current and future massively parallel computers (exascale horizon). Second, we describe a method for imposing the correct electron-nucleus (e-n) cusp in MOs expanded as a linear combination of (cusplless) Gaussian basis functions. Enforcing the e-n cusp in trial wave functions is an important asset in QMC calculations as it significantly reduces the variance of the local energy during the Monte Carlo sampling.

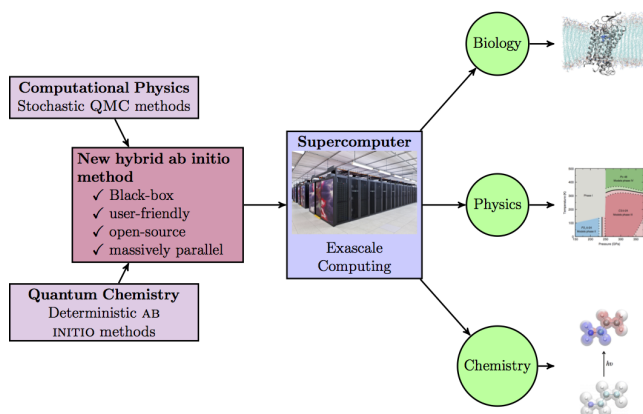


FIGURE 5.1: Concrete applications made possible thanks to the massively parallel nature of the hybrid deterministic/stochastic methods. Biology: study of the rhodopsin protein [314]; Physics: phase diagram of solid molecular hydrogen at extreme pressures [315]; Chemistry: absorption spectra in solution [316].

5.2 Explicitly-correlated FCI methods

One of the most fundamental problem of conventional electronic structure methods is their slow energy convergence with respect to the size of the one-electron basis set. This problem was already spotted thirty years ago by Kutzelnigg [88] who stated that

“traditional CI is not really bad, it only has difficulties to represent the wave function at those regions of configuration space where one interelectronic distance r_{ij} approaches zero.”

To address this problem he proposed to introduce explicitly the correlation between electrons via the introduction of the interelectronic distance r_{12} as a basis function [89, 317–320]. As mentioned in the previous chapter, this yields a prominent improvement of the energy convergence from $O(L^{-3})$ to $O(L^{-7})$ (where L is the maximum angular momentum of the one-electron basis). This idea was later generalised to more accurate correlation factors $f_{12} \equiv f(r_{12})$ [269, 270, 274–276, 291]. The resulting F12 methods achieve chemical accuracy for small organic molecules with relatively small Gaussian basis sets [233, 234, 293, 294]. For example, as illustrated by Tew and coworkers, one can obtain, at the CCSD(T) level, quintuple-zeta quality correlation energies with a triple-zeta basis [321].

Here, following Kutzelnigg’s idea, we propose to introduce the explicit correlation between electrons within the CI method via a dressing of the CI matrix [322, 323]. This method, involving effective Hamiltonian theory, has been shown to be successful in other scenarios [324]. Compared to other explicitly-correlated methods, this dressing strategy has the advantage of introducing the explicit correlation at a low computational cost. The present explicitly-correlated dressed CI method is completely general and can be applied to any type of truncated, full, or even selected CI methods [325–330]. However, for the sake of generality, we will discuss here the dressing of the FCI matrix.

5.2.1 Ansatz

Inspired by a number of previous research [331], our electronic wave function ansatz $|\Psi\rangle = |D\rangle + |F\rangle$ is simply written as the sum of a “conventional” part

$$|D\rangle = \sum_I c_I |I\rangle \quad (5.1)$$

composed by a linear combination of determinants $|I\rangle$ of coefficients c_I and an “explicitly-correlated” part

$$|F\rangle = \sum_I t_I \hat{Q} f |I\rangle \quad (5.2)$$

with coefficients t_I . The projector

$$\hat{Q} = \hat{I} - \sum_I |I\rangle\langle I| \quad (5.3)$$

ensures the orthogonality between $|D\rangle$ and $|F\rangle$, and

$$f = \sum_{i<j} \gamma_{ij} f_{ij} \quad (5.4)$$

is a correlation factor, and

$$\gamma_{ij} = \begin{cases} 1/2, & \text{for opposite-spin electrons,} \\ 1/4, & \text{for same-spin electrons.} \end{cases} \quad (5.5)$$

As first shown by Kato [109, 122] (and further elaborated by various authors [120, 123]), for small r_{12} , the two-electron correlation factor f_{12} in Eq. (5.4) must behave as

$$f_{12} = \gamma_{12} r_{12} + \mathcal{O}(r_{12}^2). \quad (5.6)$$

5.2.2 Dressing

Our primary goal is to introduce the explicit correlation between electrons at low computational cost. Therefore, assuming that $\hat{H}|\Psi\rangle = E|\Psi\rangle$, one can write, by projection over $\langle I|$,

$$c_I \left[H_{II} + c_I^{-1} \langle I|\hat{H}|F\rangle - E \right] + \sum_{J \neq I} c_J H_{IJ} = 0, \quad (5.7)$$

where $H_{IJ} = \langle I|\hat{H}|J\rangle$. Hence, we obtain the desired energy by diagonalising the dressed Hamiltonian:

$$\mathring{H}_{IJ} = \begin{cases} H_{II} + c_I^{-1} \langle I|\hat{H}|F\rangle, & \text{if } I = J, \\ H_{IJ}, & \text{otherwise,} \end{cases} \quad (5.8)$$

with

$$\langle I|\hat{H}|F\rangle = \sum_J t_J \left[\langle I|\hat{H}f|J\rangle - \sum_K H_{IK} f_{KJ} \right], \quad (5.9)$$

and $f_{IJ} = \langle I|f|J\rangle$. It is interesting to note that, in an infinite basis, we have $\langle I|\hat{H}|F\rangle = 0$, which demonstrates that our dressed CI method becomes exact in the limit of a complete one-electron basis.

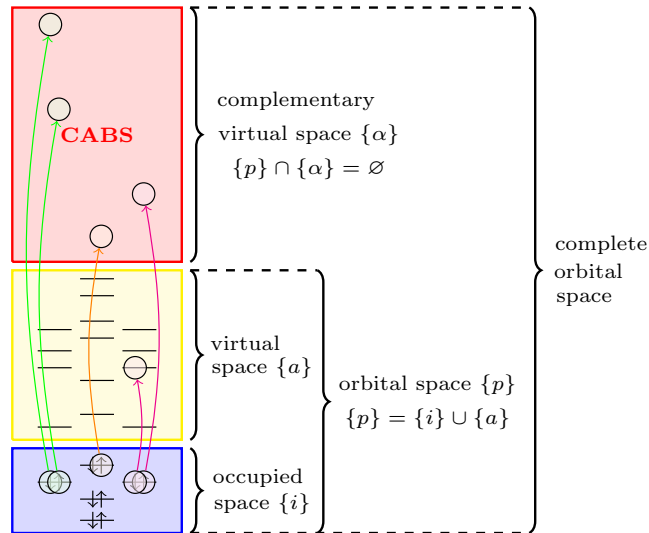


FIGURE 5.2: Schematic representation of the various orbital spaces and their notation. The arrows represent the three types of excited determinants contributing to the dressing: the pure doubles $|_{ij}^{\alpha\beta}\rangle$ (green), the mixed doubles $|_{ij}^{a\beta}\rangle$ (magenta) and the pure singles $|_i^\alpha\rangle$ (orange).

At this stage, two key comments are in order. First, as one may have realised, the coefficients t_I are unknown. However, they can be set to ensure the correct electron-electron cusp conditions [272].

This yields the following linear system of equations

$$\sum_I (\delta_{IJ} + f_{IJ}) t_J = c_I, \quad (5.10)$$

which can be easily solved using standard linear algebra packages.

Second, because Eq. (5.8) depends on the CI coefficient c_I , one must iterate the diagonalisation process self-consistently until convergence of the desired eigenvalues of the dressed Hamiltonian \hat{H} . At each iteration, we solve Eq. (5.10) to obtain the coefficients t_I and dress the Hamiltonian [see Eq. (5.8)]. In practice, we initially start with a CI vector obtained by the diagonalisation of the undressed Hamiltonian, and convergence is usually reached within few cycles. This iteration process can be also embedded in the Davidson diagonalisation process, which is also an iterative process. For pathological cases, a DIIS-like procedure may be employed [332, 333].

5.2.3 Matrix elements

Compared to a conventional CI calculation, new matrix elements are required. The simplest of them f_{IJ} — required in Eqs. (5.9) and (5.10) — can be easily computed by applying Slater-Condon rules [27]. They involve two-electron integrals over the geminal factor f_{12} . Their computation has been thoroughly studied in the literature in the last thirty years [89, 272, 273, 275, 276, 282, 286–292, 295, 296]. These can be more or less expensive to compute depending on the choice of the correlation factor.

As shown in Eq. (5.9), the present explicitly-correlated CI method also requires matrix elements of the form $\langle I | \hat{H} f | J \rangle$. These are more problematic, as they involve the computation of numerous three-electron integrals over the operator $r_{12}^{-1} f_{13}$, as well as new two-electron integrals [89, 286]. We have recently developed recurrence

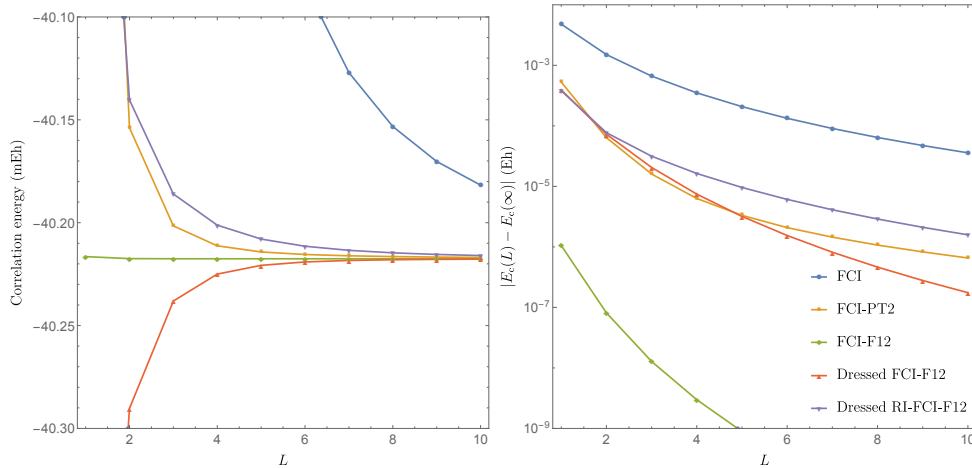


FIGURE 5.3: E_c for two electrons on a surface of a glocme of unit radius as a function of the maximum angular momentum of the basis set L . For each calculation, the maximum angular momentum of the auxiliary basis is set to $L_{\text{RI}} = 3L$.

relations and efficient upper bounds in order to compute these types of integrals [263, 265, 300, 334].

However, we will also explore a different route here. We propose to compute them using the RI approximation [89, 233, 266, 287, 335], which requires a complete basis set (CBS). This CBS is built as the union of the orbital basis set (OBS) $\{p\}$ (divided as occupied $\{i\}$ and virtual $\{a\}$ subspaces) augmented by a complementary auxiliary basis set (CABS) $\{\alpha\}$, such as $\{p\} \cap \{\alpha\} = \emptyset$ and $\langle p|\alpha\rangle = 0$ [287, 335] (see Fig. 5.2).

In the CBS, one can write

$$\hat{I} = \sum_{A \in \mathcal{A}} |A\rangle\langle A| \quad (5.11)$$

where \mathcal{A} is the set of all the determinants $|A\rangle$ corresponding to electronic excitations from occupied orbitals $\{i\}$ to the extended virtual orbital space $\{a\} \cup \{\alpha\}$. Substituting (5.11) into the first term of the right-hand side of Eq. (5.9), one gets

$$\begin{aligned} \langle I|\hat{H}|F\rangle &= \sum_J t_J \left[\sum_{A \in \mathcal{A}} H_{IA} f_{AJ} - \sum_{K \in \mathcal{D}} H_{IK} f_{KJ} \right] \\ &= \sum_J t_J \sum_{A \in \mathcal{C}} H_{IA} f_{AJ}, \end{aligned} \quad (5.12)$$

where \mathcal{D} is the set of “conventional” determinants obtained by excitations from the occupied space $\{i\}$ to the virtual one $\{a\}$, and $\mathcal{C} = \mathcal{A} \setminus \mathcal{D}$. Because f is a two-electron operator, the way to compute efficiently Eq. (5.12) is actually very similar to what is done within second-order multireference perturbation theory [336].

Although $\langle 0|\hat{H}|_i^a\rangle = 0$, note that the Brillouin theorem does not hold in the CABS, i.e. $\langle 0|\hat{H}|_i^\alpha\rangle \neq 0$. Here, we will eschew the generalized Brillouin condition (GBC) which set these to zero [89].

5.2.4 An illustrative example

To illustrate this method, we have computed the correlation energy of two electrons on a surface of a unit glocme — system we have presented earlier in the memoir — as a function of the maximum angular momentum of the basis set L . For each calculation,

the maximum angular momentum of the auxiliary (or RI) basis is set to $L_{\text{RI}} = 3L$. Note that here, because of the form of the exact wave function presented earlier, we used a correlation factor $f_{12} = r_{12}$.

Various methods have been considered:

1. the conventional FCI method which obviously corresponds to CISD here.
2. FCI-PT2 in which we compute a second-order Epstein-Nesbet perturbative correction using the auxiliary basis.
3. the FCI-F12 method where the explicitly-correlated basis function is treated variationally (i.e. no dressing).
4. the dressed FCI-F12 method presented here in which the energy is computed by projection and the dressing term is computed explicitly.
5. the same dressed FCI-F12 method where the dressing term is computed with the help of the auxiliary basis.

The results are depicted in Fig. 5.3. Few comments are in order:

- As expected, the convergence of the conventional FCI method is miserable.
- Treating the explicitly-correlated basis function variationally yields the fastest convergence but it requires the computation of expensive and numerous three- and four-electron integrals.
- the dressed FCI-F12 method significantly improves the convergence of the energy. With a relative small number of basis functions, one can reach sub-millihartree accuracy. However, the energy is not variational as it is calculated via projection.
- the PT2 correction allows to recover a significant fraction of the missing correlation energy. However, it does not produce a wave function one can use as a trial wave function for QMC calculations.
- the RI approximation induces a large error but still improve upon the conventional FCI method. Therefore, we believe that one should try to compute explicitly the three-electron integrals required in the dressed FCI-F12 method.

In regards to these results, we believe that the present dressed FCI-F12 method may be an interesting alternative for producing accurate and compact trial wave functions for DMC calculations. We hope to be able to consider more realistic systems in the near future as well as studying the nodal surfaces of these explicitly-correlated wave functions.

5.3 Self-consistent electron-nucleus cusp correction for molecular orbitals

At short interparticle distances, the Coulombic singularity dominates all other terms and, near the two-particle coalescence point, the behaviour of the exact wave function Ψ becomes independent of other details of the system [114]. In particular, early work

by Kato [109, 122], and elaborations by Pack and Byers Brown [123], showed that, as one electron at r_i approaches a nucleus of charge Z_A at r_A , we have

$$\left. \frac{\partial \langle \Psi(\mathbf{R}) \rangle}{\partial r_i} \right|_{r_i=r_A} = -Z_A \langle \Psi(\mathbf{R}) \rangle|_{r_i=r_A}, \quad (5.13)$$

where $\langle \Psi(\mathbf{R}) \rangle|_{r_i=r_A}$ is the spherical average of $\Psi(\mathbf{R})$ about $r_i = r_A$.

To remove divergences in the local energy at the electron-nucleus (e-n) coalescence points, cusp conditions such as (5.13) must be satisfied.¹ These divergences are especially harmful in DMC calculations, where they can lead to a large increase of the statistical variance, population-control problems and significant biases [67].

There are two possible ways to enforce the correct e-n cusp. One way to do it is to enforce the e-n cusp within the Jastrow factor in Eq. (1.48). This has the disadvantage of increasing the number of parameters in $J(\mathbf{R})$, and their interdependence can be tricky as one must optimise the large number of linear and non-linear parameters contained in $J(\mathbf{R})$ via a stochastic (noisy) optimization of the energy and/or its variance. However, it is frequently done in the literature thanks to some recent progress [337–339].

Here, we will follow an alternative path which consists in imposing the e-n cusp within the multideterminant expansion of Eq. (1.48). However, because one usually employs Gaussian basis functions [340] (as in standard quantum chemistry packages), the MOs $\phi_i(\mathbf{r})$ are cusplless, i.e.

$$\left. \frac{\partial \langle \phi_i(\mathbf{r}) \rangle}{\partial r} \right|_{r=r_A} = 0. \quad (5.14)$$

One solution would be to use a different set of basis functions [341] as, for instance, Slater basis functions [342, 343]. However, they are known to be troublesome, mainly due to the difficulty of calculating multicentric two-electron integrals which require expensive numerical expansions or quadratures. Nevertheless, some authors [344] have explored using wave functions built with Slater basis functions [345] while imposing the right e-n cusp afterwards.² These types of calculations can be performed with an electronic structure package such as ADF [347]. However, as far as we know, it is hard to perform large-scale calculations with Slater basis functions and the virtual space is usually poorly described. Moreover, Gaussian basis are usually of better quality than Slater-based ones due to the extensive knowledge and experience gathered by quantum chemists over the last fifty years while building robust, compact and effective Gaussian basis sets [205, 207, 348–359].

Conventional cusp correction methods usually replace the part of $\chi_\mu(\mathbf{r})$ or $\phi_i(\mathbf{r})$ close to the nuclei within a cusp-correction radius by a polynomial or a spline function which fulfils Kato cusp conditions and ensures a well-behaved local energy [360–363]. For atoms, one can also substitute Gaussian core orbitals by tabulated Slater-based ones [328, 364]. In the same vein, Toulouse and Umrigar have fitted Slater basis functions with a large number of Gaussian functions and replaced them within the QMC calculation [339]. However, it is hardly scalable for large systems due to its lack of transferability and the ever-growing number of primitive two-electron integrals to compute.

¹Note that the use of pseudopotentials would also remove the divergence at the e-n coalescence points as routinely done in QMC calculations.

²It is also possible to enforce the correct e-n cusp during the SCF process although it is rarely done [346].

Here, we propose to follow a different, alternative route by augmenting conventional Gaussian basis sets with cusp-correcting Slater basis functions. Mixed Gaussian-Slater basis sets have been already considered in the past with limited success due to the difficulty of computing efficiently mixed electron repulsion integrals [365–371]. However, we will show that, because of the way we introduce the cusp correction, the integrals required here are not that scary. For the sake of simplicity, we will focus on the HF formalism in the present study, although our scheme can also be applied to KS calculations.

5.3.1 Cusp-corrected orbitals

Assuming that the Jastrow factor does not contribute, a sufficient condition to ensure that Ψ_T (cf Eq. (1.48)) fulfils the e-n cusp (5.13) is that each (occupied and virtual) MO $\tilde{\phi}_i(\mathbf{r})$ satisfies the e-n cusp at each nuclear position \mathbf{r}_A :

$$\left. \frac{\partial \langle \tilde{\phi}_i(\mathbf{r}) \rangle}{\partial \mathbf{r}} \right|_{\mathbf{r}=\mathbf{r}_A} = -Z_A \langle \tilde{\phi}_i(\mathbf{r}) \rangle \Big|_{\mathbf{r}=\mathbf{r}_A}. \quad (5.15)$$

We also assume that the basis functions have been already orthogonalised via the standard procedure [27], i.e. $\langle \chi_\mu | \chi_\nu \rangle = \delta_{\mu\nu}$, where $\delta_{\mu\nu}$ is the Kronecker delta [29].

Here, we enforce the correct value of the e-n cusp by adding a cusp-correcting orbital to each MO:

$$\tilde{\phi}_i(\mathbf{r}) = \phi_i(\mathbf{r}) + \hat{P} \phi_i(\mathbf{r}), \quad (5.16)$$

with

$$\phi_i(\mathbf{r}) = \sum_A^M \tilde{c}_{Ai} \tilde{\chi}_A^i(\mathbf{r}), \quad (5.17)$$

where M is the number of nuclear centres and

$$\tilde{\chi}_A^i(\mathbf{r}) = \sqrt{\frac{\tilde{\alpha}_i^3}{\pi}} \exp[-\tilde{\alpha}_i |\mathbf{r} - \mathbf{r}_A|] \quad (5.18)$$

is a s-type Slater function centred on nucleus A with an orbital-dependent exponent $\tilde{\alpha}_i$. In Eq. (5.16), the projector

$$\hat{P} = \hat{I} - \sum_\mu |\chi_\mu\rangle\langle\chi_\mu| \quad (5.19)$$

(where \hat{I} is the identity operator) ensures orthogonality between $\phi_i(\mathbf{r})$ and the cusp-correcting orbital $\phi_i(\mathbf{r})$.

It is easy to show that ensuring the right e-n cusp yields the following linear system of equations for the coefficients c_{Ai} :

$$\sum_B \left[-\frac{\delta_{AB}}{Z_A} \partial_r \tilde{\chi}_A^i(\mathbf{r}_A) - \tilde{\chi}_B^i(\mathbf{r}_A) + \sum_\mu \tilde{S}_{B\mu}^i \chi_\mu(\mathbf{r}_A) \right] \tilde{c}_{Bi} = \phi_i(\mathbf{r}_A), \quad (5.20)$$

where the explicit expression of the matrix elements $\tilde{S}_{\mu A}^i = \langle \chi_\mu | \tilde{\chi}_A^i \rangle$ can be easily found using standard procedures and

$$\partial_r \tilde{\chi}_A^i(\mathbf{r}_A) \equiv \left. \frac{\partial \tilde{\chi}_A^i(\mathbf{r})}{\partial \mathbf{r}} \right|_{\mathbf{r}=\mathbf{r}_A}. \quad (5.21)$$

Equation (5.20) can be easily solved using standard linear algebra packages, and provides a way to obtain a cusp-corrected orbital $\tilde{\phi}_i(\mathbf{r})$ from a given MO $\phi_i(\mathbf{r})$. For reasons that will later become apparent, we will refer to this procedure as a one-shot (OS) calculation. Next, we are going to explain how one can optimise self-consistently the coefficients \tilde{c}_{Ai} .

5.3.2 Self-consistent dressing of the Fock matrix

So far, the coefficient \tilde{c}_{Ai} have been set via Eq. (5.20). Therefore, they have not been obtained via a variational procedure as their only purpose is to enforce the e-n cusp. However, they do depend on $\phi_i(\mathbf{r}_A)$, hence on the MO coefficients $c_{\mu i}$. We will show below that one can optimise simultaneously the coefficients \tilde{c}_{Ai} and $c_{\mu i}$ by constructing an orbital-dependent effective Fock matrix.

As it is ultimately what we wish for, the key point is to assume that $\tilde{\phi}_i(\mathbf{r})$ is an eigenfunction of the Fock operator \hat{F} , i.e.

$$\hat{F}|\tilde{\phi}_i\rangle = \tilde{\varepsilon}_i|\tilde{\phi}_i\rangle. \quad (5.22)$$

Note that, even at convergence of a conventional HF or KS calculation, the equality (5.22) is never fulfilled (unless the basis happens to span the exact orbital). This under-appreciated fact has been used by Deng et al. to design a measure of the quality of a MO [372].

Next, we project out Eq. (5.22) over $\langle\chi_\mu|$ yielding

$$\sum_\nu F_{\mu\nu}c_{\nu i} + \sum_A \tilde{c}_{Ai} \left(\tilde{F}_{\mu A}^i - \sum_\lambda F_{\mu\lambda} \tilde{S}_{\lambda A}^i \right) = \tilde{\varepsilon}_i c_{\mu i}, \quad (5.23)$$

where

$$F_{\mu\nu} = \langle\chi_\mu|\hat{F}|\chi_\nu\rangle, \quad \tilde{F}_{\mu A}^i = \langle\chi_\mu|\hat{F}|\tilde{\chi}_A^i\rangle. \quad (5.24)$$

In the general case, because we must use basis functions with non-zero derivatives at the nucleus, finding the matrix elements $\tilde{F}_{\mu A}^i$ is challenging and costly. However, because we are interested in the e-n cusp, we have found that a satisfactory approximation is

$$\tilde{F}_{\mu A}^i - \sum_\lambda F_{\mu\lambda} \tilde{S}_{\lambda A}^i \approx \tilde{h}_{\mu A}^i - \sum_\lambda H_{\mu\lambda}^c \tilde{S}_{\lambda A}^i \quad (5.25)$$

where

$$H_{\mu\nu}^c = \langle\chi_\mu|\hat{H}^c|\chi_\nu\rangle, \quad \tilde{h}_{\mu A}^i = \langle\chi_\mu|\hat{H}^c|\tilde{\chi}_A^i\rangle, \quad (5.26)$$

and \hat{H}^c is the core Hamiltonian. Note that, in Eq. (5.25), it is important to use the same approximation for both terms ($\tilde{F}_{\mu A}^i \approx \tilde{h}_{\mu A}^i$ and $F_{\mu\nu} \approx H_{\mu\nu}^c$) in order to preserve the subtle balance between the two terms. For the sake of clarity, the expression of the matrix elements $\tilde{h}_{\mu A}^i$ will not be reported here, but they can be obtained easily realising that these integrals only involve *s*-type Slater functions.

The eigenvalue problem given by Eq. (5.23) can be recast as

$$\sum_\nu \tilde{F}_{\mu\nu}^i c_{\nu i} = \tilde{\varepsilon}_i c_{\mu i}, \quad (5.27)$$

TABLE 5.1: Variational energy and its variance for various wave functions of the H atom. The energy is obtained with the decontracted STO-3G Gaussian basis set. The OS and SCD cusp-corrected energies are obtained by adding a Slater basis function of unit exponent ($\tilde{\alpha}_H = 1$) to the Gaussian basis set. The energy and variance at each iteration of the SCD process is also reported.

Basis	Cusp correction	Iteration	Energy	Variance
Gaussian	—		-0.495741	2.23×10^{-1}
Mixed	OS		-0.499270	4.49×10^{-2}
Mixed	SCD	#1	-0.499270	4.49×10^{-2}
		#2	-0.499970	3.07×10^{-6}
		#3	-0.500000	4.88×10^{-9}

where we have “dressed” the diagonal of the Fock matrix

$$\tilde{F}_{\mu\nu}^i = \begin{cases} F_{\mu\mu} + \tilde{D}_{\mu}^i & \text{if } \mu = \nu, \\ F_{\mu\nu}, & \text{otherwise,} \end{cases} \quad (5.28)$$

with

$$\tilde{D}_{\mu}^i = c_{\mu i}^{-1} \sum_A \tilde{c}_{Ai} \left(\tilde{h}_{\mu A}^i - \sum_{\lambda} H_{\mu\lambda}^c \tilde{S}_{\lambda A}^i \right). \quad (5.29)$$

The process is repeated until our convergence criteria is met, i.e. the largest absolute value of the elements of the commutator $\tilde{F}^i \mathbf{P} - \mathbf{P} \tilde{F}^i$ is lower than a given threshold, where \tilde{F}^i is the dressed Fock matrix (Eq. (5.28)) and \mathbf{P} is the density matrix with

$$P_{\mu\nu} = \sum_i^{\text{occ}} c_{\mu i} c_{\nu i}. \quad (5.30)$$

We will refer to this procedure as self-consistent dressing (SCD).

Similarly to the Perdew-Zunger self-interaction correction [170], the orbitals $\tilde{\phi}_i(\mathbf{r})$ are eigenfunctions of different Fock operators and therefore no longer necessarily orthogonal. Practically, we have found that the e-n cusp correction makes the cusp-corrected MOs $\tilde{\phi}_i$ slightly non-orthogonal. However, this is not an issue as, within QMC, one evaluates the energy via MC sampling which only requires the evaluation of the MOs and their first and second derivatives.

Obviously, as evidenced by Eq. (5.28), when $c_{\mu i}$ is small, the dressing of the Fock matrix is numerically unstable. Therefore, we have chosen not to dress the Fock matrix if $c_{\mu i}$ is smaller than a user-defined threshold τ . We have found that a value of 10^{-5} is suitable for our purposes, and we use the same value for the convergence threshold. Moreover, we have found that setting [361]

$$\tilde{\alpha}_i = \frac{\phi_i(\mathbf{r}_A)}{\hat{\phi}_i(\mathbf{r}_A)} Z_A \quad (5.31)$$

(where $\hat{\phi}_i(\mathbf{r})$ corresponds to the s -type components of $\phi_i(\mathbf{r})$ centred at \mathbf{r}_A) yields excellent results for molecular systems. In the case where $\hat{\phi}_i(\mathbf{r}_A) = 0$, the MO is effectively zero at $\mathbf{r} = \mathbf{r}_A$ and, therefore, does not need to be cusp corrected.

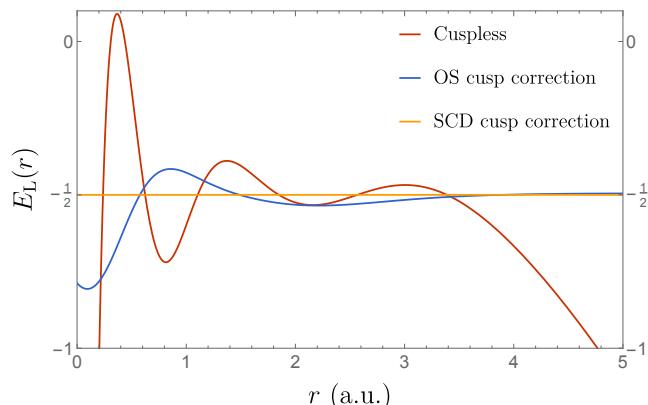


FIGURE 5.4: Local energy $E_L(r)$ for various wave functions of the H atom. The cuspless wave function is obtained with the decontracted STO-3G Gaussian basis set (red curve), and the OS and SCD cusp-corrected wave functions (blue and orange curves respectively) are obtained using $\tilde{\alpha}_H = 1$.

5.3.3 An illustrative example

Let us illustrate the present method with a simple example! For pedagogical purposes, we have computed the wave function of the hydrogen atom within a small Gaussian basis (decontracted STO-3G basis). In Fig. 5.4, we have plotted the local energy associated with this wave function as well as its OS and SCD cusp-corrected versions. The numerical results are reported in Table 5.1. As expected, the “cuspless” local energy (red curve) diverges for small r with a variational energy off by 4.3 millihartree compared to the exact value of $-1/2$. The OS cusp-correcting procedure which introduces a Slater basis function of unit exponent (but does not re-optimize any coefficients) cures the divergence at $r = 0$ and significantly improves (by roughly one order of magnitude) both the variational energy and the variance. Moreover, we observe that the long-range part of the wave function is also improved compared to the Gaussian basis set due to the presence of the Slater basis function which has the correct asymptotic decay. The SCD cusp-correcting procedure further improves upon the OS scheme, and we reach a variance lower than 10^{-8} after only 3 iterations.

Obviously, more tests are required to ensure the validity of the method but we believe that the present results are encouraging and we hope to pursue this study in the near future.

5.4 Summary

In the last chapter of this memoir, we have presented two lines of our current research. First, we have introduced a dressed version of the well-established CI method to incorporate explicitly the correlation between electrons. We have shown that the new CI-F12 method allows to fix one of the main issues of conventional CI methods, i.e. the slow convergence of the electronic energy with respect to the size of the one-electron basis set. Albeit not variational, our method is able to catch a large fraction of the basis set incompleteness error at a low computational cost compared to other variants. In particular, one eschews the computation of four-electron integrals as well as some types of three-electron integrals. We believe that the present approach could be a significant step towards the development of an accurate and efficient explicitly-correlated FCI methods.

Second, we have proposed a procedure to enforce the e-n cusp by augmenting conventional (cusplless) Gaussian basis sets with cusp-correcting Slater basis functions. Two types of procedure has been presented. In the one-shot procedure, the coefficients of the Slater functions are obtained by ensuring the correct e-n cusp at each nucleus. We have also designed a self-consistent procedure to optimise simultaneously the coefficients of the Gaussian and Slater basis functions by diagonalisation of an orbital-dependent effective Fock operator. The same procedure could potentially be employed to correct the long-range part of the electronic density with obvious application within DFT.

Conclusion

In this memoir, I have presented succinctly some of the research projects we have been pursuing in the last ten years. Moreover, I have discussed two of our current research topics in the final chapter. As concluding remarks, I would like to talk further about various research projects we would like to work on in the years to come. This is a non-exhaustive list in no particular order but I hope it will give to the reader a feeling about what we are trying to achieve.

What is the exact Green function? As mentioned earlier in the memoir, exactly solvable models are particularly valuable for testing theoretical approaches. Here, we would like to use the electrons-on-a-sphere model presented above to unveil the form of the exact Green function [373]. Green function-based methods allows an explicit incorporation of the electronic correlation effects through a summation of Feynman diagrams. Important properties such as total energies, ionisation potentials, electron affinities as well as photo-emission spectra can be obtained directly from the Green function. A particularly successful variant of these methods in electronic-structure calculations is the so-called GW approximation, which consists in evaluating the self-energy Σ starting from the Green function G using a sequence of self-consistent steps (see Fig. 5.5).

Thanks to this toy system, our preliminary results show that we might be able to compute self-consistently Σ . This will help us understand approximation such as G_0W_0 where one eschews the iterative process. More importantly, we might be able to obtain the closed-form expression of the vertex correction Γ — a quantity hardly accessible in real systems — and complete the entire five-step self-consistent process (see Fig. 5.5). This could shed lights on how to approximate wisely the vertex function in real systems.

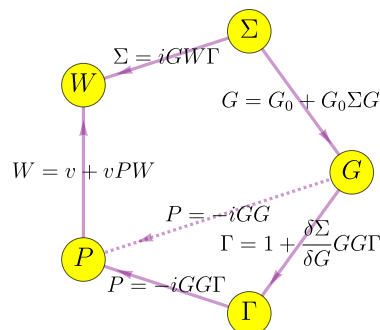


FIGURE 5.5: Hedin's pentagon [374].

GLDA correlation functional In Sec. 3.2, we have presented an exchange functional based on FUEGs. In order to create the associated correlation functional, one would need to compute accurate energies of FUEGs for various number of electrons and densities. One of the method of choice to achieve this would probably be DMC. Sadly, DMC on a curved manifold (like a D -sphere) is not as easy as one would have thought.

What are the modifications required to the VMC and DMC algorithms to perform calculations of electrons in curved manifolds? While the modifications required for the VMC algorithm are fairly straightforward [81, 375, 376], the modifications one has to do in the DMC algorithm are much more subtle. DMC on a curved manifold has received very little attention in the past. To the best of our knowledge, the only work related to this has been done by Ortiz and coworkers to calculate the energy of composite fermions on the Haldane sphere [377]. On a curved manifold, when moving the electrons, one has to make sure that the move keeps the electrons on the surface of the sphere.

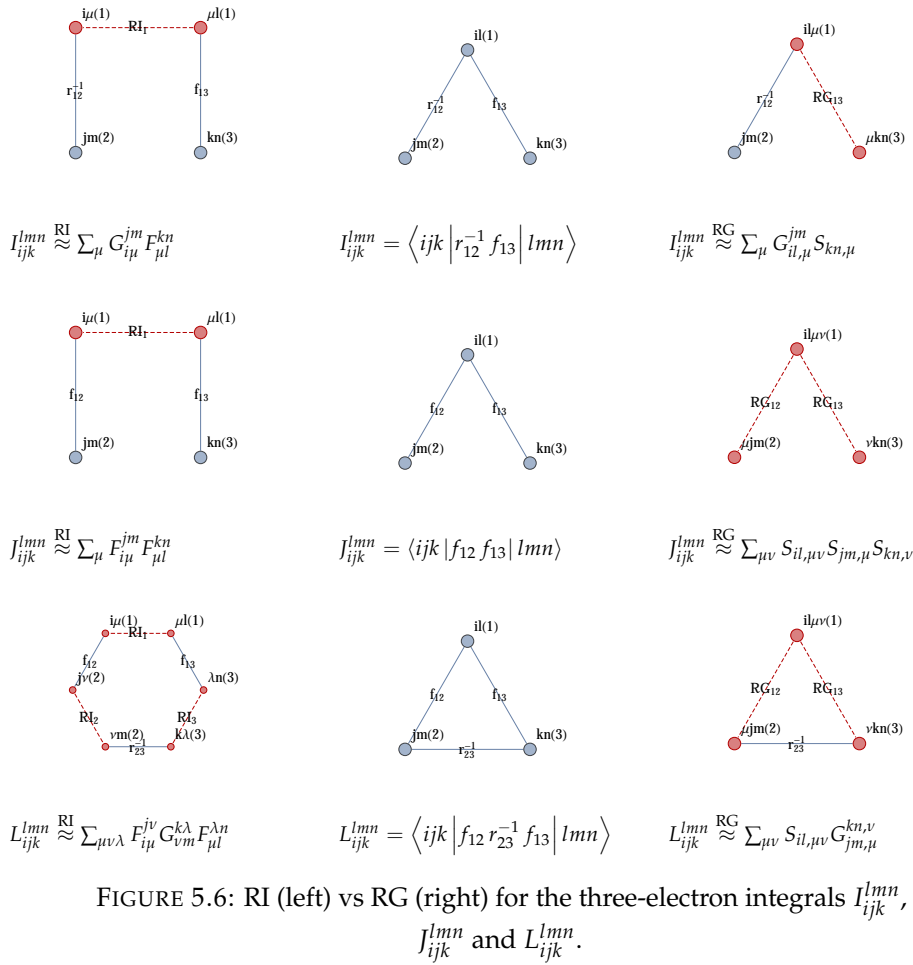
In VMC, the only required modification is the Metropolis acceptance probability [81, 376]. On a curved manifold, the DMC algorithm requires modifications in the diffusion and drift processes. The branching process is not affected by the curved nature of the manifold. The major difference appears in the calculation of the short-time approximation of the Green function

This “curved” DMC method could be efficiently implemented in the local QMC software package (QMC=Chem) developed by Scemama, Caffarel and coworkers [327]. This would allow to perform DMC calculations and obtain the near-exact energies of FUEGs required to build the three-dimensional version of the GLDA correlation functional, similarly to what we have done in the one-dimensional case [188, 189].

Symmetry-broken LDA Within DFT, the LDA correlation functional is typically built by fitting the difference between the near-exact and HF energies of the UEG, together with analytic perturbative results from the high- and low-density regimes. Near-exact energies are obtained by performing accurate DMC calculations, while HF energies are usually assumed to be the Fermi fluid HF energy. However, it has been known since the seminal work of Overhauser [378, 379] that one can obtain lower, symmetry-broken (SB) HF energies at any density [380–386]. Recently, we have computed the SBHF energies of the one-dimensional UEG [26, 187] and constructed a SB version of the LDA (SBLDA) from these results [185]. The newly designed functional, which we have named SBLDA, has shown to surpass the performance of its LDA parent in providing better estimates of the correlation energy in one-dimensional systems [184, 186, 188, 189, 387]. Based on the same methodology, we would like to design of new exchange and correlation functionals for two- and three-dimensional systems for which SBHF calculations have already been performed [380, 383–385].

Resolution of geminals The main idea behind the “resolution of geminals” (RG) is a generalisation of the resolution of the identity (RI). To explain what we mean by this, let us state the RI identity in its two-electron version, i.e.

$$\delta(r_{12}) = \sum_{\mu}^{\infty} |\chi_{\mu}(r_1)\rangle\langle\chi_{\mu}(r_2)|, \quad (5.32)$$



where $\delta(r)$ is the Dirac delta function and the one-electron basis set $\chi_{\mu}(\mathbf{r})$ is formally complete. In other words, we have just “resolved” the Dirac delta function, i.e. we wrote a two-electron function as a sum of products of one-electron functions. One can show that most of the usual two-electron operators used in quantum chemistry can be written in a similar form.

For example, one can write a Gaussian geminal, using a Gauss-Hermite quadrature, as [388]

$$G_{12} = \sum_{n\ell m} |\phi_{n\ell m}(\mathbf{r}_1)\rangle\langle\phi_{n\ell m}(\mathbf{r}_2)|, \quad (5.33)$$

with

$$\phi_{n\ell m}(\mathbf{r}) = \sqrt{8\pi^{1/2}b_n\beta_n} j_{\ell}(2\sqrt{\lambda}\beta_n r) Y_{\ell m}(\mathbf{r}), \quad (5.34)$$

where β_n and b_n are the (positive) Hermite roots and weights, and $j_n(r)$ is a spherical Bessel function of the first kind [29]. A similar expression can be found for the long-range Coulomb operator, the Slater geminal and many others.

In this way, as one inserts the RI “in-between” two operators, one can now resolve operators! This is illustrated diagrammatically in Fig. 5.6 for some of the three-electron integrals involved in explicitly-correlated methods. This procedure generates new integrals as one has to deal with spherical Bessel functions now. However, these are only one- and two-electron integrals.

A zero-variance hybrid MP2 method The stochastic MP2 algorithm developed by Hirata and coworkers [232, 308, 309, 389] has been shown to be particularly promising due to its low computational scaling and its independence towards the correlation factor [390]. We propose to investigate two potential improvements of So Hirata’s stochastic MP2 algorithm. First, following the philosophy of the multireference perturbation theory algorithm we have published recently [336], we would like to introduce a small deterministic orbital window. It would allow to catch the largest fraction of the MP2 correlation energy using a small number of MOs around the Fermi level.³ This would significantly reduce the statistical error of the stochastic part because the magnitude of the statistical error in a Monte Carlo calculation is proportional to the magnitude of the actual expectation value one is actually computing. Second, we would like to propose a zero-variance version of Hirata’s stochastic algorithm [392]. Indeed, one of the weak point of his algorithm comes from the choice of the probability distribution function. Surely, a zero-variance algorithm would significantly decrease the statistical error on the MP2 correlation energy.

Chemistry without Coulomb singularity One of the most annoying feature of the Coulomb operator is its divergence as $r_{12} \rightarrow 0$. Indeed, the exact wave function must have a well-defined cusp at electron coalescences so that the infinite Coulomb interaction is exactly cancelled by an opposite divergence in the kinetic term. Removing such a divergence would have one very important consequence: accelerating the rate of convergence of the energy with respect to the one-electron basis set (see, for example, Ref. [393]).

A well-known procedure to remove the Coulomb singularity is to use a range-separated operator [394]:

$$\frac{1}{r_{12}} = \frac{\operatorname{erfc}(\omega r_{12})}{r_{12}} + \frac{\operatorname{erf}(\omega r_{12})}{r_{12}}, \quad (5.35)$$

where $\operatorname{erf}(x)$ is the error function and $\operatorname{erfc}(x) = 1 - \operatorname{erf}(x)$ its complementary version. The parameter ω controls the separation range. For $\omega = 0$, the long-range interaction vanishes while, for $\omega \rightarrow \infty$, the short range disappears. In range-separated methods, two different methods are usually used for the short-range and long-range parts. For example, in range-separated DFT, one usually used DFT for the short-range interaction and a wave function method (such as MP2) to model the long-range part [395].

Here, we propose something slightly different. What if we approximate the Coulomb operator by its long-range component only, i.e.

$$\frac{1}{r_{12}} \approx \frac{\operatorname{erf}(\omega r_{12})}{r_{12}}, \quad (5.36)$$

with ω large enough to be chemically meaningful? The variational energy would definitely be altered by such a choice [396]. But what about the nodes? At the end of the day, the nodes are the only things which matters in DMC! Are the nodes obtained with this attenuated Coulomb operator worse than the ones obtained with the genuine, singular Coulomb operator? As stated above, the singularity of the Coulomb operator gives birth to Kato’s cusp. However, for a same-spin electron pair, the node in the wave function at $r_{12} = 0$ is produced by the antisymmetry of the

³This idea is somewhat related to the semi-stochastic FCIQMC algorithm developed by Umrigar and coworkers [391].

wave function (Pauli exclusion principle). For an opposite-spin electron pair, Kato taught us that the wave function is non-zero at $r_{12} = 0$. In other words, there can't be a node! Therefore, one could argue that removing the Coulomb singularity would have a marginal effect on the nodal surface of the electronic wave function. This is what we would like to investigate in the future.

Another possibility would be to create a local or non-local pseudopotential for the electron-electron interaction.

Bibliography

- ¹A. Fornili, P.-F. Loos, X. Assfeld, and M. Sironi, *Chem. Phys. Lett.* **427**, 236 (2006).
- ²P. F. Loos, and X. Assfeld, *J. Chem. Theor. Comput.* **3**, 1047 (2007).
- ³P. F. Loos, and X. Assfeld, *Int. J. Quantum. Chem.* **107**, 2343 (2007).
- ⁴P. F. Loos, J. Preat, A. D. Laurent, C. Michaux, D. Jacquemin, E. A. Perpète, and X. Assfeld, *J. Chem. Theor. Comput.* **4**, 637 (2008).
- ⁵E. Dumont, P. F. Loos, and X. Assfeld, *Chem. Phys. Lett.* **458**, 276 (2008).
- ⁶E. Dumont, P. F. Loos, A. D. Laurent, and X. Assfeld, *J. Chem. Theory Comput.* **4**, 171 (2008).
- ⁷E. Dumont, P. F. Loos, and X. Assfeld, *J. Phys. Chem. B* **112**, 13661 (2008).
- ⁸E. Dumont, A. D. Laurent, P. F. Loos, and X. Assfeld, *J. Chem. Theory Comput.* **5**, 1700 (2009).
- ⁹P. F. Loos, E. Dumont, A. D. Laurent, and X. Assfeld, *Chem. Phys. Lett.* **475**, 120 (2009).
- ¹⁰D. Ambrosek, P. F. Loos, X. Assfeld, and C. Daniel., *J. Inorg. Biochem.* **104**, 893 (2010).
- ¹¹P. F. Loos, and P. M. W. Gill, *Phys. Rev. A* **79**, 062517 (2009).
- ¹²P. F. Loos, and P. M. W. Gill, *J. Chem. Phys.* **131**, 241101 (2009).
- ¹³P. F. Loos, and P. M. W. Gill, *Chem. Phys. Lett.* **500**, 1 (2010).
- ¹⁴P. F. Loos, and P. M. W. Gill, *Phys. Rev. A* **81**, 052510/1–9 (2010).
- ¹⁵P. F. Loos, and P. M. W. Gill, *J. Chem. Phys.* **132**, 234111 (2010).
- ¹⁶P.-F. Loos, and P. M. W. Gill, *Phys. Rev. Lett.* **105**, 113001 (2010).
- ¹⁷P. F. Loos, and P. M. W. Gill, *Phys. Rev. Lett.* **103**, 123008 (2009).
- ¹⁸P. F. Loos, *Phys. Rev. A* **81**, 032510 (2010).
- ¹⁹P. F. Loos, and P. M. W. Gill, *Mol. Phys.* **108**, 2527 (2010).
- ²⁰P. F. Loos, and P. M. W. Gill, *Phys. Rev. Lett.* **108**, 083002 (2012).
- ²¹P. F. Loos, *Phys. Lett. A* **376**, 1997 (2012).
- ²²Y. Zhao, P. F. Loos, and P. M. W. Gill, *Phys. Rev. A* **84**, 032513/1–5 (2011).
- ²³P. F. Loos, and P. M. W. Gill, *J. Chem. Phys.* **135**, 214111 (2011).
- ²⁴P. F. Loos, and P. M. W. Gill, *Phys. Rev. B* **83**, 233102 (2011).
- ²⁵P. F. Loos, and P. M. W. Gill, *Phys. Rev. B* **84**, 033103 (2011).
- ²⁶P. F. Loos, *J. Chem. Phys.* **138**, 064108 (2013).
- ²⁷A. Szabo, and N. S. Ostlund, *Modern quantum chemistry : introduction to advanced structure theory* (Dover publications Inc., Mineola, New-York, 1989).
- ²⁸T. Helgaker, P. Jørgensen, and J. Olsen, *Molecular electronic-structure theory* (John Wiley & Sons, Ltd., 2000).

- ²⁹F. W. J. Olver, D. W. Lozier, R. F. Boisvert, and C. W. Clark, eds., *Nist handbook of mathematical functions* (Cambridge University Press, New York, 2010).
- ³⁰F. Jensen, *Introduction to computational chemistry* (Wiley, New York, 1999).
- ³¹C. J. Cramer, *Essentials of computational chemistry: theories and models* (Wiley, 2004).
- ³²P. Hohenberg, and W. Kohn, *Phys. Rev.* **136**, B864 (1964).
- ³³W. Kohn, and L. J. Sham, *Phys. Rev.* **140**, A1133 (1965).
- ³⁴R. G. Parr, and W. Yang, *Density-functional theory of atoms and molecules* (Oxford, Clarendon Press, 1989).
- ³⁵A. D. Becke, *J. Chem. Phys.* **140**, 18A301 (2014).
- ³⁶H. S. Yu, S. L. Li, and D. G. Truhlar, *J. Chem. Phys.* **145**, 130901 (2016).
- ³⁷J. P. Perdew, and K. Schmidt, *AIP Conf. Proc.* **577**, 1 (2001).
- ³⁸J. P. Perdew, A. Ruzsinszky, J. Tao, V. N. Staroverov, G. E. Scuseria, and G. I. Csonka, *J. Chem. Phys.* **123**, 062201 (2005).
- ³⁹P. A. M. Dirac, *Proc. Cam. Phil. Soc.* **26**, 376–385 (1930).
- ⁴⁰P. F. Loos, and P. M. W. Gill, *WIREs Comput. Mol. Sci.* **6**, 410 (2016).
- ⁴¹D. M. Ceperley, and B. J. Alder, *Phys. Rev. Lett.* **45**, 566 (1980).
- ⁴²S. H. Vosko, L. Wilk, and M. Nusair, *Can. J. Phys.* **58**, 1200 (1980).
- ⁴³A. D. Becke, *Phys. Rev. A* **38**, 3098 (1988).
- ⁴⁴P. M. W. Gill, *Mol. Phys.* **89**, 433 (1996).
- ⁴⁵J. P. Perdew, “Electronic structure of solids ‘91”, in, edited by P. Ziesche, and H. Eschrig, (Akademie Verlag, Berlin, 1991), p. 11.
- ⁴⁶J. P. Perdew, K. Burke, and M. Ernzerhof, *Phys. Rev. Lett.* **77**, 3865 (1996).
- ⁴⁷C. Lee, W. Yang, and R. G. Parr, *Phys. Rev. B* **37**, 785 (1988).
- ⁴⁸A. D. Becke, *J. Chem. Phys.* **88**, 1053 (1988).
- ⁴⁹F. Della Sala, E. Fabiano, and L. A. Constantin, *Int. J. Quantum Chem.* **116**, 1641 (2016).
- ⁵⁰Y. Zhao, and D. G. Truhlar, *J. Chem. Phys.* **125**, 194101 (2006).
- ⁵¹J. Wellendorff, K. T. Lundgaard, K. W. Jacobsen, and T. Bligaard, *J. Chem. Phys.* **140**, 144107 (2014).
- ⁵²J. Sun, A. Ruzsinszky, and J. P. Perdew, *Phys. Rev. Lett.* **115**, 036402 (2015).
- ⁵³J. Sun, B. Xiao, and A. Ruzsinszky, *J. Chem. Phys.* **137**, 051101 (2012).
- ⁵⁴J. Sun, R. Haunschild, B. Xiao, I. Bulik, G. E. Scuseria, and J. P. Perdew, *J. Chem. Phys.* **138**, 044113 (2013).
- ⁵⁵A. D. Becke, *J. Chem. Phys.* **98**, 5648 (1993).
- ⁵⁶J. P. Perdew, and Y. Wang, *Phys. Rev. B* **45**, 13244 (1992).
- ⁵⁷J. P. Perdew, K. Burke, and Y. Wang, *Phys. Rev. B* **54**, 16533 (1996).
- ⁵⁸A. D. Becke, *J. Chem. Phys.* **98**, 1372 (1993).
- ⁵⁹C. Adamo, and V. Barone, *J. Chem. Phys.* **110**, 6158 (1999).
- ⁶⁰C. J. Umrigar, “Quantum monte carlo methods in physics and chemistry”, in, edited by M. P. Nightingale, and C. J. Umrigar, NATO Science Series (Kluwer Academic Press, Dordrecht, 1999), pp. 129–160.

- ⁶¹M. H. Kalos, D. Levesque, and L. Verlet, *Phys. Rev. A* **9**, 2178 (1974).
- ⁶²D. M. Ceperley, and M. H. Kalos, "Monte carlo methods in statistical physics", in, edited by K. Binder, (Springer Verlag, Berlin, 1979).
- ⁶³P. J. Reynolds, D. M. Ceperley, B. J. Alder, and W. A. Lester, Jr., *J. Chem. Phys.* **77**, 5593 (1982).
- ⁶⁴J. Kolorenc, and L. Mitás, *Rep. Prog. Phys.* **74**, 026502 (2011).
- ⁶⁵C. J. Umrigar, M. P. Nightingale, and K. J. Runge, *J. Chem. Phys.* **99**, 2865 (1993).
- ⁶⁶C.-J. Huang, C. J. Umrigar, and M. P. Nightingale, *J. Chem. Phys.* **107**, 3007 (1997).
- ⁶⁷N. D. Drummond, M. D. Towler, and R. J. Needs, *Phys. Rev. B* **70**, 235119 (2004).
- ⁶⁸P. Lopez-Rios, S. Seth, N. D. Drummond, and R. J. Needs, *Phys. Rev. E* **86**, 036703 (2012).
- ⁶⁹D. M. Ceperley, *J. Stat. Phys.* **63**, 1237 (1991).
- ⁷⁰W. A. Glauser, W. R. Brown, W. A. Lester Jr., D. Bressanini, B. L. Hammond, and M. L. Koszykowski, *J. Chem. Phys.* **97**, 9200 (1992).
- ⁷¹D. Bressanini, D. M. Ceperley, and P. Reynolds, "What do we know about wave function nodes?", in *Recent advances in quantum monte carlo methods*, Vol. 2, edited by W. A. Lester Jr., S. M. Rothstein, and S. Tanaka, (World Scientific, 2001).
- ⁷²D. Bressanini, and P. J. Reynolds, *Phys. Rev. Lett.* **95**, 110201 (2005).
- ⁷³M. Bajdich, L. Mitás, G. Drobny, and L. K. Wagner, *Phys. Rev. B* **72**, 075131 (2005).
- ⁷⁴D. Bressanini, G. Morosi, and S. Tarasco, *J. Chem. Phys.* **123**, 204109 (2005).
- ⁷⁵T. C. Scott, A. Luchow, D. Bressanini, and J. D. Morgan III, *Phys. Rev. A* **75**, 060101 (2007).
- ⁷⁶L. Mitás, *Phys. Rev. Lett.* **96**, 240402 (2006).
- ⁷⁷L. Mitás, "Fermion nodes and nodal cells of noninteracting and interacting fermions", arXiv:cond-mat:/0605550 (2008).
- ⁷⁸D. Bressanini, and G. Morosi, *J. Chem. Phys.* **129**, 054103 (2008).
- ⁷⁹D. Bressanini, *Phys. Rev. B* **86**, 115120 (2012).
- ⁸⁰D. J. Klein, and H. M. Pickett, *J. Chem. Phys.* **64**, 4811 (1976).
- ⁸¹P. F. Loos, and D. Bressanini, *J. Chem. Phys.* **142**, 214112 (2015).
- ⁸²Y. Kwon, D. M. Ceperley, and R. M. Martin, *Phys. Rev. B* **58**, 6800 (1998).
- ⁸³A. Luchow, and T. C. Scott, *J. Phys. B: At. Mol. Opt. Phys.* **40**, 851 (2007).
- ⁸⁴A. Luchow, R. Petz, and T. C. Scott, *J. Chem. Phys.* **126**, 144110 (2007).
- ⁸⁵F. D. M. Haldane, *Phys. Rev. Lett.* **51**, 605 (1983).
- ⁸⁶P. F. Loos, and P. M. W. Gill, *Phys. Lett. A* **378**, 329 (2014).
- ⁸⁷A. G. Ushveridze, *Quasi-exactly solvable models in quantum mechanics* (Institute of Physics Publishing, 1994).
- ⁸⁸W. Kutzelnigg, *Theor. Chim. Acta* **68**, 445 (1985).
- ⁸⁹W. Kutzelnigg, and W. Klopper, *J. Chem. Phys.* **94**, 1985 (1991).
- ⁹⁰T. M. Henderson, and R. J. Bartlett, *Phys. Rev. A* **70**, 022512 (2004).
- ⁹¹D. Bokhan, S. Ten-no, and J. Noga, *Phys. Chem. Chem. Phys.* **10**, 3320 (2008).
- ⁹²N. R. Kestner, and O. Sinanoglu, *Phys. Rev.* **128**, 2687 (1962).

- ⁹³S. Kais, D. R. Herschbach, and R. D. Levine, *J. Chem. Phys.* **91**, 7791 (1989).
- ⁹⁴M. Taut, *Phys. Rev. A* **48**, 3561 (1993).
- ⁹⁵G. S. Ezra, and R. S. Berry, *Phys. Rev. A* **25**, 1513 (1982).
- ⁹⁶G. S. Ezra, and R. S. Berry, *Phys. Rev. A* **28**, 1989 (1983).
- ⁹⁷P. C. Ojha, and R. S. Berry, *Phys. Rev. A* **36**, 1575 (1987).
- ⁹⁸R. J. Hinde, and R. S. Berry, *Phys. Rev. A* **42**, 2259 (1990).
- ⁹⁹J. W. Warner, and R. S. Berry, *Nature* **313**, 160 (1985).
- ¹⁰⁰M. Seidl, J. P. Perdew, and S. Kurth, *Phys. Rev. Lett.* **84**, 5070 (2000).
- ¹⁰¹M. Seidl, J. P. Perdew, and S. Kurth, *Phys. Rev. A* **62**, 012502 (2000).
- ¹⁰²M. Seidl, *Phys. Rev. A* **75**, 062506 (2007).
- ¹⁰³G. Breit, *Phys. Rev.* **35**, 569 (1930).
- ¹⁰⁴P. F. Loos, and P. M. W. Gill, *J. Chem. Phys.* **138**, 164124 (2013).
- ¹⁰⁵V. Tognetti, and P. F. Loos, *J. Chem. Phys.* **144**, 054108 (2016).
- ¹⁰⁶J. D. Louck, *J. Mol. Spectrosc.* **4**, 298–333 (1960).
- ¹⁰⁷A. Ronveaux, ed., *Heun's differential equations* (Oxford University Press, Oxford, 1995).
- ¹⁰⁸A. D. Polyanin, and V. F. Zaitsev, *Handbook of exact solutions for differential equations* (Chapman & Hall/CRC, 2003).
- ¹⁰⁹T. Kato, *Commun. Pure Appl. Math.* **10**, 151 (1957).
- ¹¹⁰J. D. Baker, D. E. Freund, R. N. Hill, and J. D. Morgan III, *Phys. Rev. A* **41**, 1247 (1990).
- ¹¹¹P. M. W. Gill, and D. P. O'Neill, *J. Chem. Phys.* **122**, 094110 (2005).
- ¹¹²D. R. Herrick, and F. H. Stillinger, *Phys. Rev. A* **11**, 42 (1975).
- ¹¹³D. R. Herrick, *J. Math. Phys.* **16**, 281 (1975).
- ¹¹⁴P. F. Loos, N. J. Bloomfield, and P. M. W. Gill, *J. Chem. Phys.* **143**, 181101 (2015).
- ¹¹⁵F. Hund, *Z. Phys.* **33**, 345 (1925).
- ¹¹⁶H. N. Russell, and W. F. Meggers, *Sci. Pap. Bur. Stand.* **22**, 364 (1927).
- ¹¹⁷E. U. Condon, and G. H. Shortley, *The theory of atomic spectra* (Cambridge: University Press, 1935).
- ¹¹⁸R. J. Boyd, *Nature* **310**, 480 (1984).
- ¹¹⁹W. Kutzelnigg, and J. D. Morgan III, *J. Chem. Phys.* **96**, 4484 (1992).
- ¹²⁰J. D. Morgan III, and W. Kutzelnigg, *J. Phys. Chem.* **97**, 2425 (1993).
- ¹²¹W. Kutzelnigg, and J. D. Morgan III, *Z. Phys. D* **36**, 197 (1996).
- ¹²²T. Kato, *Trans. Am. Math. Soc.* **70**, 195 (1951).
- ¹²³R. T. Pack, and W. Byers Brown, *J. Chem. Phys.* **45**, 556 (1966).
- ¹²⁴D. P. Tew, *J. Chem. Phys.* **129**, 014104 (2008).
- ¹²⁵M. Gell-Mann, and K. A. Brueckner, *Phys. Rev.* **106**, 364 (1957).
- ¹²⁶H. A. Bethe, and E. E. Salpeter, *Quantum mechanics of one- and two-electron atoms* (Dover Publications Inc., Mineola, New-York, 1977).
- ¹²⁷H. Nakashima, and H. Nakatsuji, *J. Chem. Phys.* **127**, 224104 (2007).

- ¹²⁸E. A. Hylleraas, *Z. Phys.* **65**, 209 (1930).
- ¹²⁹J. Linderberg, *Phys. Rev.* **121**, 816 (1961).
- ¹³⁰C. Schwartz, *Phys. Rev.* **126**, 1015 (1962).
- ¹³¹L. G. Yaffe, *Rev. Mod. Phys.* **54**, 407 (1982).
- ¹³²E. Witten, *Physics Today* **33**, 38 (1980).
- ¹³³L. G. Yaffe, *Physics Today* **36**, 50 (1983).
- ¹³⁴D. J. Doren, and D. R. Herschbach, *J. Chem. Phys.* **87**, 443 (1987).
- ¹³⁵D. R. Herschbach, *J. Chem. Phys.* **84**, 838 (1986).
- ¹³⁶D. Z. Goodson, and D. R. Herschbach, *J. Chem. Phys.* **86**, 4997 (1987).
- ¹³⁷D. J. Doren, and D. R. Herschbach, *Phys. Rev. A* **34**, 2654 (1986).
- ¹³⁸D. Z. Goodson, M. López-Cabrera, D. R. Herschbach, and J. D. Morgan III, *J. Chem. Phys.* **97**, 8481 (1992).
- ¹³⁹D. Z. Goodson, and M. López-Cabrera, "Low-d regime: the one-dimensional limit", in, edited by D. R. Herschbach, J. Avery, and O. Goscinski, *Dimensional Scaling in Chemical Physics* (Kluwer Academic Publishers, Dordrecht, 1993), p. 115.
- ¹⁴⁰J. G. Loeser, and D. R. Herschbach, *J. Chem. Phys.* **86**, 2114 (1987).
- ¹⁴¹J. G. Loeser, and D. R. Herschbach, *J. Chem. Phys.* **86**, 3512 (1987).
- ¹⁴²J. G. Loeser, *J. Chem. Phys.* **86**, 5635 (1987).
- ¹⁴³S. Kais, S. M. Sung, and D. R. Herschbach, *J. Chem. Phys.* **99**, 5184 (1993).
- ¹⁴⁴L. D. Mlodinow, and N. Papanicolaou, *Ann. Phys.* **131**, 1 (1981).
- ¹⁴⁵R. J. White, and F. H. Stillinger, *J. Chem. Phys.* **52**, 5800 (1970).
- ¹⁴⁶D. C. Thompson, and A. Alavi, *Phys. Rev. B* **66**, 235118 (2002).
- ¹⁴⁷D. C. Thompson, and A. Alavi, *J. Chem. Phys.* **122**, 124107 (2005).
- ¹⁴⁸X.-Y. Pan, and V. Sahni, *J. Chem. Phys.* **119**, 7083 (2003).
- ¹⁴⁹L. H. Thomas, *Proc. Cam. Phil. Soc.* **23**, 542 (1927).
- ¹⁵⁰E. Fermi, *Z. Phys.* **36**, 902–912 (1926).
- ¹⁵¹E. Wigner, *Phys. Rev.* **46**, 1002 (1934).
- ¹⁵²W. Macke, *Z. Naturforsch. A* **5a**, 192 (1950).
- ¹⁵³L. Onsager, L. Mittag, and M. J. Stephen, *Ann. Phys.* **18**, 71 (1966).
- ¹⁵⁴F. Stern, *Phys. Rev. Lett.* **30**, 278 (1973).
- ¹⁵⁵A. K. Rajagopal, and J. C. Kimball, *Phys. Rev. B* **15**, 2819 (1977).
- ¹⁵⁶A. Isihara, and L. Ioriatti, *Phys. Rev. B* **22**, 214 (1980).
- ¹⁵⁷G. G. Hoffman, *Phys. Rev. B* **45**, 8730 (1992).
- ¹⁵⁸M. Seidl, *Phys. Rev. B* **70**, 073101 (2004).
- ¹⁵⁹J. Sun, J. P. Perdew, and M. Seidl, *Phys. Rev. B* **81**, 085123 (2010).
- ¹⁶⁰G. F. Giuliani, and G. Vignale, *Quantum theory of electron liquid* (Cambridge University Press, Cambridge, 2005).
- ¹⁶¹B. Tanatar, and D. M. Ceperley, *Phys. Rev. B* **39**, 5005 (1989).
- ¹⁶²Y. Kwon, D. M. Ceperley, and R. M. Martin, *Phys. Rev. B* **48**, 12037 (1993).
- ¹⁶³G. Ortiz, and P. Ballone, *Phys. Rev. B* **50**, 1391 (1994).

- ¹⁶⁴F. Rapisarda, and G. Senatore, *Aust. J. Phys.* **49**, 161–182 (1996).
- ¹⁶⁵G. Ortiz, M. Harris, and P. Ballone, *Phys. Rev. Lett.* **82**, 5317 (1999).
- ¹⁶⁶C. Attaccalite, S. Moroni, P. Gori-Giorgi, and G. B. Bachelet, *Phys. Rev. Lett.* **88**, 256601 (2002).
- ¹⁶⁷F. H. Zong, C. Lin, and D. M. Ceperley, *Phys. Rev. E* **66**, 036703 (2002).
- ¹⁶⁸N. D. Drummond, and R. J. Needs, *Phys. Rev. Lett.* **102**, 126402 (2009).
- ¹⁶⁹N. D. Drummond, and R. J. Needs, *Phys. Rev. B* **79**, 085414 (2009).
- ¹⁷⁰J. P. Perdew, and A. Zunger, *Phys. Rev. B* **23**, 5048 (1981).
- ¹⁷¹D. M. Ceperley, *Phys. Rev. B* **18**, 3126 (1978).
- ¹⁷²L. A. Curtiss, K. Raghavachari, P. C. Redfern, and J. A. Pople, *J. Chem. Phys.* **112**, 7374 (2000).
- ¹⁷³H. L. Woodcock III, H. F. Schaefer III, and P. R. Schreiner, *J. Phys. Chem. A* **106**, 11923 (2002).
- ¹⁷⁴A. Dreuw, and M. Head-Gordon, *J. Am. Chem. Soc.* **126**, 4007 (2004).
- ¹⁷⁵M. D. Wodrich, C. Corminboeuf, and P. Schleyer, *Org. Lett.* **8**, 3631 (2006).
- ¹⁷⁶A. J. Cohen, P. Mori-Sanchez, and W. Yang, *Science* **321**, 792 (2008).
- ¹⁷⁷D. R. B. Brittain, C. Y. Lin, A. T. B. Gilbert, E. I. Izgorodina, P. M. W. Gill, and M. L. Coote, *Phys. Chem. Chem. Phys.* **11**, 1138 (2009).
- ¹⁷⁸P. M. W. Gill, and P. F. Loos, *Theor. Chem. Acc.* **131**, 1069 (2012).
- ¹⁷⁹J. Avery, *Hyperspherical harmonics: applications in quantum theory* (Kluwer Academic, Dordrecht, 1989).
- ¹⁸⁰C. A. Coulson, and A. H. Neilson, *Proc. Phys. Soc. (London)* **78**, 831 (1961).
- ¹⁸¹P. Gori-Giorgi, and J. P. Perdew, *Phys. Rev. B* **69**, 041103 (2004).
- ¹⁸²P. M. W. Gill, D. P. O'Neill, and N. A. Besley, *Theor. Chem. Acc.* **109**, 241 (2003).
- ¹⁸³P. F. Loos, *J. Chem. Phys.* **146**, 114108 (2017).
- ¹⁸⁴P. F. Loos, C. J. Ball, and P. M. W. Gill, *Phys. Chem. Chem. Phys.* **17**, 3196 (2015).
- ¹⁸⁵F. J. M. Rogers, C. J. Ball, and P. F. Loos, *Phys. Rev. B* **93**, 235114 (2016).
- ¹⁸⁶C. J. Ball, P. F. Loos, and P. M. W. Gill, *Phys. Chem. Chem. Phys.* **19**, 3987 (2017).
- ¹⁸⁷F. J. M. Rogers, and P. F. Loos, *J. Chem. Phys.* **146**, 044114 (2017).
- ¹⁸⁸P. F. Loos, C. J. Ball, and P. M. W. Gill, *J. Chem. Phys.* **140**, 18A524 (2014).
- ¹⁸⁹P. F. Loos, *Phys. Rev. A* **89**, 052523 (2014).
- ¹⁹⁰A. D. Becke, *J. Chem. Phys.* **112**, 4020 (2000).
- ¹⁹¹A. D. Becke, *Int. J. Quantum Chem.* **23**, 1915–1922 (1983).
- ¹⁹²J. F. Dobson, *J. Chem. Phys.* **94**, 4328–4333 (1991).
- ¹⁹³C. F. von Weizsacker, *Z. Phys.* **96**, 431 (1935).
- ¹⁹⁴M. Ernzerhof, and G. E. Scuseria, *J. Chem. Phys.* **111**, 911 (1999).
- ¹⁹⁵F. G. Eich, and M. Hellgren, *J. Chem. Phys.* **141**, 224107 (2014).
- ¹⁹⁶S. Kurth, J. P. Perdew, and P. Blaha, *Int. J. Quantum Chem.* **75**, 889 (1999).
- ¹⁹⁷J. Tao, J. P. Perdew, V. N. Staroverov, and G. E. Scuseria, *Phys. Rev. Lett.* **91**, 146401 (2003).

- ¹⁹⁸J. P. Perdew, A. Ruzsinszky, G. I. Csonka, L. A. Constantin, and J. Sun, *Phys. Rev. Lett.* **103**, 026403 (2009).
- ¹⁹⁹J. Sun, B. Xiao, Y. Fang, R. Haunschuld, P. Hao, A. Ruzsinszky, G. I. Csonka, G. E. Scuseria, and J. P. Perdew, *Phys. Rev. Lett.* **111**, 106401 (2013).
- ²⁰⁰J. Sun, J. P. Perdew, and A. Ruzsinszky, *Proc. Natl. Acad. Sci. USA* **112**, 685 (2015).
- ²⁰¹J. Sun, R. C. Remsing, Y. Zhang, Z. Sun, A. Ruzsinszky, H. Peng, Z. Yang, A. Paul, U. Waghmare, X. Wu, M. L. Klein, and J. P. Perdew, *Nature Chem.* **8**, 831 (2016).
- ²⁰²B. Silvi, and A. Savin, *Nature* **371**, 683 (1994).
- ²⁰³M. Levy, and J. P. Perdew, *Phys. Rev. A* **32**, 2010 (1985).
- ²⁰⁴Y. Shao et al., *Mol. Phys.* **113**, 184 (2015).
- ²⁰⁵T. H. Dunning, Jr., *J. Chem. Phys.* **90**, 1007 (1989).
- ²⁰⁶R. A. Kendall, T. H. Dunning, Jr., and R. J. Harrison, *J. Chem. Phys.* **98**, 1358 (1992).
- ²⁰⁷D. E. Woon, and T. H. Dunning, *J. Chem. Phys.* **99**, 1914 (1993).
- ²⁰⁸D. E. Woon, and T. H. Dunning, Jr., *J. Chem. Phys.* **100**, 2975 (1994).
- ²⁰⁹D. E. Woon, and T. H. Dunning, Jr., *J. Chem. Phys.* **103**, 4572 (1995).
- ²¹⁰K. A. Peterson, and T. H. Dunning, Jr., *J. Chem. Phys.* **117**, 10548 (2002).
- ²¹¹J. Avery, *J. Phys. Chem.* **97**, 2406 (1993).
- ²¹²P. F. Loos, and P. M. W. Gill, *Mol. Phys.* **110**, 2337 (2012).
- ²¹³E. H. Lieb, and S. Oxford, *Int. J. Quantum Chem.* **19**, 427 (1981).
- ²¹⁴G. K. L. Chan, and N. C. Handy, *Phys. Rev. A* **59**, 3075 (1999).
- ²¹⁵M. M. Odashima, K. Capelle, and S. B. Trickey, *J. Chem. Theory Comput.* **5**, 798 (2009).
- ²¹⁶J. P. Perdew, A. Ruzsinszky, J. Sun, and K. Burke, *J. Chem. Phys.* **140**, 18A533 (2014).
- ²¹⁷J. Sun, J. P. Perdew, Z. Yang, and H. Peng, *J. Chem. Phys.* **144**, 191101 (2016).
- ²¹⁸S. K. Ma, and K. A. Brueckner, *Phys. Rev.* **165**, 18 (1968).
- ²¹⁹V. N. Staroverov, G. E. Scuseria, J. P. Perdew, J. Tao, and E. R. Davidson, *Phys. Rev. A* **70**, 012502 (2004).
- ²²⁰L. J. Sham, "Computational methods in band theory", in, edited by P. M. Marcus, J. F. Janak, and A. R. Williams, (Plenum (New York), 1971), p. 458.
- ²²¹L. Kleinman, *Phys. Rev. B* **30**, 2223 (1984).
- ²²²P. R. Antoniewicz, and L. Kleinman, *Phys. Rev. B* **31**, 6779 (1985).
- ²²³L. Kleinman, and S. Lee, *Phys. Rev. B* **37**, 4634 (1988).
- ²²⁴P. S. Svendsen, and U. von Barth, *Phys. Rev. B* **54**, 17402 (1996).
- ²²⁵J. P. Perdew, J. Sun, R. M. Martin, and B. Delley, *Int. J. Quantum Chem.* **116**, 847 (2016).
- ²²⁶A. Ruzsinszky, J. Sun, B. Xiao, and G. I. Csonka, *J. Chem. Theory Comput.* **8**, 2078 (2012).
- ²²⁷K. P. Huber, and G. Herzberg, *Molecular spectra and molecular structure: iv. constants of diatomic molecules* (van Nostrand Reinhold Company, 1979).
- ²²⁸P. A. M. Dirac, *Proc. Roy. Soc. (London) A* **123**, 714 (1929).

- ²²⁹C. R. Myers, C. J. Umrigar, J. P. Sethna, and J. D. Morgan III, *Phys. Rev. A* **44**, 5537 (1991).
- ²³⁰Y. I. Kurokawa, H. Nakashima, and H. Nakatsuji, *J. Chem. Phys.* **139**, 044114 (2013).
- ²³¹Y. I. Kurokawa, H. Nakashima, and H. Nakatsuji, *J. Chem. Phys.* **140**, 214103 (2014).
- ²³²A. Gruneis, S. Hirata, Y.-Y. Ohnishi, and S. Ten-no, *J. Chem. Phys.* **146**, 080901 (2017).
- ²³³C. Hattig, W. Klopper, A. Kohn, and D. P. Tew, *Chem. Rev.* **112**, 4 (2012).
- ²³⁴L. Kong, F. A. Bischo, and E. F. Valeev, *Chem. Rev.* **112**, 75 (2012).
- ²³⁵E. A. Hylleraas, *Z. Phys.* **48**, 469 (1928).
- ²³⁶E. A. Hylleraas, *Z. Phys.* **54**, 347 (1929).
- ²³⁷J. C. Slater, *Phys. Rev.* **31**, 333 (1928).
- ²³⁸D. R. Hartree, and A. L. Ingman, *Mem. Proc. Manchester Lit. Philos. Soc.* **77**, 69 (1933).
- ²³⁹S. F. Boys, *Proc. R. Soc. London, Ser. A* **258**, 402 (1960).
- ²⁴⁰K. Singer, *Proc. R. Soc. London, Ser. A* **258**, 412 (1960).
- ²⁴¹J. Rychlewski, and J. Komasa, *Explicitly correlated functions in chemistry and physics*, edited by J. Rychlewski, (Kluwer Academic Publishers, Dordrecht, 2003), p. 91.
- ²⁴²S. Bubin, M. Cafiero, and L. Adamowicz, *Adv. Chem. Phys.* **131**, 377 (2005).
- ²⁴³S. Bubin, M. Stanke, and L. Adamowicz, *J. Chem. Phys.* **131**, 044128 (2009).
- ²⁴⁴K. Szalewicz, and B. Jeziorski, *Mol. Phys.* **108**, 3091 (2010).
- ²⁴⁵K. C. Pan, and H. F. King, *J. Chem. Phys.* **53**, 4397 (1970).
- ²⁴⁶K. C. Pan, and H. F. King, *J. Chem. Phys.* **56**, 4667 (1972).
- ²⁴⁷L. Adamowicz, and A. J. Sadlej, *J. Chem. Phys.* **67**, 4298 (1977).
- ²⁴⁸L. Adamowicz, and A. J. Sadlej, *Chem. Phys. Lett.* **48**, 305 (1977).
- ²⁴⁹L. Adamowicz, and A. J. Sadlej, *J. Chem. Phys.* **69**, 3992 (1978).
- ²⁵⁰K. Szalewicz, B. Jeziorski, H. Monkhorst, and G. Zabolitzky, *Chem. Phys. Lett.* **91**, 169 (1982).
- ²⁵¹K. Szalewicz, B. Jeziorski, H. Monkhorst, and G. Zabolitzky, *J. Chem. Phys.* **78**, 1420 (1983).
- ²⁵²W. Klopper, and W. Kutzelnigg, *Chem. Phys. Lett.* **134**, 17 (1987).
- ²⁵³A. Preiskorn, and B. Zurawski, *Int. J. Quantum Chem.* **27**, 641 (1985).
- ²⁵⁴E. Clementi, *Modern techniques in computational chemistry: motecc-89* (ESCOM Science Publishers B. V., New York, 1989).
- ²⁵⁵L. E. McMurchie, and E. R. Davidson, *J. Comput. Phys.* **26**, 218 (1978).
- ²⁵⁶J. A. Pople, and W. J. Hehre, *J. Comput. Phys.* **27**, 161 (1978).
- ²⁵⁷H. F. King, and M. Dupuis, *J. Comput. Phys.* **21**, 144 (1976).
- ²⁵⁸M. Dupuis, J. Rys, and H. F. King, *J. Chem. Phys.* **65**, 111 (1976).
- ²⁵⁹J. Rys, M. Dupuis, and H. F. King, *J. Comput. Chem.* **4**, 154 (1983).
- ²⁶⁰S. Obara, and A. Saika, *J. Chem. Phys.* **84**, 3963–3974 (1986).
- ²⁶¹M. Head-Gordon, and J. A. Pople, *J. Chem. Phys.* **89**, 5777 (1988).

- ²⁶²P. M. W. Gill, *Adv. Quantum Chem.* **25**, 141 (1994).
- ²⁶³G. M. J. Barca, P. F. Loos, and P. M. W. Gill, *J. Chem. Theory Comput.* **12**, 1725 (2016).
- ²⁶⁴J. C. Womack, and F. R. Manby, *J. Chem. Phys.* **140**, 044118 (2014).
- ²⁶⁵G. M. J. Barca, P. F. Loos, and P. M. W. Gill, (in preparation).
- ²⁶⁶H. J. Werner, T. B. Adler, and F. R. Manby, *J. Chem. Phys.* **126**, 164102 (2007).
- ²⁶⁷R. A. Banchorz, F. A. Bischoff, A. Glöß, C. Hättig, S. Höfener, W. Klopper, and D. P. Tew, *J. Comput. Chem.* **32**, 2492 (2011).
- ²⁶⁸R. Rohse, W. Klopper, and W. Kutzelnigg, *J. Chem. Phys.* **99**, 8830 (1993).
- ²⁶⁹B. J. Persson, and P. R. Taylor, *J. Chem. Phys.* **105**, 5915 (1996).
- ²⁷⁰D. P. Tew, and W. Klopper, *J. Chem. Phys.* **123**, 074101 (2005).
- ²⁷¹D. P. Tew, and W. Klopper, *J. Chem. Phys.* **125**, 094302 (2006).
- ²⁷²S. Ten-no, *Chem. Phys. Lett.* **398**, 56 (2004).
- ²⁷³S. Ten-no, *J. Chem. Phys.* **126**, 014108 (2007).
- ²⁷⁴A. J. May, and F. R. Manby, *J. Chem. Phys.* **121**, 4479 (2004).
- ²⁷⁵A. J. May, E. Valeev, R. Polly, and F. R. Manby, *Phys. Chem. Chem. Phys.* **7**, 2710 (2005).
- ²⁷⁶B. J. Persson, and P. R. Taylor, *Theor. Chem. Acc.* **97**, 240 (1997).
- ²⁷⁷P. Dahle, *Accurate calculations using explicitly correlated wave functions* (PhD thesis, University of Oslo, 2004).
- ²⁷⁸P. Dahle, T. Helgaker, D. Jonsson, and P. R. Taylor, *Phys. Chem. Chem. Phys.* **9**, 3112–3126 (2007).
- ²⁷⁹P. Dahle, T. Helgaker, D. Jonsson, and P. R. Taylor, *Phys. Chem. Chem. Phys.* **10**, 3377–3382 (2008).
- ²⁸⁰S. L. Saito, and Y.-I. Suzuki, *J. Chem. Phys.* **114**, 1115 (2001).
- ²⁸¹S. Obara, and A. Saika, *J. Chem. Phys.* **89**, 1540–1559 (1988).
- ²⁸²A. Komornicki, and H. F. King, *J. Chem. Phys.* **134**, 244115 (2011).
- ²⁸³A. J. May, *Density fitting in explicitly correlated electronic structure theory* (PhD thesis, University of Bristol, 2006).
- ²⁸⁴J. C. Womack, *Evaluating many-electron molecular integrals for quantum chemistry* (PhD thesis, University of Bristol, 2015).
- ²⁸⁵G. M. J. Barca, and P. F. Loos, *Adv. Quantum Chem.*, arXiv:1703.00846 [physics.chem-ph] (in press).
- ²⁸⁶W. Klopper, and R. Rohse, *Theor. Chem. Acc.* **83**, 441 (1992).
- ²⁸⁷W. Klopper, and C. C. M. Samson, *J. Chem. Phys.* **116**, 6397 (2002).
- ²⁸⁸F. R. Manby, *J. Chem. Phys.* **119**, 4607 (2003).
- ²⁸⁹H. J. Werner, F. R. Manby, and P. J. Knowles, *J. Chem. Phys.* **118**, 8149 (2003).
- ²⁹⁰W. Klopper, *J. Chem. Phys.* **120**, 10890 (2004).
- ²⁹¹S. Ten-no, *J. Chem. Phys.* **121**, 117 (2004).
- ²⁹²F. R. Manby, H. J. Werner, T. B. Adler, and A. J. May, *J. Chem. Phys.* **124**, 094103 (2006).

- ²⁹³S. Ten-no, and J. Noga, *WIREs Comput. Mol. Sci.* **2**, 114 (2012).
- ²⁹⁴S. Ten-no, *Theor. Chem. Acc.* **131**, 1070 (2012).
- ²⁹⁵S. Reine, T. Helgaker, and R. Lind, *WIREs Comput. Mol. Sci.* **2**, 290 (2012).
- ²⁹⁶G. M. J. Barca, and P. M. W. Gill, *J. Chem. Theory Comput.* **12**, 4915 (2016).
- ²⁹⁷P. M. W. Gill, B. G. Johnson, and J. A. Pople, *Int. J. Quantum Chem.* **40**, 745 (1991).
- ²⁹⁸K. Ishida, *Int. J. Quantum Chem.* **59**, 209 (1996).
- ²⁹⁹A. K. H. Weiss, and C. Ochsenfeld, *J. Comput. Chem.* **36**, 1390 (2015).
- ³⁰⁰G. M. J. Barca, and P. F. Loos, *J. Chem. Phys.* **147**, 024103 (2017).
- ³⁰¹P. M. W. Gill, B. G. Johnson, and J. A. Pople, *Chem. Phys. Lett.* **217**, 65 (1994).
- ³⁰²J. Power, and R. M. Pitzer, *Chem. Phys. Lett.* **24**, 478 (1974).
- ³⁰³R. Ahlrichs, *Theor. Chim. Acta* **33**, 157 (1974).
- ³⁰⁴M. Haser, and R. Ahlrichs, *J. Comput. Chem.* **10**, 104 (1989).
- ³⁰⁵H. Horn, H. Weiß, M. Haser, M. Ehrig, and R. Ahlrichs, *J. Comput. Chem.* **12**, 1058 (1991).
- ³⁰⁶R. Ahlrichs, *Phys. Chem. Chem. Phys.* **8**, 3072–3077 (2006).
- ³⁰⁷P. M. W. Gill, and J. A. Pople, *Int. J. Quantum Chem.* **40**, 753 (1991).
- ³⁰⁸S. Y. Willow, K. S. Kim, and S. Hirata, *J. Chem. Phys.* **137**, 204122 (2012).
- ³⁰⁹S. Y. Willow, and S. Hirata, *J. Chem. Phys.* **140**, 024111 (2014).
- ³¹⁰G. H. Booth, A. J. W. Thom, and A. Alavi, *J. Chem. Phys.* **131**, 054106 (2009).
- ³¹¹D. M. Cleland, G. H. Booth, and A. Alavi, *J. Chem. Phys.* **134**, 024112 (2011).
- ³¹²A. J. W. Thom, *Phys. Rev. Lett.* **105**, 263004 (2010).
- ³¹³R. E. Thomas, Q. Sun, A. Alavi, and G. Booth, *J. Chem. Theory Comput.* **11**, 5316 (2015).
- ³¹⁴O. Valsson, P. Campomanes, I. Tavernelli, U. Rothlisberger, and C. Filippi, *J. Chem. Theory Comput.* **9**, 2441 (2013).
- ³¹⁵N. D. Drummond, B. Monserrat, J. H. Lloyd-Williams, C. J. Pickard, P. L. Rios, and R. J. Needs, *Nature Comm.* **6**, 7794 (2015).
- ³¹⁶C. Daday, C. Curutchet, A. Sinicropi, B. Mennucci, and C. Filippi, *J. Chem. Theory Comput.* **11**, 4825 (2015).
- ³¹⁷V. Termath, W. Klopper, and W. Kutzelnigg, *J. Chem. Phys.* **94**, 2002 (1991).
- ³¹⁸W. Klopper, and W. Kutzelnigg, *J. Chem. Phys.* **94**, 2020 (1991).
- ³¹⁹W. Klopper, R. Rohse, and W. Kutzelnigg, *Chem. Phys. Lett.* **178**, 455 (1991).
- ³²⁰J. Noga, and W. Kutzelnigg, *J. Chem. Phys.* **101**, 7738 (1994).
- ³²¹D. P. Tew, W. Klopper, C. Neiss, and C. Hattig, *Phys. Chem. Chem. Phys.* **9**, 1921 (2007).
- ³²²B. Huron, J. P. Malrieu, and P. Rancurel, *J. Chem. Phys.* **58**, 5745 (1973).
- ³²³S. Evangelisti, J.-P. Daudey, and J.-P. Malrieu, *Chem. Phys.* **75**, 91 (1983).
- ³²⁴J.-L. Heully, and J.-P. Malrieu, *Chem. Phys. Lett.* **199**, 545 (1992).
- ³²⁵E. Giner, A. Scemama, and M. Caffarel, *Can. J. Chem.* **91**, 879 (2013).

- ³²⁶A. Scemama, M. Caffarel, E. Oseret, and W. Jalby, "QMC=Chem: A Quantum Monte Carlo Program for Large-Scale Simulations in Chemistry at the Petascale Level and beyond", in *High performance computing for computational science - VECPAR 2012* (Springer Science Business Media, 2013), pp. 118–127.
- ³²⁷A. Scemama, M. Caffarel, E. Oseret, and W. Jalby, *J. Comput. Chem.* **34**, 938 (2013).
- ³²⁸A. Scemama, T. Applencourt, E. Giner, and M. Caffarel, *J. Chem. Phys.* **141**, 244110 (2014).
- ³²⁹E. Giner, A. Scemama, and M. Caffarel, *J. Chem. Phys.* **142**, 044115 (2015).
- ³³⁰M. Caffarel, T. Applencourt, E. Giner, and A. Scemama, *J. Chem. Phys.* **144**, 151103 (2016).
- ³³¹T. Shiozaki, G. Knizia, and H.-J. Werner, *J. Chem. Phys.* **134**, 034113 (2011).
- ³³²P. Pulay, *Chem. Phys. Lett.* **73**, 393 (1980).
- ³³³P. Pulay, *J. Comput. Chem.* **3**, 556 (1982).
- ³³⁴G. M. J. Barca, and P. F. Loos, *Adv. Quantum Chem.* (in press).
- ³³⁵E. F. Valeev, *Chem. Phys. Lett.* **395**, 190 (2004).
- ³³⁶Y. Garniron, A. Scemama, P. F. Loos, and M. Caffarel, *J. Chem. Phys.* **147**, 034101 (2017).
- ³³⁷J. Toulouse, and C. J. Umrigar, *J. Chem. Phys.* **126**, 084102 (2007).
- ³³⁸C. J. Umrigar, J. Toulouse, C. Filippi, S. Sorella, and R. G. Hennig, *Phys. Rev. Lett.* **98**, 110201 (2007).
- ³³⁹J. Toulouse, and C. J. Umrigar, *J. Chem. Phys.* **128**, 174101 (2008).
- ³⁴⁰S. F. Boys, *Proc. R. Soc. (London)* **A200**, 542 (1950).
- ³⁴¹L. K. McKemmish, A. T. B. Gilbert, and P. M. W. Gill, *J. Chem. Theory Comput.* **10**, 4369 (2014).
- ³⁴²J. C. Slater, *Phys. Rev.* **36**, 57 (1930).
- ³⁴³A. Bouferguene, M. Fares, and P. E. Hoggan, *Int. J. Quantum Chem.* **57**, 810 (1996).
- ³⁴⁴N. Nemec, *Phys. Rev. B* **81**, 035119 (2010).
- ³⁴⁵E. van Lenthe, and E. J. Baerends, *J. Comput. Chem.* **24**, 1142 (2003).
- ³⁴⁶P. T. A. Galek, N. C. Handy, A. J. Cohen, and G. K.-L. Chan, *Chem. Phys. Lett.* **404**, 156 (2005).
- ³⁴⁷G. te Velde, F. M. Bickelhaupt, E. J. Baerends, C. F. Guerra, S. J. A. van Gisbergen, J. G. Snijders, and T. Ziegler, *J. Comput. Chem.* **22**, 931 (2001).
- ³⁴⁸S. Huzinaga, *J. Chem. Phys.* **42**, 1293 (1965).
- ³⁴⁹W. J. Hehre, R. F. Stewart, and J. A. Pople, *J. Chem. Phys.* **51**, 2657 (1969).
- ³⁵⁰W. J. Hehre, R. Ditchfield, and J. A. Pople, *J. Chem. Phys.* **56**, 2257 (1972).
- ³⁵¹M. W. Schmidt, and K. Ruedenberg, *J. Chem. Phys.* **71**, 3951 (1979).
- ³⁵²D. F. Feller, and K. Ruedenberg, *Theor. Chim. Acta* **52**, 231 (1979).
- ³⁵³J. Almlöf, and P. R. Taylor, *J. Chem. Phys.* **86**, 4070 (1987).
- ³⁵⁴J. Almlöf, and P. R. Taylor, *J. Chem. Phys.* **92**, 551 (1990).
- ³⁵⁵C. W. Bauschlicher, and P. R. Taylor, *Theor. Chim. Acta* **86**, 13 (1993).
- ³⁵⁶K. A. Peterson, R. A. Kendall, and T. H. Dunning, *J. Chem. Phys.* **99**, 1930 (1993).

- ³⁵⁷F. Jensen, *J. Chem. Phys.* **115**, 9113 (2001).
- ³⁵⁸F. Jensen, *J. Phys. Chem. A* **111**, 11198 (2007).
- ³⁵⁹F. Jensen, *WIREs Comput. Mol. Sci.* **3**, 273 (2012).
- ³⁶⁰S. Manten, and A. Lüchow, *J. Chem. Phys.* **115**, 5362 (2001).
- ³⁶¹M. Ma, M. D. Towler, N. D. Drummond, and R. J. Needs, *Phys. Rev. B* **122**, 224322 (2005).
- ³⁶²J. Kussmann, and C. Ochsenfeld, *Phys. Rev. B* **76**, 115115 (2007).
- ³⁶³M. C. Per, S. P. Russo, and I. K. Snook, *J. Chem. Phys.* **128**, 114106 (2008).
- ³⁶⁴C. F. Bunge, J. A. Barrientos, and A. Bunge-Vivier, *At. Data Nucl. Data Tables* **53**, 113 (1993).
- ³⁶⁵L. C. Allen, *J. Chem. Phys.* **31**, 736 (1959).
- ³⁶⁶D. M. Silver, *Chem. Phys. Lett.* **7**, 511 (1970).
- ³⁶⁷G. B. Bacskay, and J. W. Linnett, *Theor. Chim. Acta* **26**, 1 (1972).
- ³⁶⁸G. B. Bacskay, and J. W. Linnett, *Theor. Chim. Acta* **26**, 14 (1972).
- ³⁶⁹G. B. Bacskay, and J. W. Linnett, *Theor. Chim. Acta* **26**, 23 (1972).
- ³⁷⁰G. B. Bacskay, *Theor. Chem. Acc.* **26**, 33 (1972).
- ³⁷¹O. P. Bugaets, and D. A. Zhogolev, *Chem. Phys. Lett.* **39**, 45 (1976).
- ³⁷²J. Deng, A. T. B. Gilbert, and P. M. W. Gill, *Can. J. Chem.* **88**, 754 (2010).
- ³⁷³J. A. Berger, P. Romaniello, F. Tandetzky, B. S. Mendoza, C. Brouder, and L. Reining, *New J. Phys.* **16**, 113025 (2014).
- ³⁷⁴L. Hedin, *Phys. Rev.* **139**, A796–A823 (1965).
- ³⁷⁵P. M. W. Gill, P. F. Loos, and D. Agboola, *J. Chem. Phys.* **141**, 244102 (2014).
- ³⁷⁶D. Agboola, A. L. Knol, P. M. W. Gill, and P. F. Loos, *J. Chem. Phys.* **143**, 084114 (2015).
- ³⁷⁷V. Melik-Alaverdian, N. E. Bonesteel, and G. Ortiz, **79**, 5286 (1997).
- ³⁷⁸A. W. Overhauser, *Phys. Rev. Lett.* **3**, 414 (1959).
- ³⁷⁹A. W. Overhauser, *Phys. Rev.* **128**, 1437 (1962).
- ³⁸⁰J. R. Trail, M. D. Towler, and R. J. Needs, *Phys. Rev. B* **68**, 045107 (2003).
- ³⁸¹F. Delyon, M. Duneau, B. Bernu, and M. Holzmann, arXiv:0807.0770v1 (2008).
- ³⁸²B. Bernu, F. Delyon, M. Duneau, and M. Holzmann, *Phys. Rev. B* **78**, 245110 (2008).
- ³⁸³B. Bernu, F. Delyon, M. Holzmann, and L. Baguet, *Phys. Rev. B* **84**, 115115 (2011).
- ³⁸⁴L. Baguet, F. Delyon, B. Bernu, and M. Holzmann, *Phys. Rev. Lett.* **111**, 166402 (2013).
- ³⁸⁵L. Baguet, F. Delyon, B. Bernu, and M. Holzmann, *Phys. Rev. B* **90**, 165131 (2014).
- ³⁸⁶F. Delyon, B. Bernu, L. Baguet, and M. Holzmann, *Phys. Rev. B* **92**, 235124 (2015).
- ³⁸⁷C. J. Ball, and P. M. W. Gill, *Mol. Phys.* **113**, 1843 (2015).
- ³⁸⁸T. Limpanuparb, and P. M. W. Gill, *J. Chem. Theory Comput.* **7**, 2353 (2011).
- ³⁸⁹C. M. Johnson, A. E. Doran, J. Zhang, E. F. Valeev, and S. Hirata, *J. Chem. Phys.* **145**, 154115 (2016).
- ³⁹⁰C. M. Johnson, S. Hirata, and S. Ten-no, *Chem. Phys. Lett.* **683**, 247 (2017).

-
- ³⁹¹F. R. Petruzielo, A. A. Holmes, H. J. Changlani, M. P. Nightingale, and C. J. Umrigar, *Phys. Rev. Lett.* **109**, 230201 (2012).
- ³⁹²R. Assaraf, and M. Caffarel, *Phys. Rev. Lett.* **83**, 4682 (1999).
- ³⁹³O. Franck, B. Mussard, E. Luppi, and J. Toulouse, *J. Chem. Phys.* **142**, 074107 (2015).
- ³⁹⁴A. Savin, "Recent developments and applications of modern density functional theory", in, edited by J. M. Seminario, (Elsevier, Amsterdam, 1996), p. 327.
- ³⁹⁵F. C. J. Toulouse, and A. Savin, *Phys. Rev. A* **70**, 062505 (2004).
- ³⁹⁶D. Prendergast, M. Nolan, C. Filippi, S. Fahy, and J. C. Greer, *J. Chem. Phys.* **115**, 1626 (2001).